Self-Assembly of Large Amyloid Fibers

Devin M. Ridgley

Dissertation submitted to the faculty of the Virginia Polytechnic Institute and State University in partial fulfillment of the requirements for the degree of

Doctor of Philosophy
In
Biological Systems Engineering

Justin R. Barone, Committee Chair
David R. Bevan
Chenming (Mike) Zhang
Scott Renneckar

May 1, 2014
Blacksburg, VA

Keywords: Amyloid, Biomaterial, Protein, Self-Assembly, Fibril, Fiber, Amino Acid

Self-Assembly of Large Amyloid Fibers

Devin M. Ridgley

ABSTRACT

Functional amyloids found throughout nature have demonstrated that amyloid fibers are potential industrial biomaterials. This work introduces a new "template plus adder" cooperative mechanism for the spontaneous self-assembly of micrometer sized amyloid fibers. A short hydrophobic template peptide induces a conformation change within a highly α-helical adder protein to form β-sheets that continue to assemble into micrometer sized amyloid fibers. This study utilizes a variety of proteins that have template or adder characteristics which suggests that this mechanism may be employed throughout nature. Depending on the amino acid composition of the proteins used the mixtures form amyloid fibers of a cylindrical (~10 μm diameter, ~2 GPa Young's modulus) or tape (5-10 μm height, 10-20 μm width and 100-200 MPa Young's modulus) morphology. Processing conditions are altered to manipulate the morphology and structural characteristics of the fibers. Spectroscopy is utilized to identify certain amino acid groups that contribute to the self-assembly process. Aliphatic amino acids (A, I, V and L) are responsible for initiating conformation change of the adder proteins to assemble into amyloid tapes. Additional polyglutamine segments (Q-blocks) within the protein mixtures will form Q hydrogen bonds to reinforce the amyloid structure and form a cylindrical fiber of higher modulus. Atomic force microscopy is utilized to delineate the self-assembly of amyloid tapes and cylindrical fibers from protofibrils (15-30 nm width) to fibers (10-20 μm width) spanning three orders of magnitude. The aliphatic amino acid content of the adder proteins' α-helices is a good predictor of high density β-sheet formation within the protein mixture. Thus, it is possible to predict the propensity of a protein to undergo conformation change into amyloid structures. Finally, *Escherichia coli* is genetically engineered to express a template protein which self-assembles into large amyloid fibers when combined with extracellular myoglobin, an adder protein. The goal of this thesis is to produce, manipulate and characterize the self-assembly of large amyloid fibers for their potential industrial biomaterial applications. The techniques used throughout this study outline various methods to design and engineer amyloid fibers of a tailored modulus and morphology. Furthermore, the mechanisms described here may offer some insight into naturally occurring amyloid forming systems.

ACKNOWLEDGMENTS

This thesis has been completed with the guidance and support of my advisor Dr. Justin Barone. I express my sincerest appreciation for his mentoring that allowed me to develop into the researcher and professional that I am today. I would like to express my thanks to my committee members Dr. David Bevan, Dr. Mike Zhang, Dr. Eva Marand and Dr. Scott Renneckar for their research suggestions and guidance over the last two years. I would also like to thank Dr. Ryan Senger and Ben Freedman for their substantial contributions to the *in vivo* expression mechanisms used in this work. Without their expertise this endeavor would have been a difficult undertaking. I am also indebted to Catlin Rippner, Elizabeth Claunch, Parker Lee and many other graduate and undergraduate students that I have had the pleasure of working with over the years. Over the last four years I have been blessed to make some great friends who have made my years at Virginia Tech so enjoyable. Finally, I would like to thank Ashely for all of her support over the years as well as my Father, Mother, Brother and Sister for their unconditional support and encouragement throughout my academic endeavors.

TABLE OF CONTENTS

LIST OF FIGURES

CHAPTER 2

CHAPTER 3

LIST OF TABLES

LIST OF EQUATIONS

CHAPTER 2

CHAPTER 4

CHAPTER 6

ABBREVIATIONS

Ac	α-casein
AFM	Atomic Force Microscopy
Al	α-lactalbumin
Am	Amylase
FT-IR	Fourier Transform-Infrared Spectroscopy
Gd	Trypsin hydrolyzed gliadin
Hm	Hemoglobin
In	Insulin
My	Myoglobin
NX	No expression of the indicated peptide
SEM	Scanning Electron Microscopy
WG	Trypsin hydrolyzed wheat gluten
X	Expression of the indicated peptide

ATTRIBUTION

Author Devin M. Ridgley is the major contributor and writer of the manuscripts shown in Chapters 2-7. Co-author Dr. Justin Barone contributed to the research strategy, conclusions and writing for each of these publications (Chapters 2-7). Co-authors Keira Ebanks (Chapter 2), Elizabeth Claunch (Chapter 4 and 6), Parker Lee (Chapters 6 and 7) and Ben Freedman (Chapter 7) all contributed to the research within these manuscripts. I want to thank each of the co-authors for their contributions to this research. At the time of the research all authors were with Dept. of Biological Systems Engineering, 203 Seitz Hall, Virginia Tech, Blacksburg VA 24061.

Chapter 1. Introduction

Nature has perfected the art of engineering robust materials over millions of years of evolution. Specifically, structural materials in nature are fiber composites. Cellulose is composed of glucose monomers and the highly rigid and tough fiber is one of the most abundant materials in nature. Proteinaceous fibers such as keratin, elastin, and collagen are composed of amino acid sequences that dictate the structural characteristics of the material.(Meyers et al., 2008) The hierarchical macromolecular self-assembly of these compounds into fibrous structures is what determines the structural properties that dictate if a material is stiff for support or highly flexible and elastic to facilitate movement.(Fratzl and Weinkamer, 2007) The method that nature employs to efficiently produce life sustaining materials should be the inspiration for future materials engineering throughout industry. Thus, in an effort to efficiently produce renewable materials we should strive to replicate naturally occurring processes.

Spider dragline silk is considered by many to be the "gold standard" of biological materials due to its high modulus and toughness.(Qin and Buehler, 2013) Spider silk is created by a pulling mechanism that takes a protein mixture, termed "dope," and draws it through the insect's silk gland, quickly evaporating the water and forming a silk strand.(Tillinghast et al., 1984) The mechanical shearing force aligns the protein β-sheets along the fiber axis. The structural properties of the silk strand can be manipulated by altering the pulling speed of the protein dope. A faster speed will create more crystalline regions making the fiber more rigid with a high modulus for structural support.(Nova et al., 2010) These fibers support the weight of a spider as it is suspended from a higher object. A lower speed will create a silk strand with varying crystalline and amorphous regions forming a strand with high extensibility and toughness.(Nova et al., 2010) These properties of the silk provide the energy dissipation required to catch prey

within the spider's web. Thus, the spider is capable of manipulating structural properties of the silk for a specific function by altering the extrusion speed. Spider silk has a higher specific modulus than steel with a greater extensibility which makes it highly desirable as an industrial biomaterial.(Smith et al., 1999; Vendrely and Scheibel, 2007; Xia et al., 2010) Indeed, synthetic spider silk from recombinant proteins has been produced and engineered to form silk strands with tailored structural and morphological properties based on the protein dope composition and post-synthetic spinning processing.(Albertson et al., 2014) While spider silk may be one of the more promising examples of nature forming robust biomaterials, it is not the only one. The silkworm *Bombyx mori* produces the fibroin protein to form silk that constitutes the cocoon of the insect.(Shen et al., 1998) This silk has a comparable elastic modulus and tensile strength to spider dragline silk, 16 ± 1 GPa and 650 ± 40 MPa respectively.(Poza et al., 2002) Insect silk has been the focus of extensive research for industrial applications such as bullet-proof vests, artificial tendons, tissue engineering scaffolds and other biomaterials.(Altman et al., 2003; Kaplan et al., 2013; Vendrely and Scheibel, 2007; Wang et al., 2006) Unfortunately, the mechanical pulling force required to align the crystalline regions of the dragline silk and the need for a coagulation bath to form the fiber during spinning has made synthetic silk too expensive for most applications.(Yu et al., 2013)

Amyloid fibers are another example of a robust proteinaceous biomaterial in nature. Amyloid fibrils also contain β -sheets. However, the β-sheets in amyloid fibrils are of much higher protein strand density than in silk and are oriented perpendicular to the fibril axis, unlike the β-sheets in spider silk.(Bouchard et al., 2000; Nelson et al., 2005) This is because amyloid fibrils are self-assembled and silk fibers require the pulling mechanism, which orients the β-sheets along the fiber axis. The formation of amyloid structures is most commonly associated with a

class of debilitating neurodegenerative diseases termed prion diseases. "Prion" is defined as a "proteinaceous infectious particle" and is commonly associated with Bovine Spongiform Encephalopy (BSE), Creutzfeldt-Jakob disease (CJD) and Scrapie for their contagious characteristics. Alzheimer's, Parkinson's and Huntington's diseases are characterized by the spontaneous misfolding of various natively stable proteins into high density β-sheet amyloid aggregates that inhibit cellular function and eventually lead to death, their classification as prion diseases is still debated.(Dobson, 2003) Amyloid Beta ($A\beta_{1\text{-}42}$) is a membrane bound protein that has been identified as the amyloid aggregate in early onset Alzheimer's disease.(Duff et al., 1996) A mutation causes the Amyloid Precurser Protein (APP) to be cleaved in a slightly different location adding two aliphatic amino acids to the 41 and 42 positions on Aβ.(Pike et al., 1995; Selkoe, 1996) The addition of two hydrophobic amino acids to the protein is enough to destabilize the protein and cause spontaneous aggregation to form amyloid plaques.(Snyder et al., 1994) Similarly, the seventeen amino acid N-terminus of the Huntington protein (HTT^{NT}) is hydrophobic.(Sivanandam et al., 2011) It is hypothesized that this region initiates aggregation and the adjacent glutamine repeat region (Q-block) stabilizes the aggregate by hydrogen bonding with itself, creating a "polar zipper" and forming a robust amyloid material.(Perutz et al., 1994; Sivanandam et al., 2011; Williamson et al., 2010) The hydrophobicity and Q-block regions have been shown to affect the aggregation of various proteins associated with prion diseases.(Chiti and Dobson, 2006; Dobson, 2001; Dobson, 2003) The fact that there is no known cure for these neurodegenerative diseases is a testament to the robustness of amyloid aggregates. Furthermore, the diversity of proteins that misfold in prion diseases suggests that there may be a common mechanism of amyloid self-assembly.

While accidental misfolding of a given protein forms fatal amyloid aggregates in some organisms, other organisms assemble amyloid fibers for functional purposes. "Functional" amyloids are produced by organisms to serve a specific need in order to perpetuate life. Barnacle cement from *Megabalanus rosa* is one of the most robust adhesives in nature. The cement is a composite material of amyloid fibers embedded within a proteinaceous polymer matrix. The fungus *Neurospora crassa* creates an extracellular amyloid matrix to protect the organism from the external environment and allow for cellular adhesion to hydrophobic surfaces.(Barlow et al., 2010; Kamino, 1996; Kamino et al., 2000; Wösten, 1994) The insect *Chrysopidae* produces amyloid silk stalks and cocoons to protect its eggs from predators.(Bauer et al., 2012; Weisman et al., 2008) The curli protein produced from gram negative bacteria forms amyloid extracellular matrices that facilitate cell adhesion and biofilm formation.(Fowler et al., 2007; Zhou et al., 2013)

It is widely accepted that any protein is capable of misfolding into a high density β-sheet amyloid aggregate given the right conditions.(Chiti and Dobson, 2006; Dobson, 2001; Dobson, 2003; Dobson et al., 1998) Generally, a protein is placed in highly denaturing conditions (pH ~2 and/or high temperature) to induce misfolding. This creates an amyloid aggregate "seed" or nucleating site that can be combined with the given protein at near physiological conditions to initiate misfolding in the natively stable protein.(Heegaard et al., 2005) This method has been extensively used throughout literature to form amyloid fibrils with a variety of proteins, such as insulin, β-microglobulin, α-lactalbumin and myoglobin.(Bouchard et al., 2000; Dzwolak et al., 2006; Dzwolak et al., 2004; Fandrich et al., 2001; Fändrich et al., 2003; Goers et al., 2002; Gosal et al., 2005; Guo and Akhremitchev, 2006; Heegaard et al., 2005; Raman et al., 2005) Typically, these amyloid fibrils are 10-20 nm in diameter with a Young's Modulus of approximately 1-3

GPa.(Adamcik et al., 2011; Knowles et al., 2007) A recent study used 4D electron microscopy to reveal a ~ 1 GPa Young's Modulus by oscillating "single amyloid beams," or a pair of hydrogen bonded β-sheets to form the characteristic amyloid cross-β conformation.(Fitzpatrick et al., 2013)

Both functional and disease causing amyloids have a modulus approaching spider silk, however the fibrils spontaneously self-assemble and require no mechanical energy input.(Adamcik et al., 2011) It is a combination of the structural properties and the relative ease of amyloid fiber self-assembly that make it a highly sought after biomaterial. Researchers have used various methods to manipulate amyloid formation for engineered biomaterial applications. Processing conditions have been adjusted to grow wide amyloid tapes with adjustable pitches.(Adamcik and Mezzenga, 2011; Davies et al., 2006) Lara *et al* used the globular protein β-lactoglobulin to self-assemble amyloid ribbons exceeding 100 nm in width.(Lara et al., 2011) Li *et al* was able to create an amyloid fibril/graphene composite that is biodegradable with shape memory properties.(Li et al., 2012) This composite material has good conductivity as well as elongation to break properties that can be refined by adjusting the amyloid fibril to graphene ratio and tailor the material for specific applications.(Solar and Buehler, 2012) Similarly, amyloid fibril hydrogels have been synthesized.(Li et al., 2011; Li and Mezzenga, 2012)

As stated above, amyloid fibrils on the nanometer scale can be synthesized with relative ease by inserting the globular protein into denaturing conditions. This process will grow and deposit amyloid fibrils of 10-20 nm in diameter which is why there has been a push to use the fibrils as a method for bottom up engineering of novel nanomaterials. Bacterial inclusion bodies (IB) were engineered to act as a tissue engineering scaffold or drug delivery mechanism.(Seras-Franzoso et al., 2013; Terzaki et al., 2013) Bolisetty *et al* utilized β-lactoglobulin fibrils to grow gold crystal

flakes.(Bolisetty et al., 2011) This method produced gold "platelets" with potential biosensing, microsensing or optical applications.(Li et al., 2013a) Similarly, amyloid fibrils were used to produce titanium dioxide (TiO_2) nanowires with potential applications within photovoltaic or other nanoelectronic devices.(Acar et al., 2013; Bolisetty et al., 2012; Sakai et al., 2013) In an effort to reduce greenhouse emissions, amyloid fibers have been designed for the selective capture of carbon dioxide.(Li et al., 2013b) Amyloid fibrils can be self-assembled from a variety of peptides or proteins. Thus, there are numerous potential applications based on the above research that shows one can turn a lot of protein starting materials into useful and functional materials. Amyloid fibrils may be functionalized with a given compound to produce a catalytic surface for large scale bioprocesses or nanoscale biosensors. The diversity of proteins that can self-assemble into fibrils may allow one to engineer composite amyloid materials with tailored structural properties. The relatively consistent size of the fibril may allow for the intelligent design of nanoscale circuits. Recent research has uncovered a variety of practical applications for the amyloid fibril as a biomaterial.

In this research the "large amyloid fiber" is introduced. This is a self-assembled amyloid fiber of similar size to naturally-occurring protein fibers such as hair and silk. This is the first time such a fiber has been observed and is unique in the size that is achieved via self-assembly and the close resemblance to natural counterparts. It is the focus of this thesis to produce, manipulate and characterize the features of micrometer sized amyloid fibers for their robust biomaterial capabilities. The large amyloid fiber is made through a unique cooperative two protein mechanism to induce conformation change in a highly hydrophobic "template" peptide and a highly α-helical "adder" protein. This mechanism spontaneously forms micrometer sized amyloid fibers in solution at near physiological conditions. The amyloid fibers (diameter=10-20

μm) produced are 3 orders of magnitude larger than the amyloid fibrils (diameter=10-20 nm) commonly reported. Here, bottom up engineering is utilized to produce hierarchical amyloid fibers with structural and morphological properties dictated by the amino acid composition of the respective protein mixtures. It is the hope of this research that large amyloid fibers will soon be utilized as functional biomaterials throughout industry as synthetic fibers, composites, tissue scaffolds or biosensors for a wide range of applications.

References

Acar, H., R. Garifullin, L. E. Aygun, A. K. Okyay, and M. O. Guler. 2013. Amyloid-like peptide nanofiber templated titania nanostructures as dye sensitized solar cell anodic materials. *J. Mater. Chem. A* 1(36):10979-10984.

Adamcik, J., A. Berquand, and R. Mezzenga. 2011. Single-step direct measurement of amyloid fibrils stiffness by peak force quantitative nanomechanical atomic force microscopy. *Appl. Phys. Lett.* 98(19):193701-193703.

Adamcik, J., and R. Mezzenga. 2011. Adjustable twisting periodic pitch of amyloid fibrils. *Soft Matter* 7(11):5437-5443.

Albertson, A. E., F. Teulé, W. Weber, J. L. Yarger, and R. V. Lewis. 2014. Effects of different post-spin stretching conditions on the mechanical properties of synthetic spider silk fibers. *J. Mech. Behav. Biomed. Mater.* 29(0):225-234.

Altman, G. H., F. Diaz, C. Jakuba, T. Calabro, R. L. Horan, J. Chen, H. Lu, J. Richmond, and D. L. Kaplan. 2003. Silk-based biomaterials. *Biomaterials* 24(3):401-416.

Barlow, D. E., G. H. Dickinson, B. Orihuela, J. L. Kulp III, D. Rittschof, and K. J. Wahl. 2010. Characterization of the adhesive plaque of the barnacle *Balanus amphitrite*: Amyloid-like nanofibrils are a major component. *Langmuir* 26(9):6549-6556.

Bauer, F., L. Bertinetti, A. Masic, and T. Scheibel. 2012. Dependence of Mechanical Properties of Lacewing Egg Stalks on Relative Humidity. *Biomacromolecules* 13(11):3730-3735.

Bolisetty, S., J. Adamcik, J. Heier, and R. Mezzenga. 2012. Amyloid Directed Synthesis of Titanium Dioxide Nanowires and Their Applications in Hybrid Photovoltaic Devices. *Adv. Funct. Mater.* 22(16):3424-3428.

Bolisetty, S., J. J. Vallooran, J. Adamcik, S. Handschin, F. Gramm, and R. Mezzenga. 2011. Amyloid-mediated synthesis of giant, fluorescent, gold single crystals and their hybrid sandwiched composites driven by liquid crystalline interactions. *J. Colloid Interface Sci.* 361(1):90-96.

Bouchard, M., J. Zurdo, E. J. Nettleton, C. M. Dobson, and C. V. Robinson. 2000. Formation of insulin amyloid fibrils followed by FTIR simultaneously with CD and electron microscopy. *Protein Sci.* 9(10):1960-1967.

Chiti, F., and C. M. Dobson. 2006. Protein misfolding, functional amyloid, and human disease. *Annual Review of Biochemistry* 75:333-366.

Davies, R. P. W., A. Aggeli, A. J. Beevers, N. Boden, L. M. Carrick, C. W. G. Fishwick, T. C. B. McLeish, I. Nyrkova, and A. N. Semenov. 2006. Self-assembling β-Sheet Tape Forming Peptides. *Supramol. Chem.* 18(5):435-443.

Dobson, C. M. 2001. The structural basis of protein folding and its links with human disease. *Philos. Trans. R. Soc., B* 356(1406):133-145.

Dobson, C. M. 2003. Protein folding and misfolding. *Nature* 426(6968):884-890.

Dobson, C. M., A. Šali, and M. Karplus. 1998. Protein Folding: A Perspective from Theory and Experiment. *Angew. Chem., Int. Ed.* 37(7):868-893.

Duff, K., C. Eckman, C. Zehr, X. Yu, C. M. Prada, J. Perez-tur, M. Hutton, L. Buee, Y. Harigaya, D. Yager, D. Morgan, M. N. Gordon, L. Holcomb, L. Refolo, B. Zenk, J.

Hardy, and S. Younkin. 1996. Increased Aβ 42(43) in brains of mice expressing mutant presenilin 1. *Nature* 383(6602):710-713.
Dzwolak, W., A. Loksztejn, and V. Smirnovas. 2006. New insights into the self-assembly of insulin amyloid fibrils: an HD exchange FT-IR study. *Biochemistry* 45(26):8143-8151.
Dzwolak, W., V. Smirnovas, R. Jansen, and R. Winter. 2004. Insulin forms amyloid in a strain-dependent manner: An FT-IR spectroscopic study. *Protein Sci.* 13(7):1927-1932.
Fandrich, M., M. A. Fletcher, and C. M. Dobson. 2001. Amyloid fibrils from muscle myoglobin. *Nature* 410(6825):165-166.
Fändrich, M., V. Forge, K. Buder, M. Kittler, C. M. Dobson, and S. Diekmann. 2003. Myoglobin forms amyloid fibrils by association of unfolded polypeptide segments. *Proc. Natl. Acad. Sci. U. S. A.* 100(26):15463-15468.
Fitzpatrick, A. W. P., S. T. Park, and A. H. Zewail. 2013. Exceptional rigidity and biomechanics of amyloid revealed by 4D electron microscopy. *Proc. Natl. Acad. Sci. U. S. A.* 110(27):10976-10981.
Fowler, D. M., A. V. Koulov, W. E. Balch, and J. W. Kelly. 2007. Functional amyloid-From bacteria to humans. *Trends Biochem. Sci.* 32(5):217-224.
Fratzl, P., and R. Weinkamer. 2007. Nature's hierarchical materials. *Prog. Mater. Sci.* 52(8):1263-1334.
Goers, J., S. E. Permyakov, E. A. Permyakov, V. N. Uversky, and A. L. Fink. 2002. Conformational Prerequisites for α-Lactalbumin Fibrillation. *Biochemistry* 41(41):12546-12551.
Gosal, W. S., I. J. Morten, E. W. Hewitt, D. A. Smith, N. H. Thomson, and S. E. Radford. 2005. Competing Pathways Determine Fibril Morphology in the Self-assembly of β2-Microglobulin into Amyloid. *J. Mol. Biol.* 351(4):850-864.
Guo, S., and B. B. Akhremitchev. 2006. Packing Density and Structural Heterogeneity of Insulin Amyloid Fibrils Measured by AFM Nanoindentation. *Biomacromolecules* 7(5):1630-1636.
Heegaard, N. H. H., T. J. D. Jørgensen, N. Rozlosnik, D. B. Corlin, J. S. Pedersen, A. G. Tempesta, P. Roepstorff, R. Bauer, and M. H. Nissen. 2005. Unfolding, Aggregation, and Seeded Amyloid Formation of Lysine-58-Cleaved β2-Microglobulin†. *Biochemistry* 44(11):4397-4407.
Kamino, K. 1996. Cement Proteins of the Acorn-Barnacle, Megabalanus rosa. *Biol. Bull. (Lancaster)* 190(3):403-409.
Kamino, K., K. Inoue, T. Maruyama, N. Takamatsu, S. Harayama, and Y. Shizuri. 2000. Barnacle cement proteins. *J. Biol. Chem.* 275(35):27360-27365.
Kaplan, D., G. H. Altman, R. Horan, and D. Horan. 2013. Spider silk based matrix. Google Patents.
Knowles, T. P., A. W. Fitzpatrick, S. Meehan, H. R. Mott, M. Vendruscolo, C. M. Dobson, and M. E. Welland. 2007. Role of Intermolecular Forces in Defining Material Properties of Protein Nanofibrils. *Science* 318(5858):1900-1903.
Lara, C. c., J. Adamcik, S. Jordens, and R. Mezzenga. 2011. General Self-Assembly Mechanism Converting Hydrolyzed Globular Proteins Into Giant Multistranded Amyloid Ribbons. *Biomacromolecules* 12(5):1868-1875.
Li, C., J. Adamcik, and R. Mezzenga. 2012. Biodegradable nanocomposites of amyloid fibrils and graphene with shape-memory and enzyme-sensing properties. *Nat. Nanotechnol.* 7(7):421-427.

Li, C., M. M. Alam, S. Bolisetty, J. Adamcik, and R. Mezzenga. 2011. New biocompatible thermo-reversible hydrogels from PNiPAM-decorated amyloid fibrils. *Chem. Commun.* 47(10):2913-2915.

Li, C., S. Bolisetty, and R. Mezzenga. 2013a. Hybrid Nanocomposites of Gold Single-Crystal Platelets and Amyloid Fibrils with Tunable Fluorescence, Conductivity, and Sensing Properties. *Adv. Mater.* 25(27):3694-3700.

Li, C., and R. Mezzenga. 2012. Functionalization of Multiwalled Carbon Nanotubes and Their pH-Responsive Hydrogels with Amyloid Fibrils. *Langmuir* 28(27):10142-10146.

Li, D., H. Furukawa, H. Deng, C. Liu, O. M. Yaghi, and D. S. Eisenberg. 2013b. Designed amyloid fibers as materials for selective carbon dioxide capture. *Proc. Natl. Acad. Sci. U. S. A.* 111(1):191-196.

Meyers, M. A., P. Y. Chen, A. Y.-M. Lin, and Y. Seki. 2008. Biological materials: Structure and mechanical properties. *Prog. Mater. Sci.* 53(1):1-206.

Nelson, R., M. R. Sawaya, M. Balbirnie, A. O. Madsen, C. Riekel, R. Grothe, and D. Eisenberg. 2005. Structure of the cross-[beta] spine of amyloid-like fibrils. *Nature* 435(7043):773-778.

Nova, A., S. Keten, N. M. Pugno, A. Redaelli, and M. J. Buehler. 2010. Molecular and Nanostructural Mechanisms of Deformation, Strength and Toughness of Spider Silk Fibrils. *Nano Lett.* 10(7):2626-2634.

Perutz, M. F., T. Johnson, M. Suzuki, and J. T. Finch. 1994. Glutamine repeats as polar zippers: their possible role in inherited neurodegenerative diseases. *Proc. Natl. Acad. Sci. U. S. A.* 91(12):5355-5358.

Pike, C. J., M. J. Overman, and C. W. Cotman. 1995. Amino-terminal Deletions Enhance Aggregation of β-Amyloid Peptides in Vitro. *J. Biol. Chem.* 270(41):23895-23898.

Poza, P., J. Pérez-Rigueiro, M. Elices, and J. Llorca. 2002. Fractographic analysis of silkworm and spider silk. *Eng. Fract. Mech.* 69(9):1035-1048.

Qin, Z., and M. J. Buehler. 2013. Spider silk: Webs measure up. *Nat. Mater.* 12(3):185-187.

Raman, B., E. Chatani, M. Kihara, T. Ban, M. Sakai, K. Hasegawa, H. Naiki, C. M. Rao, and Y. Goto. 2005. Critical Balance of Electrostatic and Hydrophobic Interactions Is Required for β2-Microglobulin Amyloid Fibril Growth and Stability. *Biochemistry* 44(4):1288-1299.

Sakai, H., K. Watanabe, Y. Asanomi, Y. Kobayashi, Y. Chuman, L. Shi, T. Masuda, T. Wyttenbach, M. T. Bowers, K. Uosaki, and K. Sakaguchi. 2013. Formation of Functionalized Nanowires by Control of Self-Assembly Using Multiple Modified Amyloid Peptides. *Adv. Funct. Mater.* 23(39):4881-4887.

Selkoe, D. J. 1996. Amyloid β-Protein and the Genetics of Alzheimer's Disease. *J. Biol. Chem.* 271(31):18295-18298.

Seras-Franzoso, J., K. Peebo, J. L. Corchero, P. M. Tsimbouri, U. Unzueta, U. Rinas, M. J. Dalby, E. Vazquez, E. García-Fruitós, and A. Villaverde. 2013. A nanostructured bacterial bioscaffold for the sustained bottom-up delivery of protein drugs. *Nanomedicine* (0):1-13.

Shen, Y., M. A. Johnson, and D. C. Martin. 1998. Microstructural Characterization of Bombyx mori Silk Fibers. *Macromolecules* 31(25):8857-8864.

Sivanandam, V. N., M. Jayaraman, C. L. Hoop, R. Kodali, R. Wetzel, and P. C. A. van der Wel. 2011. The Aggregation-Enhancing Huntingtin N-Terminus Is Helical in Amyloid Fibrils. *J. Am. Chem. Soc.* 133(12):4558-4566.

Smith, B. L., T. E. Schaffer, M. Viani, J. B. Thompson, N. A. Frederick, J. Kindt, A. Belcher, G. D. Stucky, D. E. Morse, and P. K. Hansma. 1999. Molecular mechanistic origin of the toughness of natural adhesives, fibres and composites. *Nature* 399(6738):761-763.

Snyder, S. W., U. S. Ladror, W. S. Wade, G. T. Wang, L. W. Barrett, E. D. Matayoshi, H. J. Huffaker, G. A. Krafft, and T. F. Holzman. 1994. Amyloid-beta aggregation: selective inhibition of aggregation in mixtures of amyloid with different chain lengths. *Biophys. J.* 67(3):1216-1228.

Solar, M. I., and M. J. Buehler. 2012. Composite materials: Taking a leaf from nature's book. *Nat. Nanotechnol.* 7(7):417-419.

Terzaki, K., E. Kalloudi, E. Mossou, E. P. Mitchell, V. T. Forsyth, E. Rosseeva, P. Simon, M. Vamvakaki, M. Chatzinikolaidou, A. Mitraki, and M. Farsari. 2013. Mineralized self-assembled peptides on 3D laser-made scaffolds: a new route toward 'scaffold on scaffold' hard tissue engineering. *Biofabrication* 5(4):045002-045016.

Tillinghast, E. K., S. F. Chase, and M. A. Townley. 1984. Water extraction by the major ampullate duct during silk formation in the spider, Argiope aurantia Lucas. *J. Insect Physiol.* 30(7):591-596.

Vendrely, C., and T. Scheibel. 2007. Biotechnological Production of Spider-Silk Proteins Enables New Applications. *Macromol. Biosci.* 7(4):401-409.

Wang, Y., H.J. Kim, G. Vunjak-Novakovic, and D. L. Kaplan. 2006. Stem cell-based tissue engineering with silk biomaterials. *Biomaterials* 27(36):6064-6082.

Weisman, S., H. E. Trueman, S. T. Mudie, J. S. Church, T. D. Sutherland, and V. S. Haritos. 2008. An Unlikely Silk: The Composite Material of Green Lacewing Cocoons. *Biomacromolecules* 9(11):3065-3069.

Williamson, T. E., A. Vitalis, S. L. Crick, and R. V. Pappu. 2010. Modulation of Polyglutamine Conformations and Dimer Formation by the N-Terminus of Huntingtin. *J. Mol. Biol.* 396(5):1295-1309.

Wösten, H. A. 1994. Interfacial self-assembly of a hydrophobin into an amphipathic protein membrane mediates fungal attachment to hydrophobic surfaces. *EMBO J.* 13(24):5848-5854.

Xia, X. X., Z. G. Qian, C. S. Ki, Y. H. Park, D. L. Kaplan, and S. Y. Lee. 2010. Native-sized recombinant spider silk protein produced in metabolically engineered Escherichia coli results in a strong fiber. *Proc. Natl. Acad. Sci. U. S. A.* 107(32):14059-14063.

Yu, Q., S. Xu, H. Zhang, L. Gu, Y. Xu, and F. Ko. 2013. Structure–property relationship of regenerated spider silk protein nano/microfibrous scaffold fabricated by electrospinning. *J. Biomed. Mater. Res., Part A,* DOI:10.1002/jbm.a.35051.

Zhou, Y., D. Smith, D. Hufnagel, and M. Chapman. 2013. Experimental Manipulation of the Microbial Functional Amyloid Called Curli. In *Bacterial Cell Surfaces*, 53-75. A. H. Delcour, ed: Humana Press.

Chapter 2.

Peptide Mixtures Can Self-Assemble into Large Amyloid Fibers of Varying Size and Morphology

Ridgley, D. M., K. C. Ebanks, and J. R. Barone. 2011. Peptide Mixtures Can Self-Assemble into Large Amyloid Fibers of Varying Size and Morphology. *Biomacromolecules* 12(10):3770-3779. - Reproduced with the generous permission of the American Chemical Society.

Article

pubs.acs.org/Biomac

Peptide Mixtures Can Self-Assemble into Large Amyloid Fibers of Varying Size and Morphology

Devin M. Ridgley, Keira C. Ebanks, and Justin R. Barone*

Biological Systems Engineering Department, Virginia Tech, 303 Seitz Hall, Blacksburg, Virginia 24061, United States

ABSTRACT: Peptide mixtures spontaneously formed micrometer-sized fibers and ribbons from aqueous solution. Hydrolyzed gliadin produced short, slightly elliptical fibers while hydrolyzed wheat gluten, a mixture of gliadin and glutenin, formed round fibers of similar size. Mixing hydrolyzed gliadin with increasing molar amounts of myoglobin or amylase resulted in longer, wider fibers that transitioned from round to rectangular cross section. Fiber size, morphology, and modulus were controlled by peptide mixture composition. Fourier transform infrared (FT-IR) spectroscopy results showed that peptides experienced α to β transitions forming an elementary cross-β peptide secondary structure, indicative of amyloids. Large fiber formation was observed to be dependent on hydrophobic packing between constituent peptides. A model was developed to show how the fiber morphology was influenced by the peptides in the mixture.

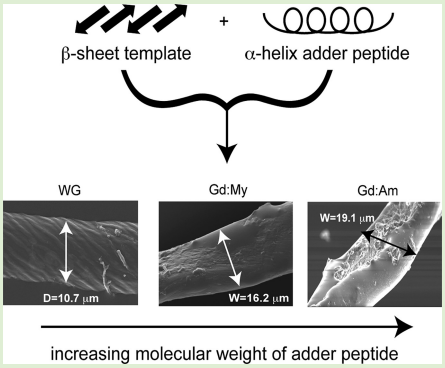

INTRODUCTION

Protein fibers find widespread structural use in nature. For instance, dragline silk must be strong and rigid to support the descent of the insect while capture silk must be tough, ductile, and sticky to capture prey.[1] β-Keratin fibers in bird feathers provide rigidity for flight. Protein molecules in silk and β-keratin have some portions in a highly organized crystalline structure known as the "β-sheet" and some regions with no organization known as "amorphous" or "random coil" regions. The ratio of β-sheets to random coils is a simple way to view the properties of the protein fiber; i.e., the more β-sheets, the stronger and more rigid the fiber, although subtleties in the amorphous region appear to contribute to the toughness greatly.[2,3] Silk has a very conservative amino acid sequence, but β-keratin has a very liberal sequence. Despite these molecular differences, both fibers are similar in size, morphology, and properties with diameters of $D \sim 10^1$ μm, aspect ratios of $L/D > 10^3$, and elastic moduli, E, of $\sim 10^1$ GPa and are extruded from the cell where the proteins are synthesized.[4] The extrusion process aligns the protein molecules and β-sheets along the fiber axis, providing a characteristic X-ray diffraction pattern and signature Amide I absorbance in Fourier transform infrared spectroscopy.[5,6] The similarities in properties appear to arise from similarities in the nanoscale morphology of the fibers.[2,3]

Spun silk and extruded β-keratin are common in nature. Nature employs a second fiber forming mechanism that appears less common. In this mechanism, fibers form spontaneously without extrusion or spinning. These fibers have a similar molecular structure to silk and β-keratin in that some regions of the protein molecules are in β-sheets and some are amorphous. However, the β-sheets are aligned perpendicular to the fiber axis and are known as "cross-β" structures. The most common of these structures are nanometer-sized cross-β fibrils, also known as "amyloids" or "prions". These nanometer-sized fibrils are most often associated with neurodegenerative or prion diseases such as Alzheimer's and Parkinson's disease.[7] Prions form when some natural event, currently unknown, allows what was once a normally functioning protein to start aggregating. There is another set of cross-β structures not implicated in disease known as "functional" amyloids.[8] These spontaneously formed structures protect bacteria and insect eggs and reinforce barnacle cement.[9−13] Interestingly, functional amyloids can be in a nanometer-sized fibril or micrometer-sized fiber form. Bacteria will put proteins into nanometer-sized cross-β structures to protect those proteins when cell environmental conditions change.[9,10,14] This appears to be a survival mechanism to allow the bacteria to proliferate whereas the protein would be damaged or denatured if not in the stable cross-β structure. Bacteria will also create large hyphae from cross-β structures for protection and proliferation.[10] Insects of the *Chrysopidae* family will deposit a highly concentrated protein solution on a plant surface that will dry into a fiber with a diameter of $\sim$20 μm and a length up to 1 cm, dimensions similar to traditional spun spider silk.[12−16] The insect then places its eggs on top of this stalk to suspend and protect them. Analysis of barnacle cements, known to be some of the most robust adhesives in nature, shows them to be fiber composites.[17−19] The reinforcing fibrous phase consists of nanometer-sized cross-β fibrils and micrometer-sized cross-β fibers.[11,20]

Evidence suggests that cross-β fibrils and fibers are more robust than silk and β-keratin. The difficulty in treating prion

Received: July 20, 2011
Revised: August 26, 2011
Published: August 31, 2011

ACS Publications © 2011 American Chemical Society

diseases is a testament to their mechanical stability, which may be why no known cure exists. Indeed, cross-β structures have been shown to be resistant to high temperature, solvents, enzymes, and severe mechanical stress.[21] The moduli of cross-β fibrils have been measured to be in the range of 2−20 GPa.[8,22−27] Comparison of β-sheets in silk and β-keratin to cross-β structures suggests that the cross-β secondary structure is thermodynamically favored and the most stable. β-Keratin fibers can be resolubilized, and upon drying, nanometer-sized cross-β fibrils can be observed but not micrometer-sized fibers.[6,28] Conversely, natural cross-β silk can be plasticized and highly deformed similar to spider silk. The egg stalk of *Chrysopa flava* or green lace wing fly was stretched in water and formed a fiber with a traditional β-sheet structure with protein chains aligned parallel to the fiber axis along the deformation.[13] Although highly favorable and stable, the cross-β structure is rarely found in nature. Nature reserves it for when it wants to destroy life (prion disease) or proliferate it (barnacle cement, egg stalks, bacteria hyphae). Therefore, nature implements mechanisms to discourage its formation, like extrusion or spinning.[29] Cross-β fibrils and fibers form spontaneously without the need for an applied deformation.

There has been growing interest in peptide-based structures in materials science because of superior mechanical properties, versatility, and ability to self-assemble.[30] This has caught the attention of engineers interested in leveraging the unusual stability and rigidity of the cross-β structure. There is a burgeoning field dedicated to utilizing amyloids as high performance bio/nanomaterials in a variety of structural and electronics applications.[23,30−34] Recently, one study was able to arrange nanometer-sized amyloid fibrils into macroscopic ordered films that were easy to manipulate and test.[35] The films had moduli of 6 GPa, which was similar to the individual fibrils. This study showed the amazing ability to build hierarchical structures from the nanometer to the micrometer scale while retaining properties, which may be a very unique feature of natural systems because synthetic systems typically show a large degradation of properties over the same scale. Here, functional cross-β fibers and ribbons 10−30 μm across and several millimeters long are reported that have been spontaneously formed from peptide mixtures. The fibers were formed from a hydrolyzed gliadin "template" and were round or rectangular in cross section. Round and rectangular fibers were formed by adding a small and large, respectively, molecular weight α-helix "adder" peptide. First, nanometer-sized cross-β fibrils self-assembled that continued to assemble into micrometer-sized fibers through hydrophobic interactions. The fibers had moduli in the range of 0.1−2 GPa depending on the adder peptide, showing another example of the unique ability of natural systems to retain properties over several orders of magnitude of scale.

EXPERIMENTAL SECTION

Wheat Gluten (WG) Hydrolysis and Self-Assembly. 2 g of WG (MP Biomedicals, LLC, Solon, OH) was dissolved in 80 mL of deionized water at 37 °C to achieve a concentration of 25 mg/mL. 30 mg of trypsin (type I from bovine pancreas, Sigma-Aldrich, St. Louis, MO) was then added to the solution to give an enzyme-to-substrate ratio of 1:67 w/w. Solution pH was adjusted to 8 with 1 M NaOH. Solution conditions were maintained at pH 8 and 37 °C for 3 weeks, and FT-IR spectra collected periodically to monitor hydrolysis and self-assembly.

Gliadin (Gd) Hydrolysis. 20 g of Gd (TCI America, Portland, OR, UniProt P04721) was dissolved in 800 mL of deionized water at 37 °C. Trypsin was then added at 1:67 w/w enzyme-to-substrate ratio, and the solution was incubated for 72 h at pH 8 and 37 °C. The solution was then poured into Teflon-coated aluminum foil trays and allowed to dry at room temperature under the fume hood. The incubation time was determined to be long enough for hydrolysis but short enough to avoid peptide aggregation.

Peptide Mixtures and Self-Assembly. Amylase (Am, α-amylase, from *Bacillus licheniformis*, Sigma-Aldrich, Saint Louis, MO, UniProt P06278) and myoglobin (My, from equine skeletal muscle, Sigma-Aldrich, St. Louis, MO, UniProt P68082) were dissolved in 10 mL of deionized water at varying molar fractions with dried Gd (Gd:My 1:0, 0.62:0.38, 0.36:0.64, 0.16:0.84, 0:1; Gd:Am 1:0, 0.85:0.15, 0.66:0.34, 0.39:0.61, 0:1). The solutions were 25 mg/mL, which was shown to be in a concentration region where there was strong cross-β formation over reasonable times[36] and greater than the 10 mg/mL used in another study on amyloid formation in peptide mixtures.[37] Solution pH was adjusted to 8 with 1 M NaOH and incubated at 37 °C for 3 weeks.

Fourier Transform Infrared (FT-IR) Spectroscopy. Attenuated total reflectance (ATR) FT-IR spectra of the incubating solutions were recorded periodically on a Thermo Nicolet 6700 FT-IR spectrometer (Thermo Fisher Scientific Inc., Waltham, MA) with a 45° ZnSe crystal trough. The spectra were collected using 256 scans at 4 cm^{-1} resolution from 4000 to 525 cm^{-1}. The spectrum of the solvent without peptide was used as a background and then subtracted from the solution spectrum to reveal the peptide absorbances. Deconvolution of the amide I band into individual components was accomplished with OMNIC v7.3 software. The spectral region 1725−1575 cm^{-1} of the original spectrum was fit with Gaussian/Lorentzian peaks at low sensitivity and full width at half-height of 3.857. All spectra were fit using a constant baseline correction and a target noise of 10.0. The absorbance assignment is shown in Table 1.

Table 1. Assignment of Amide I Absorbances

amide I structural assignment	wavenumber (cm^{-1})
cross-β	1611−1630
β-sheet	1630−1637
random coil	1637−1647
α-helix	1647−1662
β-turn	1662−1678; 1689−1699
antiparallel β-sheet	1679−1688

Fiber Formation. Incubated solutions were dried on Teflon-coated aluminum foil under the fume hood at ambient conditions. Although some fibers were observed in solution after about a week, fiber formation was maximized by drying after several weeks.

Thioflavin-T (Th-T) Binding Assay. Fluorophore Th-T was used to confirm the core cross-β structure of the self-assembled fibers. 20 μL of peptide solution was dried on a glass slide, stained with 1% Th-T solution for 10 min, and gently washed with deionized H_2O. Spatially resolved fluorescence images of the Th-T stained fibers were taken using a Zeiss Axio Imager M1 microscope. Th-T dye was excited at ~480 nm, and emission was collected at ~510 nm through a 10× objective.

Scanning Electron Microscopy (SEM). Fibers formed from dried solution were mounted onto aluminum SEM stubs with double-sided tape. Scanning electron micrographs were obtained using a LEO 1550 field-emission SEM (Zeiss, Peabody, MA) with a 4−6 mm working distance, 5 kV accelerating voltage, and an In-lens SE-detector. Fiber dimensions were obtained on 10−15 fibers each for WG, Gd, and Gd:My fibers and 4−8 fibers each for Gd:Am fibers, the latter not being as prolific in fiber formation.

Nanoindentation. Fibers were mounted on SEM stubs for nanoindentation. Nanoindentation experiments were performed at room temperature using a Hysitron Triboindenter (Minneapolis, MN) with a 90° conical diamond tip. Experiments were in displacement-controlled (DC) mode with a maximum displacement of 1000 nm at a rate of 100 nm/s. The reduced modulus, E_r, was determined according

to Oliver and Pharr[38]

$$E_r = \frac{S\sqrt{\pi}}{2\sqrt{A_c}} \quad (1)$$

where A_c was the contact area and S was the unloading stiffness. The fiber elastic modulus (Young's modulus), E_f, was related to the reduced modulus by

$$\frac{1}{E_r} = \frac{1-\nu_f^2}{E_f} + \frac{1-\nu_t^2}{E_t} \quad (2)$$

where ν_f and ν_t were Poisson's ratio of the fiber and indenter tip, respectively. The elastic modulus and Poisson's ratio of the indenter tip were 1140 GPa and 0.07, respectively, as given by the instrument's manufacturer. The fiber elastic modulus was calculated from eq 2 assuming ν_f was 0.3, which was used in previous nanoindentation studies on amyloid fibrils and was a typical value for polymers.[39,40]

RESULTS AND DISCUSSION

Self-Assembly. Self-assembly over time was monitored using FT-IR spectroscopy. Typical spectra, shown in Figure 1 for Gd:My 0.36:0.64 mole fraction, display structural changes with time. The amide I absorbance, originally centered around 1650 cm^{-1}, began to shift at 3 days to a cross-β structure centered around 1621 cm^{-1}. The cross-β structure became stronger with time. Peptide secondary structure components were resolved through deconvolution of the amide I absorbance. Particularly, the cross-β secondary structure can be resolved and has been shown to correlate well with X-ray diffraction (XRD) and circular dichroism (CD) data on cross-β formation.[36,41−43] All of the spectra were deconvoluted and changes in the α-helix and cross-β content plotted as a function of time as shown in Figure 2 for Gd:My mixtures. In this representation, there was a clear primary transition in the secondary structure with a loss of α-helix and gain in cross-β and the secondary structure changes are defined in Figure 2. For low My content, the transition happened in a few days but took more than a week for Gd:My 0.16:0.84 mol:mol. There was no delay in the Am mixtures, and all transitions happened within the same time, about 96 h. The results for WG, Gd:My, and Gd:Am are tabulated in Table 2, where x_{adder} is the mole fraction of protein added to Gd.

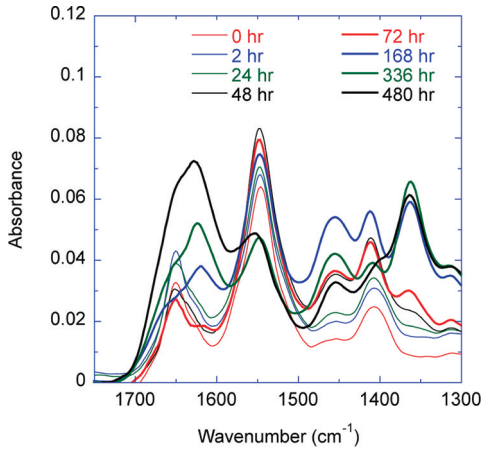

Figure 1. FT-IR spectra of Gd:My 0.36:0.64 illustrating the peak shift from ~1650 to ~1620 cm^{-1} and the change in peak intensities at ~1410 and 1365 cm^{-1} over 480 h.

The core cross-β structural arrangement of the self-assembled fibers was confirmed with a thioflavin-T (Th-T) binding assay. Fibrillar cross-β structures are highly organized and have long channels made by the regular repeat of residues and run along the length of the cross-β sheet. It has been argued that Th-T is more likely to bind to these channels than to native nanocrystalline β-sheet structures that do not have such long-range organization.[44] So Th-T has been extensively used to detect the presence of cross-β structures. Figure 3 shows a representative fluorescence microscopy snapshot of a Th-T stained WG fiber. Strong fluorescence from the core of the fiber indicated cross-β structural arrangement.

The amide I absorbance was not the only spectral feature that changed with time. The CH_3 asymmetric deformation around 1410 cm^{-1}, $\delta_{as}(CH_3)$, and CH_3 symmetric deformation around 1365 cm^{-1}, $\delta_s(CH_3)$, were very weak but grew in intensity with self-assembly. In Figure 1, it can be seen that these two absorbances change differently with self-assembly.

Fiber Size and Morphology. The fibers obtained from drying the solutions were imaged in SEM. Pure Gd fibers were slightly elliptical and WG fibers were round in cross section. WG was a mixture of hydrolyzed Gd (42 wt %) and high and low molecular weight glutenin, GtH (12 wt %, UniProt P08488) and GtL (46 wt %, UniProt P10386) peptides, respectively, and these fibers contained a tight, regularly defined pitch on the surface. The addition of My or Am to the peptide mixture caused the fibers to become longer, wider, and more rectangular in cross section with a higher pitch (Figure 4).

Fiber Mechanical Properties. Nanoindentation results revealed that self-assembled WG had a consistently higher modulus than Gd, Gd:My, or Gd:Am fibers and ribbons, with the latter being about equal in modulus (Figure 5).

Fiber Structure and Correlation to Properties. The present work was motivated by initial observations of micrometer-sized fiber formation in tryptic hydrolysates of wheat gluten.[36] Hydrolyzed WG peptides consistently displayed round, micrometer-sized fibers with a cross-β secondary structure. This was interesting because other studies on cross-β formation in proteins and peptides displayed only nanometer-sized fibril formation. Initially, it was hypothesized that a component of the peptide mixture was responsible for fiber formation because unhydrolyzed WG at pH 8 and 37 °C would not spontaneously form cross-β fibrils or fibers. However, WG has been shown to form fibrils under severe denaturing conditions, consistent with many other studies on cross-β fibril formation in the literature.[45−47] The current understanding of cross-β fibril formation is that fibrils form through main chain interactions that are independent of the amino acid sequence.[48] Accumulating evidence suggests that virtually any peptide can fibrillate when provided the right conditions.[49,50] These are usually extreme denaturing conditions of low pH, high temperature, high stress, or high ionic strength that disrupt the protein's ability to fold based on side chain interactions, straightening the peptide and allowing main chain interactions to dominate. Therefore, the same trypsin hydrolysis experiments were carried out on the gliadin and glutenin components of WG. Gliadin displayed strong cross-β formation as evidenced by XRD and FT-IR while glutenin did not.[36] Hydrolyzed Gd also formed micrometer-sized fibers that were smaller in diameter and length than WG fibers. Examination of tryptic fragments of WG revealed the 3-22 peptide of gliadin (Gd20), the 162-207 peptide of gliadin (Gd46), and the 203-277 peptide of the low molecular weight glutenin subunit (GtL75)

dx.doi.org/10.1021/bm201005k | Biomacromolecules 2011, 12, 3770−3779

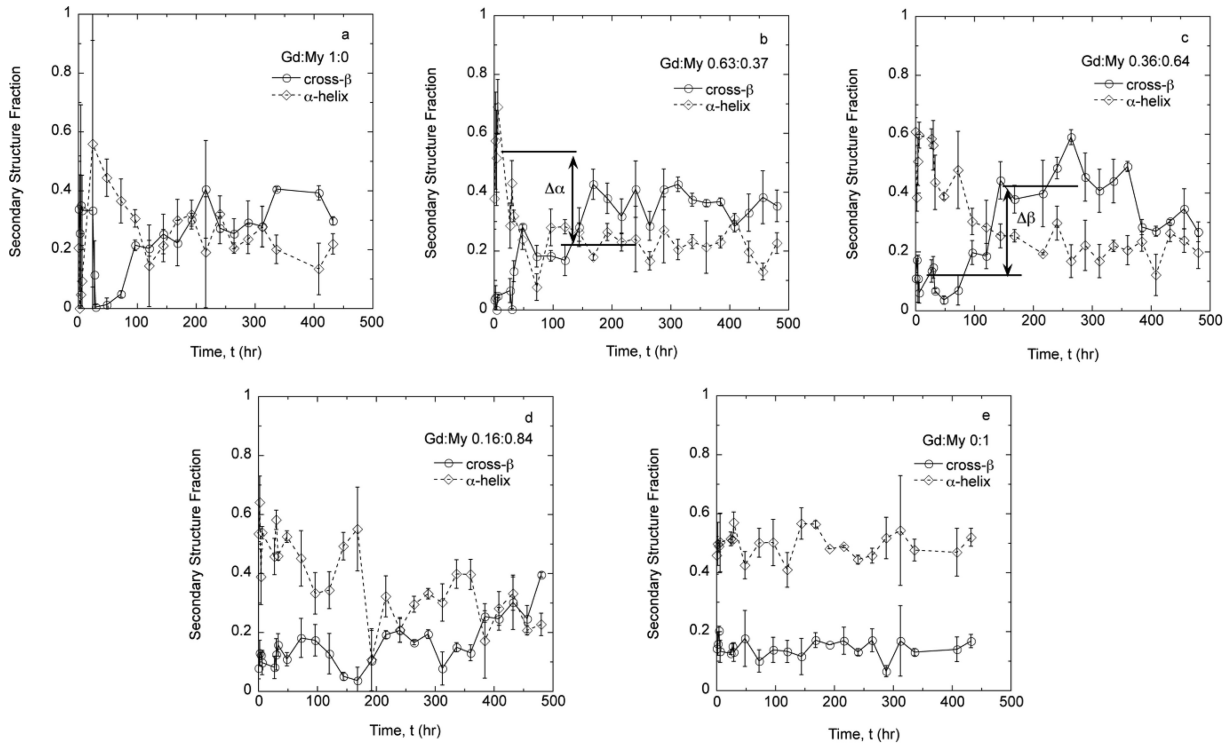

Figure 2. Fraction of cross-β and α-helix secondary structure was determined through deconvolution of the FT-IR amide I peak in Gd:My mixtures as a function of time. (a) Gd:My 1:0, (b) Gd:My 0.63:0.37, (c) Gd:My 0.36:0.64, (d) Gd:My 0.16:0.84, (e) Gd:My 0:1 mol:mol.

Table 2. Summary of FT-IR Spectral Changes in Self-Assembled Peptide Mixtures[a]

mixture	x_{adder}	Δcross-β	Δα-helix	$\Delta(\delta_s/\delta_{as})$	t_e (h)	t_f (h)
Gd:My	0	0.30	0.33	1.63	81	193
	0.37	0.26	0.23	2.72	139	311
	0.64	0.29	0.31	1.69	95	432
	0.84	0.10	0.20	0.53	168	410
	1.00	0.00	0.00	0.40	0	0
Gd:Am	0.15	0.20	0.09	1.93	96	169
	0.34	0.11	0.02	1.65	98	171
	0.61	0.10	0.07	1.03	99	144
	1.00	0.11	0.10	0.58	97	167
WG (Gd:GtL)	0.49	0.35	0.33	2.77	168	431

[a] x_{adder} is mole fraction of My, Am, or GtL; Δcross-β, Δα-helix, and $\Delta(\delta_s/\delta_{as})$ are change in cross-β, α-helix, and ratio of symmetric CH_3 to asymmetric CH_3 deformation, respectively; t_e and t_f are transition times for elementary unit and fiber formation, respectively.

to have a high propensity for cross-β formation as determined by multiple prediction algorithms.[51] In hydrolyzed WG, the mole fraction of Gd:GtL was 0.51:0.49, which is shown in Table 2. All three peptides had high α-helix content, but Gd20 was considered hydrophobic (positive GRAVY) compared to Gd46 and GtL75, which were considered hydrophilic (negative GRAVY, Table 3). α to β transitions as measured by FT-IR spectroscopy were observed in hydrolyzed WG solutions that formed fibers (Figure 6a).

Replacing glutenin with My or Am affected the α to β transition, $\delta_s(CH_3)$ and $\delta_{as}(CH_3)$ absorbances, and fiber morphology. The observed changes offered insight into the multiple peptide self-assembly process and how large fibers formed. Self-assembly based on complementary charge was eliminated as a possible mechanism because of the low level of

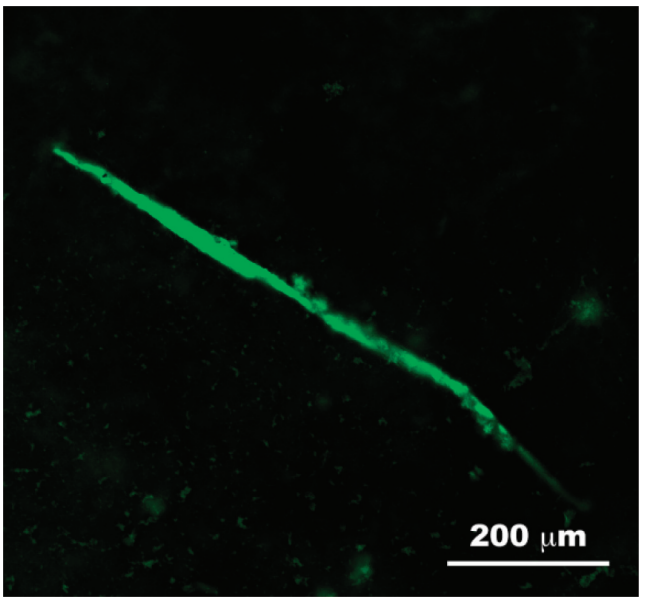

Figure 3. Th-T binding in WG fibers reveals the cross-β secondary structure.

charge at pH 8, and it has been shown that peptides need a large percentage of charged amino acids to self-assemble based on this mechanism.[31,52] In addition, not all peptide mixtures displayed a charge mismatch. Cross-β formation was approximately equal to α-helix loss in the peptide secondary structure, indicating an α to β transition was important in forming elementary units prior to fiber formation. Indeed, α-helical peptides have been shown to undergo α to β transitions more readily on hydrophobic surfaces.[53,54] Pure My had no conformation change and displayed no aggregation on any

dx.doi.org/10.1021/bm201005k | Biomacromolecules 2011, 12, 3770–3779

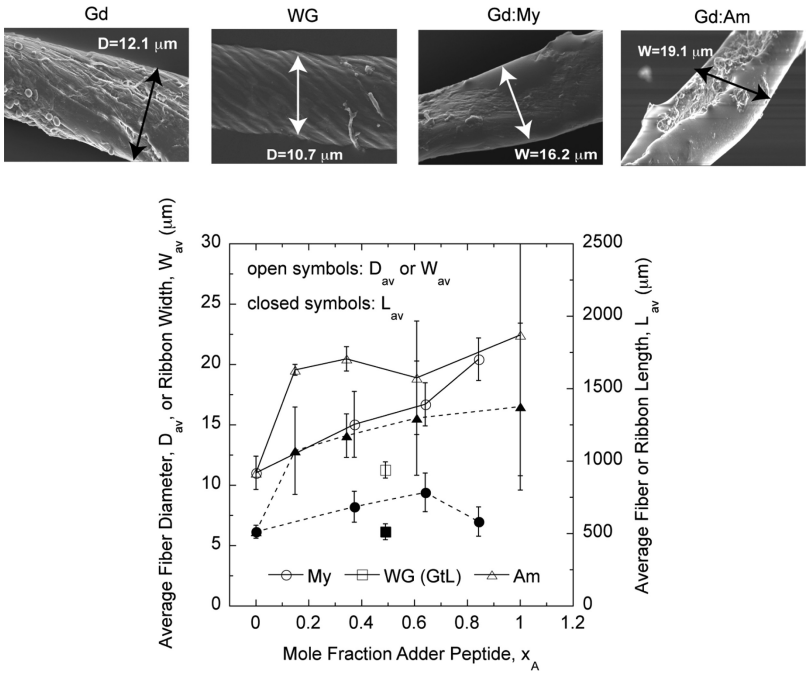

Figure 4. Top: scanning electron micrographs illustrating the difference in width and morphology of Gd, WG, Gd:My, and Gd:Am fibers. Bottom: fibers increased in size as the ratio of My and Am increased in respective Gd:My and Gd:Am mixtures.

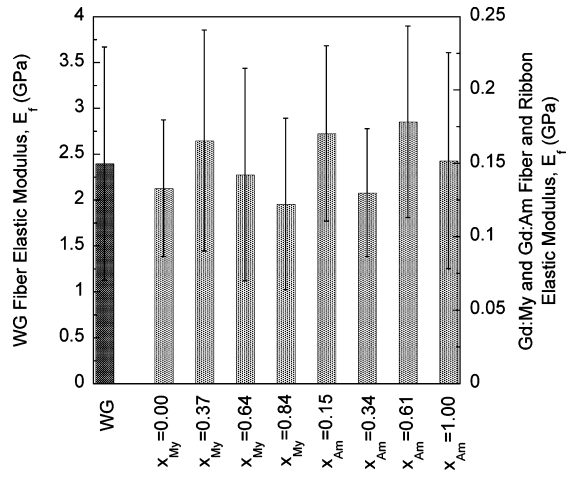

Figure 5. Fiber modulus, E_f, as determined by nanoindentation.

scale at the experimental conditions although it can at more severe denaturing conditions.[55,56] All peptide mixtures displayed a primary α to β transition, represented by $\Delta\alpha$, Δcross-β, and t_e in Table 2. For WG, Gd:Am, and Gd:My of low My content, only a primary transition was observed, with conformational change saturating after t_e. For Gd:My 0.36:0.64 and 0.16:0.84, there were secondary transitions at about 375 h. Gd:My 0.36:0.64 lost cross-β at the expense of random coil (data not shown and the only increase in random coil content). Gd:My 0.16:0.84 lost α-helix and gained cross-β in two steps, at 168 and 375 h. This secondary transition was not consistent with an α-helical "intermediate" phase characterized by conversion of random coils to α-helices and then β-sheets, an important mechanism in amyloid fibril formation in disease forming peptides in hydrophobic environments.[57−60] The fraction of α-helix in My and Am was n_α = 0.76 and 0.25, respectively. The fraction of alanine (A), isoleucine (I), leucine (L), and valine (V) in the α-helices was ϕ_α = 0.36 for both My and Am. We can now define a parameter $f_1 = n_a\phi_\alpha$ that we hypothesize is the potential of the α-helix to unravel into β-sheets on a more hydrophobic surface and f_1 = 0.27 and 0.09 for My and Am, respectively, which were similar to $\Delta\alpha$ values in Table 2. A similar analysis for WG components revealed f_1 = 0.31 and 0.13 for Gd46 and GtL75, respectively. The f_1 value for Gd46 was consistent with the conformational change in Gd and WG, although a mixture of peptides may have influenced conformational change in WG. The correlation of f_1 to conformational change suggested that hydrophobic regions of the α-helix were converting to cross-β. For Gd:My mixtures of low Gd content, conversion did not appear to occur in one step and was inhibited for Gd:My 0.16:0.84. Since My did not undergo an α to β transition on its own, it was heavily dependent on the template to do so, and the transition was a longer, multistep process with a scarcity of template. Am underwent an α to β transition on its own and appeared to control the α to β transition in the presence of the template, but the presence of the template positively influenced fiber formation and affected fiber size and morphology. It has recently been predicted that α-helices should be of a minimum size of about 40 amino acids to undergo an α to β transition under mechanical stretching.[61] Predicted (PSIPRED) α-helical domains in Gd46, GtL75, My, and Am were shorter than this critical length as were, for instance, α-helical domains in Aβ(1−40) and α-synuclein, two common peptides studied in the amyloid literature and implicated in disease. This indicated that α to β transitions from environmental changes in the absence of deformation had a shorter critical length.

Considering $\delta_s(CH_3)$ as a measure of up and down CH_3 vibration and $\delta_{as}(CH_3)$ as a measure of side to side CH_3 vibration, the ratio $\delta_s(CH_3)/\delta_{as}(CH_3)$ can be used to quantify packing of CH_3 groups on A, I, L, and V side groups, which were plentiful especially in Gd20.[62] Figure 6 shows the change in $\delta_s(CH_3)/\delta_{as}(CH_3)$ for each peptide mixture, and the overall change for each is listed in Table 2. The ratio $\delta_s(CH_3)$/

dx.doi.org/10.1021/bm201005k|Biomacromolecules 2011, 12, 3770−3779

Table 3. Properties of Peptides and Proteins[a]

peptide	α (%)	no. aa	MW	AI	GRAVY	pI	− (%)	+ (%)	TANGO
Gd20	85	20	2060	171.0	1.820	9.4	0.0	5.0	1477
Gd46	87	46	5422	108.0	−0.328	6.4	4.3	2.2	207
GtL75	47	75	8465	89.7	−0.668	5.4	2.7	1.3	771
My	76	154	17083	88.8	−0.381	7.2	13.6	13.6	624
Am	25	512	58549	69.6	−0.607	6.3	12.1	10.6	N/A

[a] α is % α-helix; no. aa is number of amino acids; MW is molecular weight in g/mol; AI is aliphatic index; GRAVY is grand average of hydropathicity; pI is isoelectric point; −, + are percentage of negative and positive amino acids, respectively; TANGO is a measure of cross-β potential.

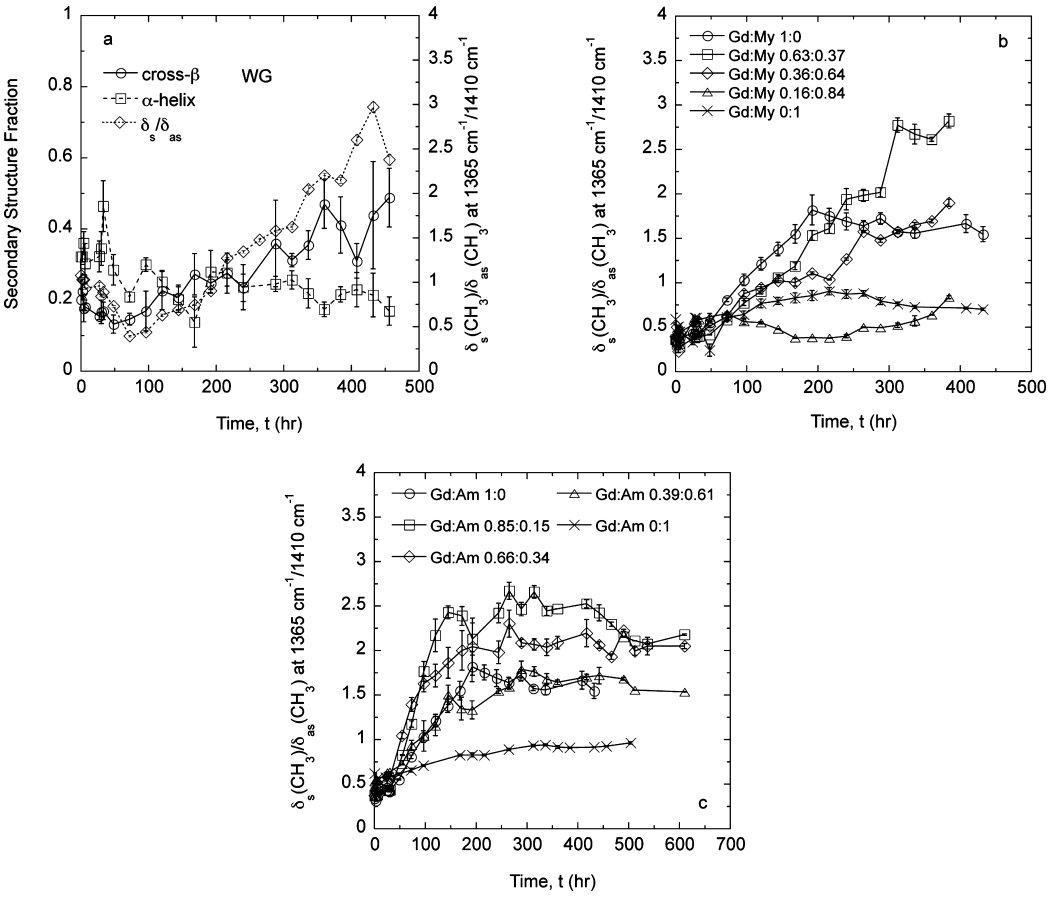

Figure 6. (a) Secondary structure change and $\delta_s(CH_3)/\delta_{as}(CH_3)$ change for WG. $\delta_s(CH_3)/\delta_{as}(CH_3)$ change for (b) Gd:My and (c) Gd:Am mixtures.

$\delta_{as}(CH_3)$ steadily increased over all time, showing up and down vibration favored over side to side vibration or increased packing of hydrophobic groups. The change in $\delta_s(CH_3)/\delta_{as}(CH_3)$ continued for a longer period of time than α to β transitions, delineated by t_f in Table 2. Longer hydrophobic groups on amino acid side chains[63] and substituted onto the peptide[64] have been shown to facilitate aggregation.

Based on the FT-IR, SEM, and nanoindentation results, a fiber formation mechanism was developed involving a combination of peptides: (1) short, hydrophobic peptides in hydrolyzed Gd with a high cross-β potential, like Gd20, experienced an α to β transition upon release from the protein and formed a stable cross-β "template"; (2) hydrophobic regions in the α-helices of longer, hydrophilic α-helical containing peptides interacted with the template to undergo an α to β transition, "adding" into the structure to form an elementary unit, anticipated to be a nanometer-sized structure; (3) elementary units added together through hydrophobic interactions to form large fibers. Fiber size, morphology, and properties were governed by the adder protein molecular weight and fraction of α-helices that were hydrophobic. The hypothesis was tested by changing glutenin (containing GtL75) to My, a longer protein with a majority of α-helix, and Am, a longer protein with less α-helix relative to the overall chain length (Table 3). Both My and Am readily added into the structure although not to the extent that glutenin did as evidenced by the lower Δcross-β. These events led to elementary unit formation, which has been shown to be β-sheet "tapes" of 4−8 nm width, 0.5−1 nm thickness, and length determined by peptide concentration.[65−67] Tapes can now interact with each other to form larger structures. Two morphology extremes can result from this interaction: (1) tapes completely straighten out and stack to yield flat fibrils with a laminated morphology, or (2) tapes twist around each other to form a cylindrical fibril.[67−69] Natural amino acids exist in the left-handed conformation, so tapes can have a twist. The

dx.doi.org/10.1021/bm201005k | Biomacromolecules 2011, 12, 3770−3779

fibrils were 10−20 nm in diameter, meaning they were composed of several tapes. An example of several fibrils is shown in Figure 7a. It was found that the twisted morphology

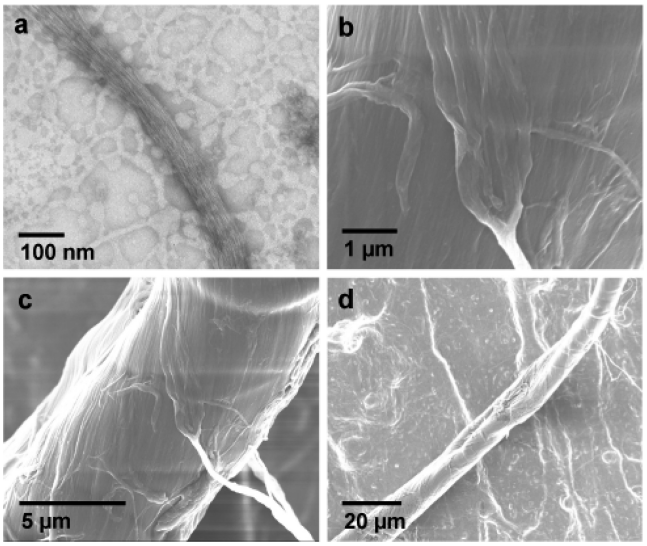

Figure 7. Hierarchy of scale for WG fibers showing (a, b) nanometer-sized fibrils twisting into a (c, d) micrometer-sized fiber.

was thermodynamically favored and the one most often observed.[66] Each time a tape added into the growing fibril, it adjusted its twist to be accommodated into the structure. Eventually, the cost to adjust was too much for any tape and this determined the final fibril size. It has been theorized that fibrils could twist around one another to form larger fibers.[67] This is observed in Figure 7 where fibrils twisted around one another to continue to build the large fiber. Peptide mixtures appeared to facilitate this process. Recent studies have shown that individual fibrils interact through hydrophobic interactions and that electrostatic interactions provide the twist.[70,71] Screening of the electrostatic interactions of β-lactoglobulin fibrils yielded the laminated morphology.[72] FTIR data presented here showed that α to β transitions and hydrophobic interactions were important in elementary unit formation, but hydrophobic interactions alone were important in large fiber assembly.

The morphology changes and range of fiber moduli gave insight into how much of the adder peptides added into the structure. My did not show any conformation change and did not display aggregation on any scale. Upon addition to hydrolyzed Gd, the change in conformation remained similar to that of Gd before decreasing at concentrations above 0.64 mole fraction My. Pure Am showed some ribbon formation but no discernible conformation change and only slight hydrophobic packing. Am seemed to template itself, which may be possible based on its molecular weight and that there was a long hydrophobic portion near the N-terminus. Pure Am showed very little fiber formation so the conformation change may not be discernible in the FTIR spectrum; instead, it was dominated by the majority of unassembled protein. Upon addition to hydrolyzed Gd, the conformation change in the mixtures was always that of pure Am, no matter the mole fraction. Therefore, conformation change in My mixtures was heavily dependent on the template while the Am mixtures were not. WG displayed a higher Δcross-β than pure Gd, suggesting that indeed several peptides in the hydrolysate, i.e., Gd20, Gd46, and GtL75, were involved in self-assembly. WG and Gd:My 0.63:0.37 showed the most hydrophobic packing, but each system showed a similar, general trend of a steady decrease in $\delta_s(CH_3)/\delta_{as}(CH_3)$ for increasing addition of adder protein. Gd peptides were more hydrophobic than the adder proteins and peptides so the behavior was consistent with increased molar addition of adder. The addition of adder protein resulted in increased fiber size and a transition from round to rectangular fibers. Am fibers were the largest followed by My and then WG and Gd fibers, which were about equal in size, suggesting that fiber size was dependent on adder peptide molecular weight. However, the amount of peptide participating in the cross-β structure was dependent on the α-helix content, specifically how hydrophobic the α-helices were, defined by f_1, with Am having the least involvement. Fiber length can also be correlated with twisting.[67] The lower twist of Gd:My and Gd:Am fibers may have contributed to the longer length.

Gd, Gd:My, and Gd:Am fibers all possessed similar modulus, around 0.15 GPa. The WG fibers had significantly higher modulus, around 2 GPa, a range consistent with reported values for amyloid fibrils and natural protein fibers.[8,22,24−27,39,73] A new technique to directly measure amyloid fibril modulus has recently been developed, reporting values of 1.3−2.1 GPa[26] and 3.7 ± 1.1 GPa,[25] showing that the results obtained through the less direct nanoindentation method were similar. WG had a consistently higher modulus and also had the highest cross-β content and hydrophobic packing. Considering the fibers as possessing ordered β-sheet regions and less ordered amorphous or semiamorphous regions, the higher modulus could result from the higher cross-β content. In the context of recent work, this would make the WG fibers stiffer but perhaps not as tough as Gd:My or Gd:Am fibers.[2,3] The increased amount of cross-β content would limit rearrangement of amorphous regions to limit toughness. The increased hydrophobic packing would add to the overall rigidity and stability of the structure. For some mixtures, the WG cross-β content was much higher than Gd:My and Gd:Am mixtures, but only slightly higher for others, so the cross-β content alone probably cannot explain the much larger modulus for WG fibers. An analysis of the amino acid composition showed that Gt peptides, particularly GtL75, had a lot of glutamine (Q), with significant Q-blocks or glutamine repeats, known to facilitate cross-β formation, whereas My and Am had no Q-blocks.[74−78] Gd contained a long Q-block in the 23-162 tryptic fragment, but this peptide had no predicted β-aggregation potential. The absence of Q-blocks in Gd fibers may be the reason for the lower modulus. Comparison of the CH_2 rock and wag absorbance at 1080 cm^{-1}, $\gamma_{r,w}(CH_2)$, to the C−N stretching absorbance at 1016 cm^{-1}, ν(CN), by plotting the ratio shows that $\gamma_{r,w}(CH_2)/\nu(CN) < 1$ and constant for WG (Figure 8). However, the value decreased and was greater than 1 for Gd, Gd:My, and Gd:Am, saturating at the same point as the α to β transition. For WG fibers, glutamine would have CH_2 from its side group, and these packed similarly to the amide group, spectral evidence that GtL75 was involved in the aggregation. This may have indicated that increased hydrogen bonding between Q side groups reinforced the structure, resulting in a much higher modulus. A peptide with a large amount of Q was 3 times more twisted than one of similar length but with less Q, indicating that Q increased aggregation efficiency and that attractive forces between Q side groups stabilized the cross-β structure.[67] For Gd, Gd:My, and Gd:Am, there was little glutamine aggregated in the structure and limited amino acid side group

dx.doi.org/10.1021/bm201005k|*Biomacromolecules* 2011, 12, 3770−3779

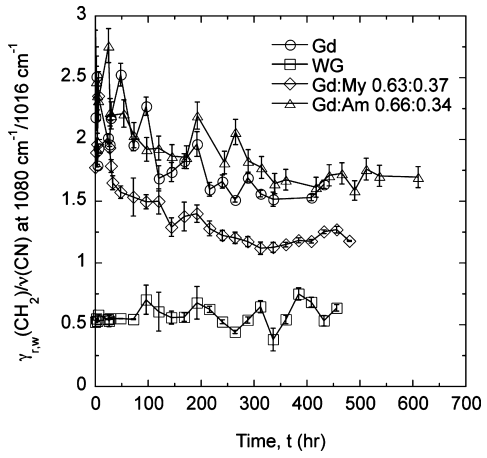

Figure 8. Comparison of the ratios of $\gamma_{r,w}(CH_2)$ at 1080 cm^{-1} to $\nu(CN)$ at 1016 cm^{-1} between WG, Gd, Gd:My, and Gd:Am, demonstrating the difference between the side group interaction of the systems without Q-blocks (Gd:My and Gd:Am) and the system with Q-blocks (WG).

bonding. Instead, side group CH_2, such as those on I and L, physically packed but did not hydrogen bond. The fibers still contained 20% or less of unassembled α-helix, which can undergo α to β transitions under mechanical deformation, acting as an energy dissipation mechanism and increasing modulus.[61] Given the similar amount of α-helix content in each fiber, it was difficult to decouple this mechanism from the more obvious differences in cross-β content, hydrophobic packing, and glutamine interactions.

On a larger scale, overall fiber twisting can contribute to the fiber properties. Highly twisted fibers can be unraveled under tensile deformation and act as a toughening mechanism.[27] Hydrogen bonds increase or decrease depending on compressive or tensile deformation, respectively. Both of these mechanisms could contribute to the overall mechanical response of the fibers, and it would be interesting to study them as a function of applied deformation.

Figure 9 shows a schematic of how two different peptide mixtures can result in two different micrometer-sized fiber morphologies. The top route was exemplified by WG fibers and the bottom route by Gd:Am or Gd:My fibers. Predominantly straight peptides resulted in tapes that could twist into fibrils and fibrils that could twist into cylindrical fibers (WG). Peptides with a lot of unassembled chain length assembled into tapes that had difficulty twisting into cylindrical fibers because of the large amount of random coil peptide decorating the outside of the tape, resulting in flat ribbons (Gd:Am, Gd:My). The pitch, h, was small for cylindrical WG fibers ($h_{fiber} \sim 2.4$ μm) because of tight twisting, but large for Gd:My and Gd:Am ribbons ($h_{ribbon} \sim 200$ μm) because of frustrated twisting. All fibrils adding into WG fibers were highly twisted, while fibrils adding into Gd:Am or Gd:My ribbons were straighter with globules on the surface. The globules were agglomerates that were a result of dangling chain ends. Given the much larger modulus of WG fibers compared to Gd:Am and Gd:My, tight twisting may be indicative of increased interactions between peptides in the WG fiber, which was facilitated by more Q. Gd fibers showed a composite behavior between the two. Fibrils formed that twisted into semielliptical fibers because the adder peptide, Gd46, did not possess much dangling chain ends. Some random coils existed because globules were observed on the surface of the Gd fibers (Figure 4) but none on the WG fibers (Figure 9). However, the lack of Q meant that the twisting was not as tight as WG fibers, resulting in a more shallow pitch (Figure 4) and reduced modulus.

The morphologies observed appeared to be much larger versions of twisted β-sheet tapes (WG) and infinite stacks (Gd:Am and Gd:My) reported for much shorter peptide sequences.[65,67,68,72] Right-handed and left-handed twists were observed in the same systems. For instance, Figure 7 shows a left-handed twist for WG fibers but Figure 9 a right-handed twist. The Gd:My ribbon in Figure 9 twists right, but we observed others twisting left. The L-chirality of natural amino acids predicted left-handed helicity of fibers formed from twisting cross-β fibrils together.[67] A survey of the literature showed many instances of several fibrils twisting together to form larger structures of 10^1-10^2 nm diameter with left-handed helicity. However, there were some exceptions. A peptide of $(VK)_4$-VPPT-$(KV)_4$ showed a laminated or "infinite stack" morphology because the bulky diproline in the middle prevented it from twisting.[67,68] The same laminated morphology was observed in β-lactoglobulin fibrils at high ionic strength to screen electrostatic interactions and reduce twist.[72] A diphenylalanine (F) peptide produced smooth fibers with no helicity.[23] The peptide SAA_{1-12} displayed right-handed helicity and contained a diphenylalanine and two other phenylalanines in its 12 amino acid structure.[79] GtL75, for example, had P and F next to and in-between Q-blocks. The bulky amino acids could have alternated twisting in longer chain peptides once the chain was far enough away from the bulky interruption to begin twisting again. In other words, P, F, or some combination of them in the peptide sequence may have acted as a twisting "roadblock": the fibril twisted one way until it reached a roadblock and then straightened out and, if it was long enough, began twisting in the other direction somewhere down the fibril, away from the roadblock.

CONCLUSION

Peptide mixtures showed the ability to self-assemble beyond the nanometer scale into large, micrometer-sized fibers with a cross-β secondary structure. The continued assembly from the nanometer to the micrometer scale was driven by hydrophobic packing of aliphatic amino acid side groups on elementary units. By adding peptides of varying length and α-helix content to hydrolyzed gliadin, fibers and ribbons of varying size and morphology were produced. The amount of the peptide participating in the cross-β structure was dependent on the hydrophobicity of the initial α-helical content of the peptide. The adder peptide molecular weight controlled the fiber size. If α-helix content was low and molecular weight high, then there was a significant portion of unassembled peptide that did not allow for twisting into round fibers, instead producing ribbons. Finally, fiber modulus could be controlled through increased cross-β content, hydrophobic packing, and hydrogen bonding interactions between amino acid side groups, which were evidenced by the Q-blocks in WG. Therefore, on the basis of the presented results, it is possible to design large robust fibers of differing morphology and modulus based on the characteristics of the template and adder peptides. The proposed mechanism may be one utilized by nature to self-assemble cross-β fibrils and fibers. Aβ42, HTT, and CB-4 peptides implicated in Alzheimer's disease, Huntington's disease, and barnacle cement, respectively, all have "templating" properties.[21,80−84] Similarly, ApoE4, HAP1, and CB-2 peptides

dx.doi.org/10.1021/bm201005k|Biomacromolecules 2011, 12, 3770−3779

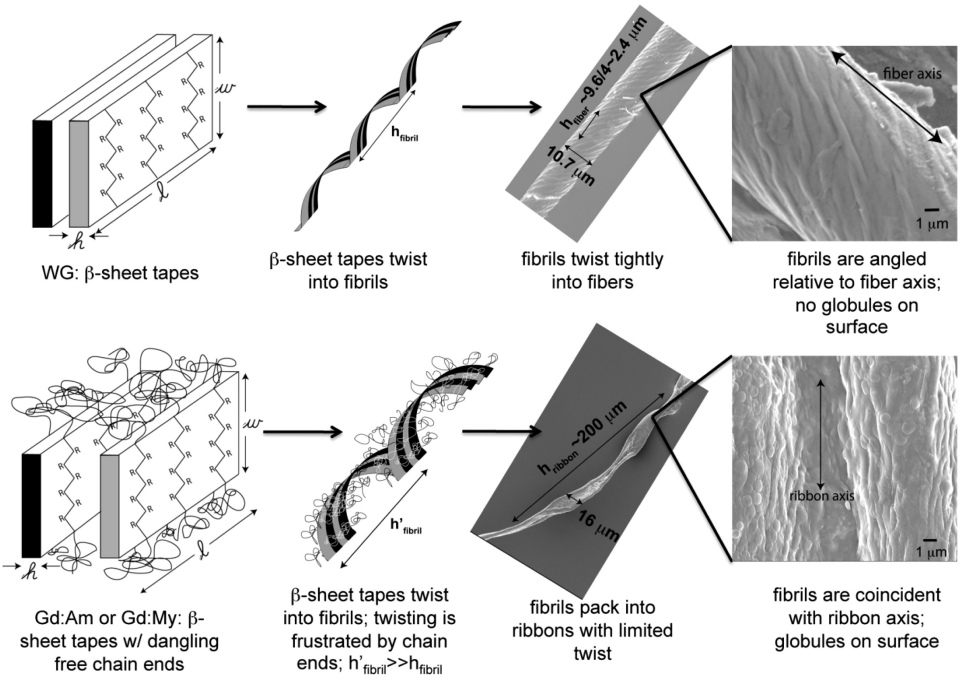

Figure 9. Schematic depicting the effect of dangling free chain ends that do not participate in cross-β aggregation on the final length, diameter, and morphology of amyloid fibers and ribbons.

implicated in Alzheimer's disease, Huntington's disease, and barnacle cement, respectively, all have "adder" properties. These peptides are found naturally together and may act similarly to the templated self-assembly process described here.

AUTHOR INFORMATION

Corresponding Author

*E-mail: jbarone@vt.edu. Phone: (540) 231-0680.

ACKNOWLEDGMENTS

Generous funding through NSF-CMMI-0856262 and the USDA funded Virginia Tech Biodesign and Bioprocessing Research Center is gratefully acknowledged.

REFERENCES

(1) Omenetto, F. G.; Kaplan, D. L. *Science* **2010**, *329* (5991), 528–531.
(2) Keten, S.; Buehler, M. J. *J. R. Soc., Interface* **2010**, *7* (53), 1709–1721.
(3) Nova, A.; Keten, S.; Pugno, N. M.; Redaelli, A.; Buehler, M. J. *Nano Lett.* **2010**, *10* (7), 2626–2634.
(4) Vincent, J. *Structural Biomaterials*; Princeton University Press: Princeton, NJ, 1990.
(5) Fraser, R. D. B.; MacRae, T. P. *Conformation in Fibrous Proteins and Related Synthetic Polypeptides*; Academic Press: New York, 1973.
(6) Fraser, R. D. B.; MacRae, T. P. Molecular Structure and Mechanical Properties of Keratins. In *Symposia of the Society for Experimental Biology, No. XXXIV, The Mechanical Properties of Biological Materials*; Vincent, J. F. V., Currey, J. D., Eds.; Cambridge University Press: New York, 1980; pp 211–246.
(7) Chiti, F.; Dobson, C. M. *Annu. Rev. Biochem.* **2006**, *75*, 333–366.
(8) Knowles, T. P. J.; Buehler, M. J. *Nature Nanotechnol.* **2011**, *6* (8), 469–479.
(9) Fowler, D. M.; Koulov, A. V.; Balch, W. E.; Kelly, J. W. *Trends Biochem. Sci.* **2007**, *32* (5), 217–224.
(10) Gebbink, M. F. B. G.; Claessen, D.; Bouma, B.; Dijkhuizen, L.; Wosten, H. A. B. *Nat. Rev. Microbiol.* **2005**, *3*, 333–341.
(11) Barlow, D. E.; Dickinson, G. H.; Orihuela, B.; Kulp, J. L. III; Rittschof, D.; Wahl, K. J. *Langmuir* **2010**, *26* (9), 6549–6556.
(12) Parker, K. D.; Rudall, K. M. *Nature* **1957**, *179*, 905–906.
(13) Geddes, A. J.; Parker, K. D.; Atkins, E. D.; Beighton, E. *J. Mol. Biol.* **1968**, *32*, 343–358.
(14) Wang, X.; Hammer, N. D.; Chapman, M. R. *J. Biol. Chem.* **2008**, *283* (31), 21530–21539.
(15) Lucas, F.; Shaw, J. T. B.; Smith, S. G. *Nature* **1957**, *179*, 906–907.
(16) Rudall, K. M. Silk and other cocoon proteins. In *Comparative Biochemistry: A Comprehensive Treatise. Constituents of Life Part B*; Florkin, M., Mason, H. S., Eds.; Academic Press: New York, 1962; Vol. *IV*.
(17) Naldrett, M. J.; Kaplan, D. J. *Marine Biol.* **1997**, *127*, 629–635.
(18) Kamino, K.; Inoue, K.; Maruyama, T.; Takamatsu, N.; Harayama, S.; Shizuri, Y. *J. Biol. Chem.* **2000**, *275* (35), 27360–27365.
(19) Nakano, M.; Shen, J.-R.; Kamino, K. *Biomacromolecules* **2007**, *8*, 1830–1835.
(20) Sullan, R. M. A.; Gunari, N.; Tanur, A. E.; Chan, Y.; Dickinson, G. H.; Orihuela, B.; Rittschof, D.; Walker, G. C. *Biofouling* **2009**, *25* (3), 263–275.
(21) Sanan, D. A.; Weisgraber, K. H.; Russell, S. J.; Mahley, R. W.; Huang, D.; Saunders, A.; Schmechel, D.; Wisniewski, T.; Frangione, B.; Roses, A. D.; Strittmatter, W. J. *J. Clin. Invest.* **1994**, *94*, 860–869.
(22) Smith, J. F.; Knowles, T. P. J.; Dobson, C. M.; MacPhee, C. E.; Welland, M. E. *Proc. Natl. Acad. Sci. U. S. A.* **2006**, *103* (43), 15806–15811.
(23) Kol, N.; Adler-Abramovich, L.; Barlam, D.; Shnek, R. Z.; Gazit, E.; Rousso, I. *Nano Lett.* **2005**, *5*, 1343–1346.
(24) Knowles, T. P.; Fitzpatrick, A. W.; Meehan, S.; Mott, H. R.; Vendruscolo, M.; Dobson, C. M.; Welland, M. E. *Science* **2007**, *318*, 1900–1903.
(25) Adamcik, J.; Berquand, A.; Mezzenga, R. *Appl. Phys. Lett.* **2011**, *98*, 193701.
(26) Sweers, K.; van der Werf, K.; Bennink, M.; Subramaniam, V. *Nano Res. Lett.* **2011**, *6* (1), 1–10.
(27) Paparcone, R.; Keten, S.; Buehler, M. J. *J. Biomech.* **2010**, *43*, 1196–1201.
(28) Filshie, B.K.; Fraser, R. D. B.; MacRae, T. P.; Rogers, G. E. *Biochem. J.* **1964**, *92*, 19.

(29) Jin, H.-J.; Kaplan, D. L. *Nature* **2003**, *424*, 1057−1061.
(30) Cherny, I.; Gazit, E. *Angew. Chem., Int. Ed.* **2008**, *47* (22), 4062−4069.
(31) Gazit, E. *Chem. Soc. Rev.* **2007**, *32*, 1263−1269.
(32) Adler-Abramovich, L.; Perry, R.; Sagi, A.; Gazit, E.; Shabat, D. *ChemBioChem* **2007**, *8*, 859−862.
(33) Reches, M.; Gazit, E. *Science* **2003**, *300*, 625−627.
(34) Scheibel, T.; Parthasarathy, R.; Sawicki, G.; Lin, X.-M.; Jaeger, H.; Lindquist, S. L. *Proc. Natl. Acad. Sci. U. S. A.* **2003**, *100*, 4527−4532.
(35) Knowles, T. P. J.; Oppenheim, T. W.; Buell, A. K.; Chirgadze, D. Y.; Welland, M. E. *Nature Nanotechnol.* **2010**, *5* (3), 204−207.
(36) Athamneh, A.; Barone, J. R. *Smart Mater. Struct.* **2009**, *18*, 104024.
(37) MacPhee, C. E.; Dobson, C. M. *J. Am. Chem. Soc.* **2000**, *122*, 12707−12713.
(38) Oliver, W. C.; Pharr, G. M. *J. Mater. Res.* **1992**, *7* (6), 1564−1583.
(39) del Mercato, L. L.; Maruccio, G.; Pompa, P. P.; Bochiccio, B.; Tamburro, A. M.; Cingolani, R.; Rinaldi, R. *Biomacromolecules* **2008**, *9* (3), 796−803.
(40) Guo, S.; Akhremitchev, B. B. *Biomacromolecules* **2006**, *7* (5), 1630−1636.
(41) Zurdo, J.; Guijarro, J. I.; Dobson, C. M. *J. Am. Chem. Soc.* **2001**, *123*, 8141−8142.
(42) Kreplak, L.; Doucet, J.; Dumas, P.; Briki, F. *Biophys. J.* **2004**, *87* (1), 640−647.
(43) Sunde, M.; Blake, C. C. F. *Q. Rev. Biophys.* **1998**, *31* (1), 1−39.
(44) Krebs, M. R. H.; Bromley, E. H. C.; Donald, A. M. *J. Struct. Biol.* **2005**, *149* (1), 30−37.
(45) Bernardin, J. E.; Kasarda, D. D. *Cereal Chem.* **1973**, *50*, 529−536.
(46) Bernardin, J. E.; Kasarda, D. D. *Cereal Chem.* **1973**, *50*, 735−744.
(47) Kasarda, D. D.; Bernardin, J. E.; Thomas, R. S. *Science* **1967**, *155* (3759), 203−205.
(48) Fandrich, M.; Dobson, C. M. *EMBO J.* **2002**, *21*, 5682−5690.
(49) Dobson, C.M. *Trends Biochem. Sci.* **1999**, *24* (9), 329−332.
(50) Uversky, V.N.; Fink, A. L. *Biochim. Biophys. Acta* **2004**, *1698* (2), 131−153.
(51) Maurer-Stroh, S.; Debulpaep, M.; Kuemmerer, N.; de la Paz, M. L.; Martins, I. C.; Reumers, J.; Morris, K. L.; Copland, A.; Serpell, L.; Serrano, L.; Schymkowitz, J. W. H.; Rousseau, F. *Nature Methods* **2010**, *7* (3), 237−242.
(52) Dzwolak, W.; Marszalek, P. E. *Chem. Commun.* **2005**, 5557−5559.
(53) Sethuraman, A.; Belfort, G. *Biophys. J.* **2005**, *88*, 1322−1333.
(54) Sethuraman, A.; Vedantham, G.; Imoto, T.; Przybycien, T.; Belfort, G. *Proteins: Struct., Funct., Bioinform.* **2004**, *56*, 669−678.
(55) Fandrich, M.; Forge, V.; Buder, K.; Kittler, M.; Dobson, C. M.; Diekmann, S. *Proc. Natl. Acad. Sci. U. S. A.* **2003**, *100* (26), 15463−15468.
(56) Vilasi, S.; Dosi, R.; Iannuzzi, C.; Malmo, C.; Parente, A.; Irace, G.; Sirangelo, I. *FEBS Lett.* **2006**, *580* (6), 1681−1684.
(57) Kirkitadze, M. D.; Condron, M. M.; Teplow, D. B. *J. Mol. Biol.* **2001**, *312* (5), 1103−1119.
(58) Giacomelli, C. E.; Norde, W. *Biomacromolecules* **2003**, *4* (6), 1719−1726.
(59) Valerio, M.; Porcelli, F.; Zbilut, J. P.; Giuliani, A.; Manetti, C.; Conti, F. *ChemMedChem* **2008**, *3* (5), 833−843.
(60) Giacomelli, C. E.; Norde, W. *Macromol. Biosci.* **2005**, *5* (5), 401−407.
(61) Qin, Z.; Buehler, M. J. *Phys. Rev. Lett.* **2010**, *104*, 198304.
(62) Gunzler, H.; Gremlich, H.-U. *IR Spectroscopy*; Wiley-VCH: Weinheim, 2002.
(63) Hammes, G.G.; Schullery, S. E. *Biochemistry* **1968**, *7* (11), 3882−3887.
(64) Lowik, D. W.P. M.; Garcia-Hartjes, J.; Meijer, J. T.; van Hest, J. C. M. *Langmuir* **2004**, *21* (2), 524−526.
(65) Nyrkova, I. A.; Semenov, A. N.; Aggeli, A.; Bell, M.; Boden, N.; McLeish, T. C. B. *Eur. Phys. J. B* **2000**, *17*, 499−513.
(66) Nyrkova, I. A.; Semenov, A. N.; Aggeli, A.; Boden, N. *Eur. Phys. J. B* **2000**, *17*, 481−497.
(67) Aggeli, A.; Nyrkova, I. A.; Bell, M.; Harding, R.; Carrick, L.; McLeish, T. C. B.; Semenov, A. N.; Boden, N. *Proc. Natl. Acad. Sci. U. S. A.* **2001**, *98* (21), 11857−11862.
(68) Lamm, M. S.; Rajagopal, K.; Schneider, J. P.; Pochan, D. J. *J. Am. Chem. Soc.* **2005**, *127* (47), 16692−16700.
(69) Nagarkar, R. P.; Hule, R. A.; Pochan, D. J.; Schneider, J. P. *J. Am. Chem. Soc.* **2008**, *130* (13), 4466−4474.
(70) Adamcik, J.; Jung, J.-M.; Flakowski, J.; De Los Rios, P.; Dietler, G.; Mezzenga, R. *Nature Nanotechnol.* **2010**, *5* (6), 423−428.
(71) Bolisetty, S.; Adamcik, J.; Mezzenga, R. *Soft Matter* **2011**, *7*, 493−499.
(72) Adamcik, J.; Mezzenga, R. *Soft Matter* **2011**, *7* (11), 5437−5443.
(73) Wenger, M.P. E.; Bozec, L.; Horton, M. A.; Mesquida, P. *Biophys. J.* **2007**, *93* (4), 1255−1263.
(74) Perutz, M. F.; Johnson, T.; Suzuki, M.; Finch, J. T. *Proc. Natl Acad. Sci. U. S. A.* **1994**, *91*, 5355−5358.
(75) DePace, A. H.; Santoso, A.; Hillner, P.; Weissman, J. S. *Cell* **1998**, *93*, 1241−1252.
(76) Scherzinger, E.; Sittler, A.; Schweiger, K.; Heiser, V.; Lurz, R.; Hasenbank, R.; Bates, G. P.; Lehrach, H.; Wanker, E. E. *Proc. Natl. Acad. Sci. U. S. A.* **1999**, *96* (8), 4604−4609.
(77) Chen, S.; Berthelier, V.; Bradley Hamilton, J.; O'Nuallain, B.; Wetzel, R. *Biochemistry* **2002**, *41*, 7391−7399.
(78) Sikorski, P.; Atkins, E. *Biomacromolecules* **2005**, *6* (1), 425−432.
(79) Rubin, N.; Perugia, E.; Goldschmidt, M.; Fridkin, M.; Addadi, L. *J. Am. Chem. Soc.* **2008**, *130* (14), 4602−4603.
(80) Baumann, M. H.; Kallijarvi, J.; Lankinen, H.; Soto, C.; Haltia, M. *Biochem. J.* **2000**, *349*, 77−84.
(81) Aleshkov, S.; Abraham, C. R.; Zannis, V. I. *Biochemistry* **1997**, *36* (34), 10571−10580.
(82) Cerf, E.; Gustot, A.; Goormaghtigh, E.; Ruysschaert, J.-M.; Raussens, V. *FASEB J.* **2011**, *25* (5), 1585−1595.
(83) Sivanandam, V. N.; Jayaraman, M.; Hoop, C. L.; Kodali, R.; Wetzel, R.; van derWel, P. C. A. *J. Am. Chem. Soc.* **2011**, *133* (12), 4558−4566.
(84) Kamino, K.; Odo, S.; Maruyama, T. *Biol. Bull.* **1996**, *190* (3), 403−409.

Chapter 3.

The Effect of Processing on Large, Self-Assembled Amyloid Fibers

Ridgley, D. M., E. C. Claunch, and J. R. Barone. 2012. The effect of processing on large, self-assembled amyloid fibers. *Soft Matter* 8(40):10298-10306. - Reproduced with the generous permission of the Royal Society of Chemistry.

View Article Online / Journal Homepage / Table of Contents for this issue
Dynamic Article Links

Soft Matter

Cite this: *Soft Matter*, 2012, **8**, 10298

www.rsc.org/softmatter

PAPER

The effect of processing on large, self-assembled amyloid fibers

Devin M. Ridgley, Elizabeth C. Claunch and Justin R. Barone*

Received 27th June 2012, Accepted 8th August 2012
DOI: 10.1039/c2sm26496j

Published on 23 August 2012. Downloaded by Virginia Tech on 04/03/2014 16:48:51.

It has been shown that micrometer-sized amyloid fibers can spontaneously self-assemble from peptide mixtures. Varying the molar ratio and type of peptides in the mixture affected fiber morphology and properties. Here, the same peptide mixtures at constant molar ratio are studied at different processing conditions to note influences on fiber formation. This study illustrates that changes in solution pH, temperature, and ionic strength can also influence the extent of fiber formation. In addition, processing variables greatly affect the size, morphology, and modulus of large amyloid fibers. Fibers segregate into two classes: flat ribbons or tapes of low modulus and cylindrical fibers of high modulus. Cylindrical cross-sections appear to result from twisted tapes and processing conditions can affect the transition from flat to cylindrical. Solution conditions could prevent or enhance the twisting transition, depending on the amino acid composition of the peptides in the mixture. The most robust fiber properties result from cylindrical fibers with diameters of 10–20 μm. The transition from flat to cylindrical appears to be highly influenced by the glutamine (Q) or lysine (K) content of the peptides. Thus it is possible to design useful, macroscopic fibers with predictable shape and properties.

Introduction

Over the past several decades there has been growing interest in the production of naturally occurring materials by replicating biological processes honed over millions of years of evolution. Silk, keratin, and collagen are just a few examples of naturally occurring materials that are composed of proteins assembled from the molecular level to form large, robust fibers.[1,2] These structures are particularly interesting because they assemble into fibers with different material properties unique to the given function.[3] For instance, silk spun from insects can vary in rigidity and toughness.[4] Dragline silk is rigid to provide structural support while capture silk is tough with high extensibility to catch prey.[5] The properties of spider silk are governed by the secondary structure of the proteins constituting the silk. Dragline silk is primarily composed of organized β-sheets that give the fiber more rigidity and strength to support the weight of the spider. Capture silk contains more amorphous regions that allow the fiber to absorb more energy without breaking.[6,7] Silk fibers are produced from an extensional strain applied when the insect excretes a small amount of silk onto a surface and then descends. Silk solution is extruded at high deformation through the silk gland while water is simultaneously evaporated, forming the silk fiber with β-sheets aligned along the fiber axis.[4] The extensional deformation overcomes the free energy barrier required for fiber formation and is a determining factor in the final structure of the fiber and therefore its properties. It is a "pushing" or "pulling" mechanism that is responsible for the formation of a host of natural fibers where β-sheets are aligned along the fiber axis.[8] There has been an extensive effort to replicate the processing that spiders have perfected and manipulate the structural properties of artificial spider silk. One such method is to produce spider dragline silk in *E. coli*.[9–11] The extracted artificial silk is then solubilized and electrospun under high deformation to form the silk fiber and align the β-sheets along the fiber.[12] Using this method, artificial spider dragline silk can vary in size and strength depending on the protein mixture composition and the force applied to "draw" the fibroin.[12]

Alternatively, there is another class of biological fibrous structures known as amyloids. Amyloids spontaneously self-assemble without the application of a mechanical strain and contain a cross-β secondary structure, which has the β-sheets oriented perpendicular to the fibril axis.[13–16] While a large body of work focuses on cross-β structures in pathogenic "prion" diseases,[13,15–17] there are instances of "functional" amyloids that occur in nature as a mechanism for survival and preservation.[15,18,19] For instance, barnacle cement has been shown to be one of the most robust adhesives in nature and uses alternating hydrophobic and hydrophilic amino acid regions to form an insoluble cross-β fibril, which contributes to the strength of the adhesive.[20–22] The bacterium *Streptomyces coelicolor* and fungus *Neurospora crassa* use amyloids to form protective coatings and hyphae.[19,23] *Chrysopidae* form cross-β silks to protect their eggs.[24,25] Amyloid fibrils have been shown to have moduli comparable to spider silk and can be formed without electrospinning.[12] Amyloid fibrils have also shown great solvent and temperature resistance and the fact that no known cure exists for

Biological Systems Engineering Department, Virginia Tech, 303 Seitz Hall, Blacksburg, VA 24061, USA. E-mail: jbarone@vt.edu

This journal is © The Royal Society of Chemistry 2012

View Article Online

Published on 23 August 2012. Downloaded by Virginia Tech on 04/03/2014 16:48:51.

prion disease is a testament to the robustness of the cross-β structure.[26] The outstanding physical properties and observed functional role of amyloids in nature serve as an inspiration to use the self-assembled structures in advanced materials.[27]

The majority of studies have focused on proteins and peptides such as insulin, myoglobin, β_2-microglobulin, and Aβ(1–40 and 42) that are able to form nanometer-sized cross-β fibrils under specific conditions.[15,18,27–36] Virtually any peptide or protein can form a cross-β structure as long as the experimental conditions exist to straighten it out so that it can strongly hydrogen bond to another straight peptide and form the highly organized cross-β structure.[26] These conditions are usually far from physiological and the self-assembly does not exceed the nanometer scale. The diversity of the peptides and proteins that are known and/or implicated in a host of natural amyloid forming systems suggests that amyloidosis is a result of general peptide properties.[37] In other words, there is likely a universal mechanism for the formation of both prions and functional amyloids that explains how fibrils and fibers form at physiological conditions.

Previous research has shown that it is possible to form micrometer-sized amyloid fibers *in vitro* with peptide mixtures derived from (1) tryptic hydrolysates of wheat gluten (WG) and (2) trypsin-hydrolyzed gliadin (Gd) with unhydrolyzed myoglobin (My) or amylase (Am) at near physiological conditions.[38,39] The described mechanism is consistent with a model that implicates a nucleation site or chaperone molecule in the initiation of fibril formation.[40–43] First, a "template" peptide is too hydrophobic to remain in solution and aggregates to form a stable cross-β structure. Hydrophobic amino acids exist next to each other so there are still some hydrophobic groups exposed to the solvent. A second, soluble, α-helical "adder" peptide has its hydrophobic groups on α-helices. The adder peptide by itself is stable in aqueous solution and does not show conformation change as measured with FT-IR spectroscopy.[38] Upon interaction with a template, the hydrophobic groups on the adder prefer the more stable template and unravel, undergoing an α to β conformational change and adding into the aggregate.[38] It has been shown that α to β transitions readily occur on hydrophobic surfaces.[44,45] Fourier transform-infrared (FT-IR) spectroscopy shows that the loss of α-helix releases a large fraction of aliphatic amino acids (A, I, L, and V) that allow for hydrophobic interactions of peptide side groups.[38] The hydrophobic interactions facilitate cross-β formation.[46,47] Wheat gluten is a combination of gliadin and glutenin proteins and the tryptic hydrolysate results in cylindrical fibers of high modulus at pH 8 and 37 °C. Gliadin hydrolysis produces peptides with "template" properties. Glutenin peptides have "adder" properties. Replacing the glutenin fraction with myoglobin or amylase results in rectangular tapes of low modulus at the same conditions. So the morphology and Young's modulus of the fibers are dependent on the molecular weight and amino acid composition of the adder peptide and the ratio of template to adder peptide.[38]

A recent study by Adamcik *et al.* has shown that the size and morphology of already self-assembled, nanometer-sized amyloid fibrils can be manipulated by altering the ionic strength of the solution.[46,47] Additional evidence suggests that there is a fine balance between electrostatic and hydrophobic interactions required for fibril stabilization.[33] Previous studies have shown that nanometer-sized cross-β fibrils can be formed at high and low pH, high ionic strength, and/or high temperature from peptides and proteins that would not aggregate at physiological conditions.[1,26,29,30,33,46,48] Thus, changes in solution conditions can play an integral role in the self-assembly and morphological features of amyloid fibrils. This study builds on previous research by investigating the effects of solution pH, ionic strength, and temperature on inter-peptide interactions at the molecular level and how they influence the formation of micrometer-sized cross-β structures in two systems where the adder peptide or protein is varied. The results show that it is possible to manipulate the size, morphology, and rigidity of spontaneously self-assembled amyloid fibers formed from inexpensive peptide mixtures.

Experimental

Wheat Gluten (WG) hydrolysis and self-assembly

2 g of WG (MP Biomedicals, LLC, Solon, OH) was dissolved in 80 ml of de-ionized water at 37 °C to achieve a concentration of 25 mg ml^{-1}. 30 mg of trypsin (Type I from bovine pancreas, Sigma-Aldrich, St. Louis, MO) was then added to the solution to give an enzyme-to-substrate ratio of 1 : 67 w/w and the pH was adjusted to 8 with 1 M NaOH. Solution conditions were maintained at pH 8 and 37 °C for one day to allow for hydrolysis. The solution was then divided into seven 20 ml samples: four maintained at 37 °C and pH's 4, 6, 8, and 10 with 1 M NaOH or 1 M HCl as needed and three maintained at pH 8 and temperatures 22, 60 and 80 °C for a period of 20 days. FT-IR spectra were captured daily for 20 days to monitor self-assembly. WG is a mixture of hydrolyzed gliadin (Gd, UniProt P04721, 0.49 mole fraction) and high and low molecular weight glutenin, GtH (UniProt P08488, 0.06 mole fraction) and GtL (UniProt P10386, 0.45 mole fraction) peptides. In this mixture, Gd20 is the template peptide with Gd46 and GtL75 acting as the adder peptides (see peptide properties in Table 3 of Ridgley *et al.*).[38,49]

Gliadin (Gd) hydrolysis

20 g of Gd (TCI America, Portland, OR) was dissolved in 800 ml of de-ionized water at 37 °C. Trypsin was then added at 1 : 67 w/w enzyme-to-substrate ratio and the solution incubated for 72 hours at pH 8 and 37 °C. The solution was then poured into Teflon-coated aluminum foil trays and allowed to dry at room temperature under a fume hood. The incubation time was determined to be long enough for hydrolysis but short enough to avoid peptide aggregation.

Gd:My mixtures

Myoglobin (My, from equine skeletal muscle, Sigma-Aldrich, St. Louis, MO, UniProt P68082) was dissolved in 10 ml de-ionized water at a molar ratio of 0.36 : 0.64 (Gd:My) with dried Gd. Seven solutions of 25 mg ml^{-1} were created, which was shown to be in a concentration region where there was strong cross-β formation over reasonable times[38,39] and greater than the 10 mg ml^{-1} used in another study on amyloid formation in peptide mixtures.[50] Four solutions were maintained at 37 °C and pH was adjusted to pH 4, 6, 8, and 10 with 1 M NaOH or 1 M HCl as needed and three maintained at pH 8 and temperatures 22, 60 and 80 °C for a period of 20 days. FT-IR spectra were collected daily for 20 days to monitor self-assembly. In this mixture, Gd20

View Article Online

Published on 23 August 2012. Downloaded by Virginia Tech on 04/03/2014 16:48:51.

was the template peptide and My the adder protein (see peptide properties in Table 3 of Ridgley *et al.*).[38]

Ionic strength

100 mM NaCl WG and Gd:My solutions were prepared in the same manner as above at pH 8, 25 mg ml^{-1}, and incubated at 37 °C for 20 days. 100 mM NaCl has been shown to alter the self-assembly[51] and morphology[46] of amyloid fibrils.

Final fiber formation

After 20 days, WG and Gd:My solutions were dried on Teflon-coated aluminum foil under the fume hood at ambient conditions.

Fourier transform infrared (FT-IR) spectroscopy

Attenuated total reflectance (ATR) FT-IR spectra of the incubating solutions were recorded periodically on a Thermo Nicolet 6700 FT-IR Spectrometer (Thermo Fisher Scientific Inc., Waltham, MA) with a 45° ZnSe crystal trough. The spectra were collected using 256 scans at 4 cm^{-1} resolution from 4000–525 cm^{-1}. The spectrum of the solvent without peptide was used as a background and then subtracted from the peptide solution spectrum to reveal the peptide absorbances. Deconvolution of the Amide I band into individual components was accomplished in the same manner as previously reported.[38]

Raman spectroscopy

Raman spectra were collected on the dried amyloid fibers mounted on aluminum foil. Spectra were taken with a 785 nm laser from a Senterra Raman dispersive spectrometer (Bruker, Billerica, MA) at a power of 100 mW through a 100× objective. Spectra were baseline corrected to account for slight background fluorescence with OPUS 6.5 software.

Scanning Electron Microscopy (SEM)

Fibers formed from dried solution were mounted onto aluminum SEM stubs with double-sided tape. Scanning electron micrographs were obtained using a LEO 1550 field-emission SEM (Zeiss, Peabody, MA) with a 4–6 mm working distance, 5 kV accelerating voltage, and an In-lens SE-detector.

Nanoindentation

Fibers were mounted on stainless steel stubs for nanoindentation. Nanoindentation experiments were performed at room temperature using a Hysitron Triboindenter (Minneapolis, MN) with a 90° conical diamond tip. Experiments were in displacement-controlled (DC) mode with a maximum displacement of 1000 nm at a rate of 100 nm s^{-1}. Fiber, E_f, or tape, E_t, elastic (Young's) modulus was determined as previously reported.[38,52]

Results and discussion

Fibers at constant temperature

Table 1 summarizes the fiber morphologies that result from various peptide mixtures at various processing conditions. When incubated at pH 8 and 37 °C, Gd:My solutions resulted in rectangular cross-section tapes of width, W, while WG solutions resulted in cylindrical cross-section fibers of diameter, D (Fig. 1).[38] The micrometer-sized tapes and fibers were hierarchical and appeared to result from the aggregation of smaller fibrils. The smaller fibrils formed an angle, γ, relative to the tape or fiber axis and were separated by a distance h_t or h_f for tapes or fibers, respectively, which defined the "pitch".[34,35,46,47,53–56] Larger scale twisting of the tapes and fibers was observed resulting in another level of pitch, h'. At pH 8 and 100 mM NaCl, WG formed flat, rectangular cross-section tapes instead of cylinders (Fig. 2). While purely cylindrical fibers were observed for WG at pH 4 and 8, a mixed morphology of cylinders and tapes was

Table 1 Gd:My and WG fiber morphologies at various solution conditions[a]

		pH				
T		4	6	8	10	100 mM NaCl
22 °C	WG			▬		
	Gd:My			●/▬		
37 °C	WG	●	●/▬	●	●/▬	▬
	Gd:My	●/▬	▬	●/▬	▬	▬
60 °C	WG			▬		
	Gd:My			●/▬		
80 °C	WG			▬		
	Gd:My			●/▬		

[a] Note: Gd:My at pH 8 is listed with a mixed morphology at each temperature to show that is was a tape that gradually twisted from high h' at 22 °C to low h' at 80 °C. The circles depict a cylindrical fiber, rectangles depict a tape, and both circles and rectangles illustrate that the system produces both morphologies.

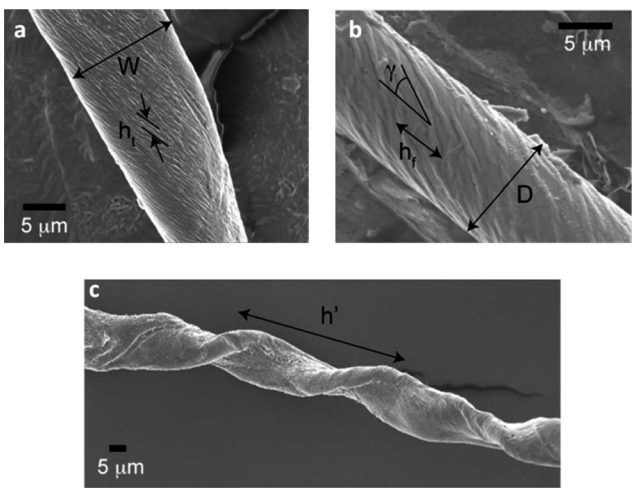

Fig. 1 SEM images depicting the measurements for tape width (W), tape pitch (h_t), fiber diameter (D), fiber pitch (h_f), fibril angle with respect to the fiber axis (γ) and the overall fiber pitch (h').

 This journal is © The Royal Society of Chemistry 2012

View Article Online

Published on 23 August 2012. Downloaded by Virginia Tech on 04/03/2014 16:48:51.

observed at pH 6 and 10. At pH 4, Gd:My fibers had both rectangular and cylindrical cross-sections. All other Gd:My tapes at 37 °C had a rectangular cross-section. Fiber production at pH 6 and 10 was less than pH 8 and greatly reduced at pH 4 for both systems.

Fibers at constant pH

WG produced tapes at pH 8 and 22, 60, and 80 °C. Gd:My produced tapes that had an increasing twist, or decreasing h', as temperature increased from 22 °C to 80 °C (Fig. 2b) while h_t was relatively constant. At 60 °C and 80 °C, Gd:My tapes began to tightly twist into cylinders (Fig. 3). Fiber production was very low at 60 and 80 °C in both peptide systems.

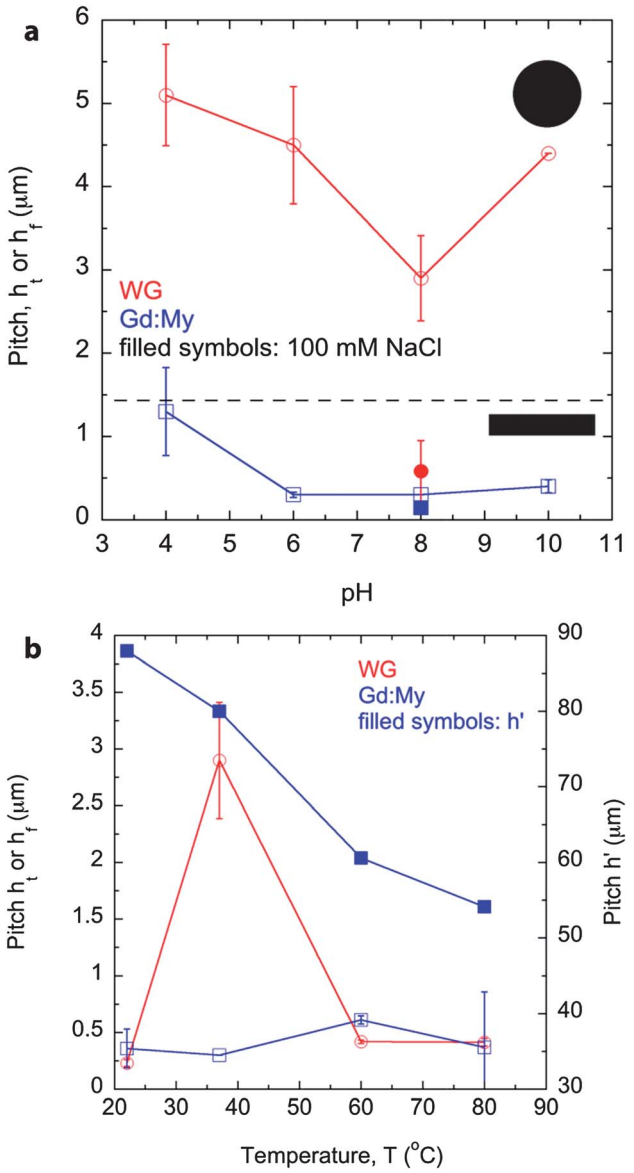

Fig. 2 WG and Gd:My pitch at (a) pH's 4, 6, 8, 10 and 100 mM NaCl at a constant 37 °C. Red is WG, blue is Gd:My, and filled symbols are mixtures incubated with 100 mM NaCl; (b) temperatures 22, 37, 60 and 80 °C at a constant pH 8. Red is WG, blue is Gd:My, and filled symbols are the large scale pitch, h', from Gd:My tapes twisting.

Fiber properties

Simple geometric considerations relate γ to h, $\gamma(^\circ) = 360x/h$.[34,35,46,47,53–56] Rectangular tapes displayed nearly constant fiber moduli, E_f, with fiber twist angle, γ. However, at $\gamma = 23^\circ$, cylindrical fibers formed and modulus increased dramatically (Fig. 4). Fiber production, morphology, and properties of large self-assembled amyloid fibers were influenced by processing conditions. Samples were monitored with FT-IR for 20 days. The Amide I was deconvoluted into its secondary structure components including the cross-β region assigned at 1611–1630 cm^{-1}.[38] The large fibers contained a core cross-β structure that developed with time. The data plotted in Fig. 5 represent the largest change in cross-β structure for each sample, with some samples exhibiting secondary structure change earlier than others. It was observed that a gain in cross-β was concurrent with a loss of α-helix.[38]

Also shown is a "hydrophobic packing" parameter defined as the change in the ratio of the symmetric CH_3 deformation at

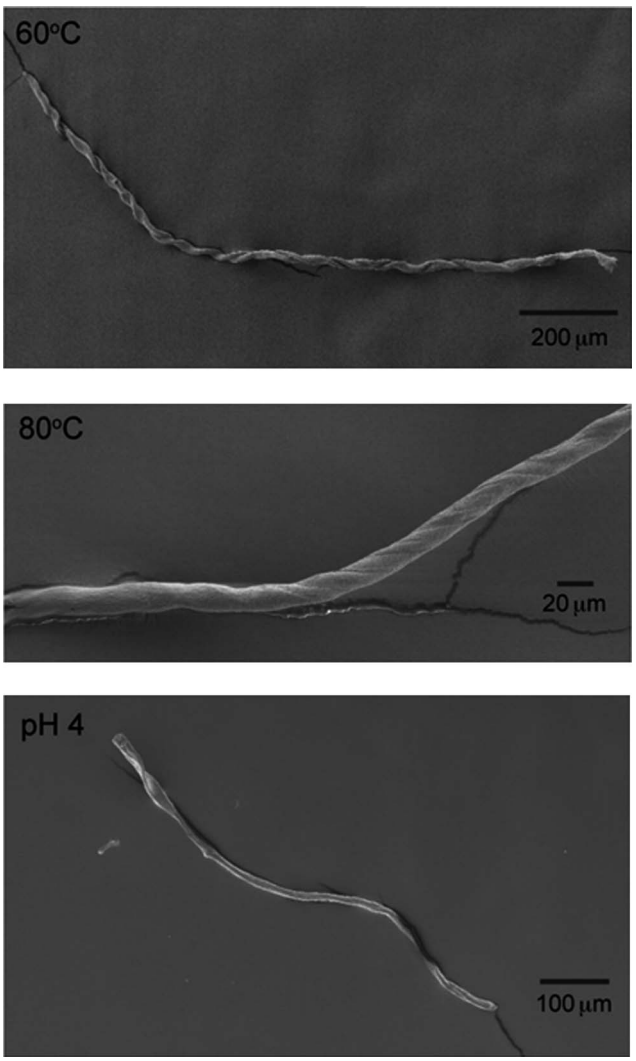

Fig. 3 SEM images of Gd:My tapes twisting into cylindrical fibers at pH 8 and 60 and 80 °C and pH 4 and 37 °C. Note at pH 4 how the fiber on the left hand side of the picture is rectangular and the fiber is twisted on the right hand side of the picture.

View Article Online

Published on 23 August 2012. Downloaded by Virginia Tech on 04/03/2014 16:48:51.

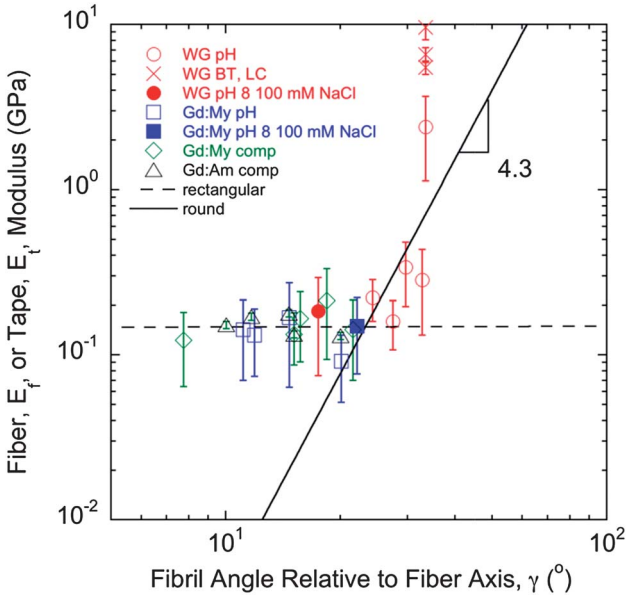

Fig. 4 WG and Gd:My tape and fiber modulus, E_t and E_f, can be differentiated by the fibril angle relative to the fiber axis, γ.

1365 cm^{-1}, δ_s, to the asymmetric CH_3 deformation at 1410 cm^{-1}, δ_{as}. In other words, this parameter shows the ability of CH_3 groups on plentiful alanine (A), isoleucine (I), leucine (L), and valine (V) amino acids (Fig. 6) to interdigitate with one another so that a positive value is indicative of "packing".[57] The change in cross-β was directly correlated with the change in δ_s/δ_{as} showing cross-β formation was driven by hydrophobic interactions between the side groups on A, I, L, and V. Some peptide mixtures showed a slightly negative $\Delta(\delta_s/\delta_{as})$. The original construction of the parameter was to quantify up and down movement of the CH_3 group (δ_s) compared to side-to-side movement of the CH_3 group (δ_{as}) so that positive $\Delta(\delta_s/\delta_{as})$ values showed close packing or interdigitation. The negative values observed may indicate that CH_3 amino acid side groups interacted weakly in those systems and there was no "packing" as defined here. This resulted in low values of cross-β and fiber formation.

Although it has been shown that pure mixtures of the peptides in previous research formed fibers and ribbons, the crude mixtures contained a host of peptides, *i.e.*, WG contained peptides hydrolyzed from Gd, GtL, and GtH while Gd:My contained peptides hydrolyzed from Gd.[38,49] Considering all the peptides in the mixture at each pH, WG and Gd:My were overwhelmingly positively charged at pH 4 and 6 and negatively charged at pH 10. However, at pH 8 WG was 84% positively and 16% negatively charged and Gd:My was 39% positively and 61% negatively charged. The largest secondary structure changes were found at pH 8 so charge attraction facilitated inter-peptide interactions. At high or low pH, secondary structure change decreased as did fiber production. Having a predominantly positive (low pH) or negative (high pH) charge on the mixtures caused peptides to repel each other in solution, which hindered interaction and therefore aggregation and secondary structure change. The peptides in the mixtures had high aliphatic indices (AI) indicative of the amount of A, I, L, and V (Fig. 6).[38] The fact that a small amount of fibers did form at pH values above and below the pI of the peptide mixtures suggested that the

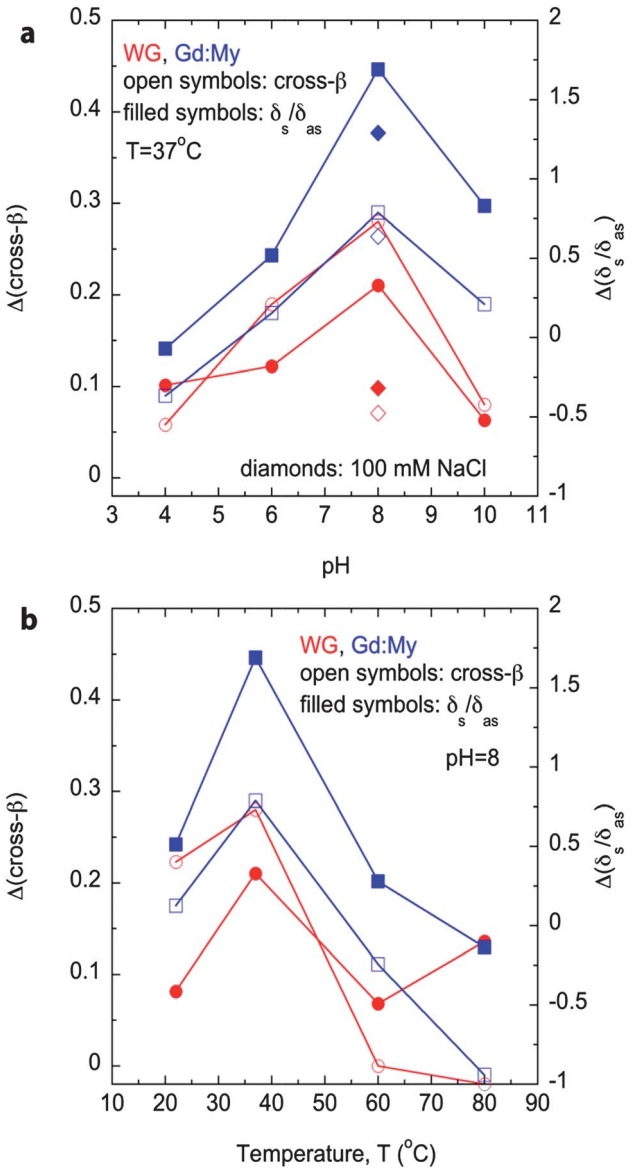

Fig. 5 WG and Gd:My values for the overall change in cross-β, Δ(cross-β), and CH_3 hydrophobic packing, $\Delta(\delta_s/\delta_{as})$, at (a) pH's 4, 6, 8, 10 and 100 mM NaCl at a constant 37 °C and (b) temperatures 22, 37, 60 and 80 °C at a constant pH 8. Red is WG, blue is Gd:My, open symbols are Δ(cross-β), and filled symbols $\Delta(\delta_s/\delta_{as})$.

abundance of hydrophobic groups could overcome charge repulsion to aggregate peptides.

To further explore the effect of peptide charge and hydrophobic interactions on peptide aggregation within the mixtures, both WG and Gd:My at pH 8 and 37 °C were incubated in 100 mM NaCl. WG produced tapes instead of cylinders and Gd:My continued to produce tapes. Hydrophobic interactions and cross-β formation were greatly decreased in the WG mixture but were only slightly decreased in the Gd:My mixture (Fig. 5). The peptides were not salted out at 100 mM NaCl because hydrophobic interactions decreased and the ionic strength of the solution was several orders of magnitude greater than the molar concentration of positive and negative charges on the peptides in solution thus all peptide charge was screened. Ionic strength did

 This journal is © The Royal Society of Chemistry 2012

View Article Online

Published on 23 August 2012. Downloaded by Virginia Tech on 04/03/2014 16:48:51.

Gd20

TFLILALLAI VATTATTAVR

Gd46

SQVLQQSTYQ LLQELCCQHL WQIPEQSQCQ AIHNVVHAII LHQQQK

GtL75

AIIYSIILQE QQQVQGSIQS QQQQPQQLGQ CVSQPQQQSQ QQLGQQPQQQ
QLAQGTFLQP HQIAQLEVMT SIALR

My

MGLSDGEWQQ VLNVWGKVEA DIAGHGQEVL IRLFTGHPET LEKFDKFKHL
KTEAEMKASE DLKKHGTVVL TALGGILKKK GHHEAELKPL AQSHATKHKI
PIKYLEFISD AIIHVLHSKH PGDFGADAQG AMTKALELFR NDIAAKYKEL
GFQG

Fig. 6 The amino acid sequences of the template peptide (Gd20) and the adder peptides Gd46, GtL75, and myoglobin (My) present in the WG and Gd:My solutions.

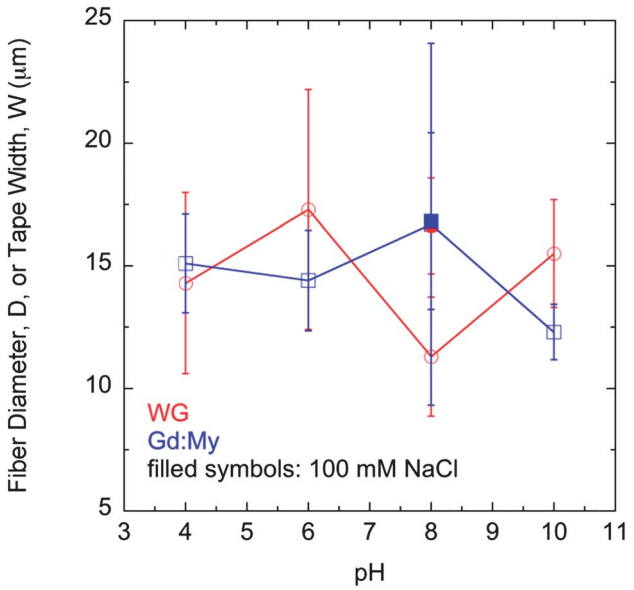

Fig. 7 Fiber diameter (D) or tape width (W) for WG and Gd:My systems at pH's 4, 6, 8, 10 and 100 mM NaCl at a constant 37 °C. Red is WG, blue is Gd:My, and filled symbols are mixtures incubated with 100 mM NaCl.

not affect the width of the tapes (Fig. 7) but did decrease total fiber formation. Na^+ and Cl^- ions screened charge on the peptides and did not allow for the facilitation of peptide aggregation that complementary charge provided at pH 8. However, aggregation still occurred through some hydrophobic interactions and allowed for modest secondary structure change. Other studies have shown how screening peptide charge can balance repulsive forces and change the state of aggregation at a given pH.[51,58,59]

At pH 4, 6, and 10, WG still formed cylindrical fibers but less of them compared to pH 8 with pH 6 and 10 forming tapes as well. Twisting into a cylinder would be consistent with the charge repulsion model offered by Adamcik and Mezzenga who showed that already formed amyloid fibrils twisted into cylinders when placed into low ionic strength solutions but remained flat tapes when placed in high ionic strength solutions.[46] Mixed morphologies of tapes and cylinders on the same fiber were observed at pH 6 and 10. At pH 8, there was still some positive charge that could have influenced twisting of the WG tapes into cylinders.[60] At 100 mM NaCl, the charge on WG peptides was fully neutralized and did not allow the tape to twist. Gd:My produced tapes at all pH and ionic strength even though it carried a net positive charge at low and high pH. At pH 4 there was a mixed morphology of tapes and cylinders, with cylinders resulting from charge repulsion.

Solution temperature produced the most interesting experimental results. Fiber formation and secondary structure change were maximized at 37 °C. Amyloid fibril formation has been shown to maximize at a critical temperature for other aggregating peptide systems so the results in Fig. 5 are consistent with previous studies.[61] Interestingly, WG showed the cylindrical cross-section only at 37 °C while Gd:My tapes could be induced to twist into cylinders at high temperature. Higher temperatures did not promote increased hydrophobic interactions as shown in Fig. 5. WG and Gd:My peptides formed fibrils and then tapes through hydrophobic interactions. However, twisting could not be fully explained by a charge repulsion model because of the lack of cylinders at conditions where there was a lot of like charge that would have resulted in repulsion and twisting. Gd:My cylindrical fibers and flat tapes could be segregated by plotting the ratio of the ν(CN) absorbance at 1016 cm^{-1} to the $\gamma_{r,w}(CH_2)$ absorbance at 1080 cm^{-1} (Fig. 8a). Thus, final fiber morphology could be predicted from FT-IR data gathered in solution during aggregation. Loss of the ν(CN) absorbance relative to the $\gamma_{r,w}(CH_2)$ absorbance (a lower ratio) resulted in cylinders. My contained a significant amount of lysine (K) with some glutamine (Q), which were amino acids with amines and amides, respectively, in the side group (Fig. 6) and would contribute to ν(CN).[62,63] So FT-IR analysis suggested that more K and Q added into the structure and hydrogen bonded to induce twisting resulting in a loss of ν(CN). The conditions where Gd:My twisted into cylinders would have been sufficiently denaturing to allow increased straightening of a My chain.[32,50,64] Curiously, overall aggregation was not increased, even at pH 8 and 60 °C and 80 °C, as evidenced by the lower overall secondary structure change (Fig. 5) with moderate final cross-β contents of 20% and 19%, respectively, which were lower than at milder conditions (Fig. 5). Clearly, temperature had some detrimental effect on overall aggregation, which was preferred at closer to physiological conditions.

The same analysis could not be used to predict WG fibers and tapes. Instead, plotting the ratio of $\gamma_{r,w}(NH_2)$ at 1103 cm^{-1} to $\gamma_{r,w}(CH_2)$ was able to differentiate some, but not all, of the WG cylinders from the tapes (Fig. 8b). Gd46 and GtL75 peptides contained significant amounts of glutamine repeat units or "Q-blocks". Q-blocks are known facilitators of cross-β formation and are implicated in prion diseases such as Huntington's disease.[65–69] Q-blocks facilitated the addition of WG peptides into the aggregated structure as shown with FT-IR spectroscopy.[70] Q-blocks have also been shown to positively influence twisting of cross-β ribbons into helicoids and cylinders.[34] The fact that ν(CN)/$\gamma_{r,w}(CH_2)$ could not differentiate morphology suggested that Q aggregation occurred in WG at each condition. Q contained an amide on the amino acid side group that would have contributed to $\gamma_{r,w}(NH_2)$. So the state of the Q amide side group can better differentiate the morphology, although not completely. Amides on Q in WG could rock back and forth but

View Article Online

Published on 23 August 2012. Downloaded by Virginia Tech on 04/03/2014 16:48:51.

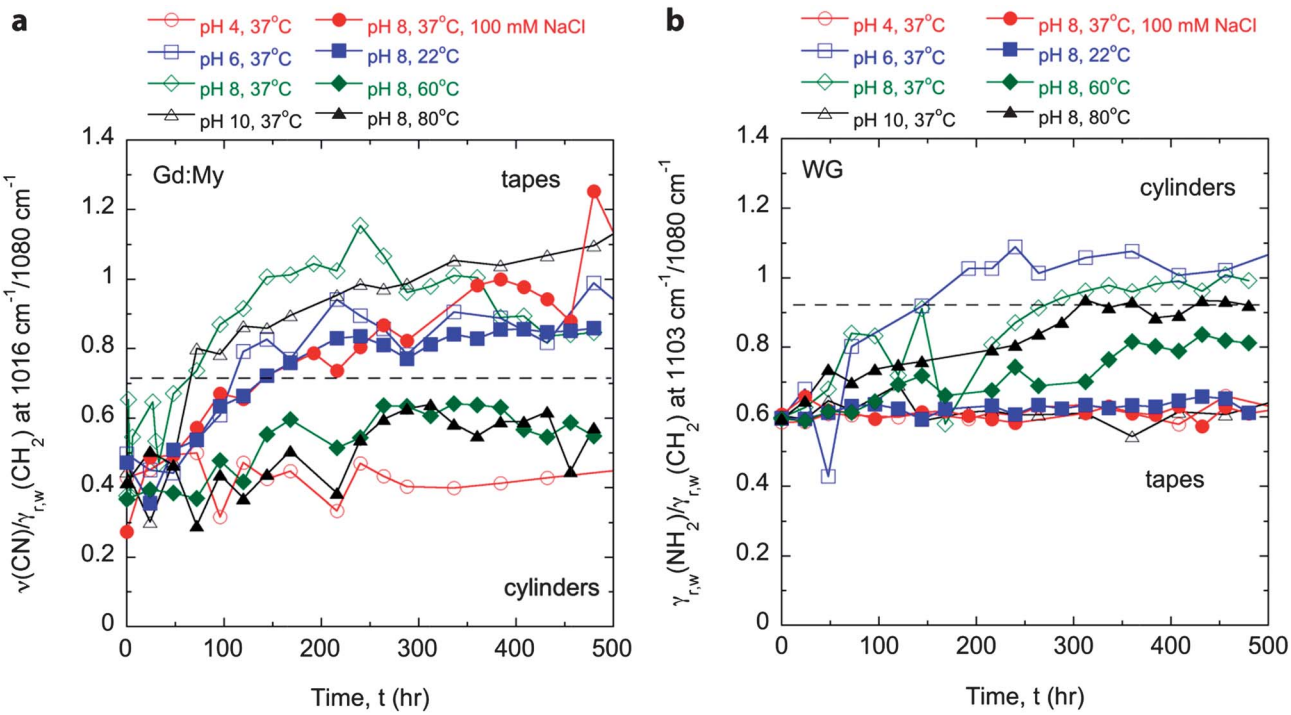

Fig. 8 Prediction of final fiber morphology from solution FT-IR observations. Gd:My cylinders showed $\nu(CN)/\gamma_{r,w}(CH_2)$ ratio less than 0.7 at long time. WG displayed a cylindrical morphology when $\gamma_{r,w}(NH_2)/\gamma_{r,w}(CH_2)$ ratio was greater than 0.9 at long time. Error bars are within the symbols.

not stretch, indicating that cylinders had vertically constrained Q side groups with some horizontal mobility. This may be because amide side groups on Q have a preferred hydrogen bonding direction in the aggregated structure.

Although peptide charge has been shown to influence twisting of self-assembled β-sheet ribbons, other sequence features can affect twisting as well.[34,71,72] Under certain conditions, Q and K in the adder protein or peptide could make more adder available to the template. This would facilitate hydrogen bonding and potentially hydrophobic interactions on the amino acid side groups and allow the structure to twist. At pH 8, the lysine was predominantly positively charged with a $pK_R = 10.5$ of the side group that may have influenced twisting. Analogous to the Q on WG peptides, which have no acid–base property, it seemed more likely that K simply facilitated hydrogen bonding interactions and induced twisting in the Gd:My system. In addition, the length of the adder peptide may play a role. My had twice the molecular weight of GtL75 and three times the molecular weight of Gd46. Thus, it required more interaction with the template to straighten and add. There were 7.32×10^{-6} moles of My in the mixture. Fig. 5 shows the gain in cross-β for Gd:My at pH 8 and 37 °C to be 29%, which was the fraction of My added into the self-assembled structure. Thus, $(1 - 0.29)(7.32 \times 10^{-6}) = 5.2 \times 10^{-6}$ moles of My did not add into the structure. Using a similar analysis for Gd46 and GtL75 results in 13 and 9.9 times more unassembled My protein compared to Gd46 and GtL75, respectively. At pH 4, the conditions were sufficiently denaturing to perhaps cause a My chain to straighten more than at other conditions, which was consistent with observed aggregation at low pH for peptides that did not aggregate at other conditions.[32,50,64] However, charge repulsion still hindered overall

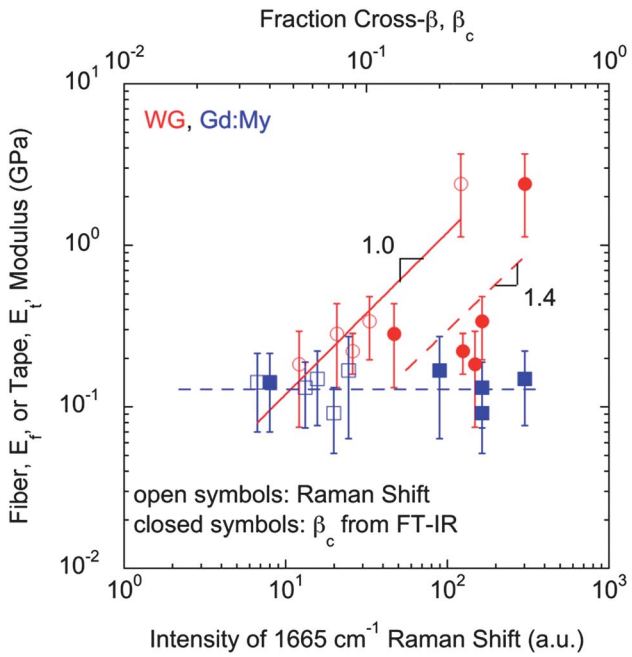

Fig. 9 Fiber and tape modulus depended similarly on the β-sheet fraction formed in solution (measured with FT-IR) and the β-sheet fraction in the final dried fiber or tape (measured with Raman spectroscopy).

aggregation, which was why Δ(cross-β) was lower than at other conditions. A model has been presented for how this unassembled chain length impedes twisting.[38] The cylindrical cross-section observed in this study did not result from extrusion through a spinneret or hair follicle, like silk and keratin fibers,

 This journal is © The Royal Society of Chemistry 2012

View Article Online

Published on 23 August 2012. Downloaded by Virginia Tech on 04/03/2014 16:48:51.

respectively. Twisting appeared to be more influenced by an abundance of Q or K in the adder peptide. Q and K contain amide and amine groups, respectively, that can further hydrogen bond. Morphologically, twisted cylindrical fibers showed a high twist angle, γ, and a higher modulus (Fig. 4). Molecularly, the more twisted fibers contained more β-sheet structure, which could be observed two ways as shown in Fig. 9. First, the cross-β fraction, β_c, found through deconvolution of the FT-IR Amide I absorbance in solution was greater in higher modulus fibers. The values in Fig. 9 represent the highest cross-β fraction corresponding to the largest Δ(cross-β) in Fig. 5. The dried fibers were also analyzed using Raman spectroscopy and the 1665 cm^{-1} Raman shift, indicative of β-sheet structures, is plotted in Fig. 9.[73] There was good agreement between the two techniques indicating that a lot of structure formation happened in solution and that final dried fiber properties could be predicted from the solution analysis. The difference in scaling between the two techniques is likely a result of drying. The tape modulus was independent of γ and β-structures indicating that a common interaction produced the rigidity, such as weaker hydrophobic interactions, and that higher modulus resulted from enhanced hydrogen bonding through Q or K that also resulted in the twisted morphology.

Conclusion

Hydrophobic interactions caused aggregation in template peptides at very short times. Exposed hydrophobic groups induced α to β transitions on adder peptides that added onto the template over longer times, which could be monitored with FT-IR spectroscopy. Fibrils formed that aggregated into flat tapes. The self-assembly over these scales appeared to be mostly driven by hydrophobic interactions that could be enhanced by complementary charge on peptides in the mixture. Flat tapes had nearly constant modulus of about $E_t \sim 0.15$ GPa. Peptide charge during self-assembly was altered by changing solution pH or ionic strength. Some tapes twisted into cylinders. Repulsive charge along the flat tapes had at most a secondary effect on twisting. FT-IR showed that side chains of glutamine and lysine, which have a large hydrogen bonding potential, primarily induced twisting. The increased hydrogen bonding resulted in highly twisted cylindrical fibers of high modulus. The fiber modulus directly correlated with the fiber twist, which resulted from increased β-sheet formation. Twisted fibers had moduli from $E_f \sim 0.2$ to 2.5 GPa. This study showed that it was possible to produce large, macroscopic fibrous structures with tailored morphology and properties by altering solution conditions.

Acknowledgements

Generous funding through NSF-CMMI-0856262 and the USDA funded Virginia Tech Biodesign and Bioprocessing Research Center is gratefully acknowledged.

References

1 P. Fratzl and R. Weinkamer, *Prog. Mater. Sci.*, 2007, **52**, 1263–1334.
2 M. A. Meyers, P.-Y. Chen, A. Y.-M. Lin and Y. Seki, *Prog. Mater. Sci.*, 2008, **53**, 1–206.
3 P. Fratzl, *Curr. Opin. Colloid Interface Sci.*, 2003, **8**, 32–39.
4 F. Vollrath, *Nature*, 2001, **410**, 541.
5 F. G. Omenetto and D. L. Kaplan, *Science*, 2010, **329**, 528–531.
6 A. Nova, S. Keten, N. M. Pugno, A. Redaelli and M. J. Buehler, *Nano Lett.*, 2010, **10**, 2626–2634.
7 S. Keten and M. J. Buehler, *J. R. Soc. Interface*, 2010, **7**, 1709–1721.
8 X. Chen, Z. Shao and F. Vollrath, *Soft Matter*, 2006, **2**, 448–451.
9 M. B. Hinman, J. A. Jones and R. V. Lewis, *Trends Biotechnol.*, 2000, **18**, 374–379.
10 S. R. Fahnestock and S. L. Irwin, *Appl. Microbiol. Biotechnol.*, 1997, **47**, 23–32.
11 J. P. O'Brien, S. R. Fahnestock, Y. Termonia and K. H. Gardner, *Adv. Mater.*, 1998, **10**, 1185–1195.
12 A. Seidel, O. Liivak, S. Calve, J. Adaska, G. Ji, Z. Yang, D. Grubb, D. B. Zax and L. W. Jelinski, *Macromolecules*, 2000, **33**, 775–780.
13 C. M. Dobson, *Trends Biochem. Sci.*, 1999, **24**, 329–332.
14 C. M. Dobson, A. Sali and M. Darplus, *Angew. Chem., Int. Ed.*, 1998, **37**, 868–893.
15 F. Chiti and C. M. Dobson, *Annu. Rev. Biochem.*, 2006, **75**, 333–366.
16 C. M. Dobson, *Nature*, 2003, **426**, 884–890.
17 S. B. Prusiner, *Proc. Natl. Acad. Sci. U. S. A.*, 1998, **95**, 13363–13383.
18 T. P. J. Knowles and M. J. Buehler, *Nat. Nanotechnol.*, 2011, **6**, 469–479.
19 D. M. Fowler, A. V. Koulov, W. E. Balch and J. W. Kelly, *Trends Biochem. Sci.*, 2007, **32**, 217–224.
20 D. E. Barlow, G. H. Dickinson, B. Orihuela, J. L. Kulp, D. Rittschof and K. J. Wahl, *Langmuir*, 2010, **26**, 6549–6556.
21 K. Kamino, S. Odo and T. Maruyama, *Biol. Bull.*, 1996, **190**, 403–409.
22 K. Kamino, K. Inoue, T. Maruyama, N. Takamatsu, S. Harayama and Y. Shizuri, *J. Biol. Chem.*, 2000, **275**, 27360–27365.
23 M. F. B. G. Gebbink, D. Claessen, B. Bouma, L. Dijkhuizen and H. A. B. Wosten, *Nat. Rev. Microbiol.*, 2005, **3**, 333–341.
24 K. D. Parker and K. M. Rudall, *Nature*, 1957, **179**, 905–906.
25 S. Weisman, H. E. Trueman, S. T. Mudie, J. S. Church, T. D. Sutherland and V. S. Haritos, *Biomacromolecules*, 2008, **9**, 3065–3069.
26 T. Fukuma, A. Mostaert and S. Jarvis, *Tribol. Lett.*, 2006, **22**, 233–237.
27 T. P. J. Knowles, T. W. Oppenheim, A. K. Buell, D. Y. Chirgadze and M. E. Welland, *Nat. Nanotechnol.*, 2010, **5**, 204–207.
28 M. Bouchard, J. Zurdo, E. J. Nettleton, C. M. Dobson and C. V. Robinson, *Protein Sci.*, 2000, **9**, 1960–1967.
29 M. Fandrich, M. A. Fletcher and C. M. Dobson, *Nature*, 2001, **410**, 165–166.
30 W. S. Gosal, I. J. Morten, E. W. Hewitt, A. Smith, N. H. Thomson and S. E. Radford, *J. Mol. Biol.*, 2005, **351**, 850–864.
31 K. Hasegawa, I. Yamaguchi, S. Omata, F. Gejyo and H. Naiki, *Biochemistry*, 1999, **38**, 15514–15521.
32 T. P. Knowles, A. W. Fitzpatrick, S. Meehan, H. R. Mott, M. Vendruscolo, C. M. Dobson and M. E. Welland, *Science*, 2007, **318**, 1900–1903.
33 B. Raman, E. Chatani, M. Kihara, T. Ban, M. Sakai, K. Hasegawa, H. Naiki, C. M. Rao and Y. Goto, *Biochemistry*, 2005, **44**, 1288–1299.
34 A. Aggeli, I. A. Nyrkova, M. Bell, R. Harding, L. Carrick, T. C. B. McLeish, A. N. Semenov and N. Boden, *Proc. Natl. Acad. Sci. U. S. A.*, 2001, **98**, 11857–11862.
35 R. P. W. Davies, A. Aggeli, A. J. Beevers, N. Boden, L. M. Carrick, C. W. G. Fishwick, T. C. B. McLeish, I. A. Nyrkova and A. N. Semenov, *Supramol. Chem.*, 2006, **18**, 435–443.
36 S. Barghorn, P. Davies and E. Mandelkow, *Biochemistry*, 2004, **43**, 1694–1703.
37 F. Chiti, P. Webster, N. Taddei, A. Clark, M. Stefani, G. Ramponi and C. M. Dobson, *Proc. Natl. Acad. Sci. U. S. A.*, 1999, **96**, 3590–3594.
38 D. M. Ridgley, K. C. Ebanks and J. R. Barone, *Biomacromolecules*, 2011, **12**, 3770–3779.
39 A. Athamneh and J. R. Barone, *Smart Mater. Struct.*, 2009, **18**, 104024.
40 K. C. Gokhale, G. P. Newnam, M. Y. Sherman and Y. O. Chernoff, *J. Biol. Chem.*, 2005, **280**, 22809–22818.
41 Y. Chernoff, S. Lindquist, B. Ono, S. Inge-Vechtomov and S. Liebman, *Science*, 1995, **268**, 880–884.
42 J. T. Jarrett and P. T. Lansbury, *Biochemistry*, 1992, **31**, 12345–12352.
43 L. M. Shinchuk, D. Sharma, S. E. Blondelle, N. Reixach, H. Inouye and D. A. Kirschner, *Proteins: Struct., Funct., Bioinf.*, 2005, **61**, 579–589.

View Article Online

44 A. Sethuraman and G. Belfort, *Biophys. J.*, 2005, **88**, 1322–1333.
45 A. Sethuraman, G. Vedantham, T. Imoto, T. Przybycien and G. Belfort, *Proteins: Struct., Funct., Bioinf.*, 2004, **56**, 669–678.
46 J. Adamcik and R. Mezzenga, *Soft Matter*, 2011, **7**, 5437–5443.
47 S. Bolisetty, J. Adamcik and R. Mezzenga, *Soft Matter*, 2011, **7**, 493–499.
48 M. I. Ivanova, M. R. Sawaya, M. Gingery, A. Attinger and D. Eisenberg, *Proc. Natl. Acad. Sci. U. S. A.*, 2004, **101**, 10584–10589.
49 The fibers formed here are from a complex mixture of peptides produced from the hydrolysate. We have since synthesized the individual peptides and shown that the pure mixtures behave the same.
50 C. E. MacPhee and C. M. Dobson, *J. Am. Chem. Soc.*, 2000, **122**, 12707–12713.
51 L. M. Carrick, A. Aggeli, N. Boden, J. Fisher, E. Ingham and T. A. Waigh, *Tetrahedron*, 2007, **63**, 7457–7467.
52 W. C. Oliver and G. M. Pharr, *J. Mater. Res.*, 1992, **7**, 1564–1583.
53 I. A. Nyrkova, A. N. Semenov, A. Aggeli, M. Bell, N. Boden and T. C. B. McLeish, *Eur. Phys. J. B*, 2000, **17**, 499–513.
54 I. A. Nyrkova, A. N. Semenov, A. Aggeli and N. Boden, *Eur. Phys. J. B*, 2000, **17**, 481–497.
55 J. Adamcik, A. Berquand and R. Mezzenga, *Appl. Phys. Lett.*, 2011, **98**, 193701.
56 J. Adamcik, J.-M. Jung, J. Flakowski, P. De Los Rios, G. Dietler and R. Mezzenga, *Nat. Nanotechnol.*, 2010, **5**, 423–428.
57 G. Vriend and C. Sander, *J. Appl. Crystallogr.*, 1993, **26**, 47–60.
58 Z. Luo, B. Akerman, S. Zhang and B. Norden, *Soft Matter*, 2010, **6**, 2260–2270.
59 J. C. Stendahl, M. S. Rao, M. O. Guler and S. I. Stupp, *Adv. Funct. Mater.*, 2006, **16**, 499–508.
60 C. Li, J. Adamcik and R. Mezzenga, *Nat. Nanotechnol.*, 2012, **7**, 421–427.
61 S. Srisailam, H.-M. Wang, T. K. S. Kumar, D. Rajalingam, V. Sivaraja, H.-S. Sheu, Y.-C. Chang and C. Yu, *J. Biol. Chem.*, 2002, **277**, 19027–19036.
62 H. Gunzler and H. U. Gremlich, *IR Spectroscopy*, Wiley-VCH, Weinheim, 2002.
63 A. Barth, *Prog. Biophys. Mol. Biol.*, 2000, **74**, 141–173.
64 J. F. Smith, T. P. Knowles, C. M. Dobson, C. E. MacPhee and M. E. Welland, *Proc. Natl. Acad. Sci. U. S. A.*, 2006, **103**, 15806–15811.
65 M. F. Perutz, T. Johnson, M. Suzuki and J. T. Finch, *Proc. Natl. Acad. Sci. U. S. A.*, 1994, **91**, 5355–5358.
66 A. H. DePace, A. Santoso, P. Hillner and J. S. Weissman, *Cell*, 1998, **93**, 1241–1252.
67 E. Scherzinger, A. Sittler, K. Schweiger, V. Heiser, R. Lurz, R. Hasenbank, G. P. Bates, H. Lehrach and E. E. Wanker, *Proc. Natl. Acad. Sci. U. S. A.*, 1999, **96**, 4604–4609.
68 S. Chen, V. Berthelier, J. Bradley Hamilton, B. O'Nuallain and R. Wetzel, *Biochemistry*, 2002, **41**, 7391–7399.
69 P. Sikorski and E. Atkins, *Biomacromolecules*, 2005, **6**, 425–432.
70 D. M. Ridgley, K. C. Ebanks and J. R. Barone, *Biomacromolecules*, 2011, **12**, 3770–3779.
71 V. Castelletto, I. W. Hamley, J. Adamcik, R. Mezzenga and J. Gummel, *Soft Matter*, 2012, **8**, 217–226.
72 V. Castelletto, I. W. Hamley, R. A. Hule and D. Pochan, *Angew. Chem., Int. Ed.*, 2009, **121**, 2353–2356.
73 N. C. Maiti, M. M. Apetri, M. G. Zagorski, P. R. Carey and V. E. Anderson, *J. Am. Chem. Soc.*, 2004, **126**, 2399–2408.

Published on 23 August 2012. Downloaded by Virginia Tech on 04/03/2014 16:48:51.

This journal is © The Royal Society of Chemistry 2012

Chapter 4.

Characterization of Large Amyloid Fibers and Tapes with Fourier-Transform Infrared (FT-IR) and Raman Spectroscopy

Ridgley, D. M., E. C. Claunch, and J. R. Barone. 2013. Characterization of Large Amyloid Fibers and Tapes with Fourier-Transform Infrared (FT-IR) and Raman Spectroscopy. *Appl. Spectrosc.* 57:1417-1426. - Reproduced with generous permission of the Society for Applied Spectroscopy.

Characterization of Large Amyloid Fibers and Tapes with Fourier Transform Infrared (FT-IR) and Raman Spectroscopy

Devin M. Ridgley, Elizabeth C. Claunch, Justin R. Barone*

Biological Systems Engineering Department, Virginia Tech, 303 Seitz Hall, Blacksburg, VA 24061 USA

Amyloids are self-assembled protein structures implicated in a host of neurodegenerative diseases. Organisms can also produce "functional amyloids" to perpetuate life, and these materials serve as models for robust biomaterials. Amyloids are typically studied using fluorescent dyes, Fourier transform infrared (FT-IR), or Raman spectroscopy analysis of the protein amide I region, and X-ray diffraction (XRD) because the self-assembled β-sheet secondary structure of the amyloid can be easily identified with these techniques. Here, FT-IR and Raman spectroscopy analyses are described to characterize amyloid structures beyond just identification of the β-sheet structure. It has been shown that peptide mixtures can self-assemble into nanometer-sized amyloid structures that then continue to self-assemble to the micrometer scale. The resulting structures are flat tapes of low rigidity or cylinders of high rigidity depending on the peptides in the mixture. By monitoring the aggregation of peptides in solution using FT-IR spectroscopy, it is possible to identify specific amino acids implicated in β-sheet formation and higher order self-assembly. It is also possible to predict the final tape or cylinder morphology and gain insight into the structure's physical properties based on observed intermolecular interactions during the self-assembly process. Tapes and cylinders are shown to both have a similar core self-assembled β-sheet structure. Soft tapes also have weak hydrophobic interactions between alanine, isoleucine, leucine, and valine that facilitate self-assembly. Rigid cylinders have similar hydrophobic interactions that facilitate self-assembly and also have extensive hydrogen bonding between glutamines. Raman spectroscopy performed on the dried tapes and fibers shows the persistence of these interactions. The spectroscopic analyses described could be generalized to other self-assembling amyloid systems to explain property and morphological differences.

Index Headings: **Amyloid; Fourier Transform Infrared Spectroscopy; FT-IR; Raman Spectroscopy; Protein; Amino Acid.**

INTRODUCTION

Under certain conditions, peptides and proteins have been shown to aggregate into structures known as "amyloids." All amyloids have one distinct feature: that the constituent peptides or proteins transform from a non-β-sheet secondary structure, i.e., random coil and/or α-helix, to a β-sheet secondary structure. There is a large body of work on the aggregation of spontaneously misfolded proteins into amyloids associated with neurodegenerative "prion" diseases such as Alzheimer's, Parkinson's, and Huntington's diseases.[1,2] There is another, less studied class of amyloid in nature termed the "functional amyloid" that barnacles, bacteria, and fungi use as a method of self-preservation by facilitating attachment of the organism to a substrate or into a biofilm.[3–10] It is generally accepted that any peptide or protein is capable of misfolding into an amyloid given the right conditions, which are usually denaturing.[1,3,11–20] Thus, in vitro techniques can be used to mimic nature's amyloid self-assembly processes either to study prion disease progression or to design new biomaterials.[21,22]

Amyloids can exist as amorphous aggregates, which are random globules of self-assembled, β-structured proteins.[23] Amorphous aggregates are important to prion disease progression.[2] Amyloids can also exist as self-assembled fibrils 2–10 nm wide and >100 nm long.[11,14,16,23–48] These nanometer-sized fibrils are the most studied amyloid because of relevance to prion disease progression and potential use as nanomaterials. In some instances, amyloid tapes and fibers >150 nm wide and many millimeters long have been predicted and observed.[20,22,49–52] From a materials science perspective, the in vitro self-assembly of amyloid fibrils is interesting because they have a modulus similar to spider silk and a specific modulus rivaling steel.[5,53–55] Amyloid fibrils can be distinguished by the fact that the protein chain axis in the β-sheet is perpendicular to the fibril axis, which can be discerned by rotating the specimen in an X-ray diffraction (XRD) or polarized infrared or Raman experiment to reference the chain axis.[56–59] In contrast, native silk and β-keratin fibers containing β-sheets have the protein chain axis oriented along the fiber axis.[56,59] To differentiate the two, the amyloid fibril β-sheet has been termed the "cross-β" structure. *Chrysopa* silk is a protein fiber with the cross-β structure.[56,57,60] Protein isolated from the gland of this insect also forms the cross-β structure. However, a water swollen *Chrysopa* stalk will align its protein chains along the axis of deformation when stretched.[56] Other proteins have shown similar behavior.[59] Thus, silk and β-keratin proteins are aligned along the fiber axis because of the pultrusion or extrusion deformation, respectively, required for fiber formation.[61]

A number of techniques have been employed to study amyloid structures. In disease pathology, dyes such as Thioflavin-T, Thioflavin-S, and Congo Red have been used because they specifically bind to available hydrogen bonding sites inside β-sheets.[33,62,63] Once the dyes bind they are excited with a laser of a designated wavelength and fluoresce to reveal amyloid structures in vivo and in vitro.[64,65] However, this technique only reveals the presence of aggregated β-structures and their location, which is advantageous in identifying disease pathology. More complete analysis of the amyloid structure can be performed using XRD, especially on fibrils with preferential molecular orientation.[11,56,57,59,60,66,67] Unfortunately, XRD is not very convenient. Using Fourier transform infrared (FT-IR) spectroscopy, protein secondary structure can be determined by studying the amide I absorbance, which is much more convenient and, when done correctly, can be quite powerful.[68] The protein amide I absorbance describes the state of the carbonyl in the peptide bond.[69,70] The position of the amide I absorbance has been shown to correspond to the different protein secondary structures, which are summarized in

Received 26 February 2013; accepted 2 August 2013.
* Author to whom correspondence should be sent. E-mail: jbarone@vt.edu.
DOI: 10.1366/13-07059

0003-7028/13/6712-1417/0
© 2013 Society for Applied Spectroscopy

TABLE I. FT-IR amide I secondary structure assignments.

Wavenumber (cm^{-1})	Assignment
1605–1625	High strand density β-sheet usually indicative of amyloid
1615–1625	Range used for single β-structure fit
1625–1635	Low strand density β-sheet usually indicative of native, non-amyloid β-structures
1635–1644	Random coil
1645–1665	α-helix
1666–1699	β-turn, antiparallel β-sheet

Table I.[59,71–75] These assignments have been confirmed with XRD and circular dichroism (CD).[66,67,76–78] Amyloid formation can be characterized by a shift in the amide I absorbance from the random coil and/or α-helix conformation to the β-sheet conformation, which is a shift to lower wavenumber.[11] Although not absolute, on average, the amide I position appears at lower wavenumber for amyloids (~1615 cm^{-1}) than for native β-sheets (~1630 cm^{-1}).[79,80] The difference does not arise from the amount of β-sheet or the ratio of antiparallel to parallel β-sheet, but differences in the β-sheet twist angle and number of protein chains or "strands" per β-sheet.[55,81] The lower wavenumber position of amide I for amyloids originates in lower β-sheet twist angle and more strands per β-sheet.[79] Secondary structure can also be analyzed using Raman spectroscopy. Assignments are similar to those found with FT-IR except for the β-sheet, which appears at a Raman shift of ~1670 cm^{-1}.[82–87] Explicit information about the β-sheet amyloid core has been obtained using deep ultraviolet resonance Raman (DUVRR) spectroscopy.[88] Hydrogen–deuterium exchange DUVRR can isolate the β-sheet core, which will not have an easy exchange, from chemical groups outside of the β-sheet that can readily exchange.[89] The same technique showed the influence of peptide amino acid sequence on the core amyloid β-sheet structure.[90] $A\beta_{34–42}$ and $A\beta_{1–40}$ are peptides important in Alzheimer's disease. $A\beta_{34–42}$ fibrils had an antiparallel β-sheet structure similar to globular proteins, while $A\beta_{1–40}$ had a parallel β-sheet structure significantly different from globular proteins.[91]

Recent research shows that it is possible to spontaneously self-assemble micrometer-sized amyloid fibers from (1) tryptic hydrolysates of wheat gluten (WG) and (2) a mixture of trypsin-hydrolyzed gliadin and unhydrolyzed myoglobin (Gd:My).[21,22,65] WG is a combination of gliadin and glutenin proteins, and the peptides produced from hydrolysis self-assemble into cylindrical fibers of high modulus. Replacing the hydrolyzed glutenin fraction with unhydrolyzed myoglobin results in rectangular tapes of low modulus. By themselves, the glutenin peptides and myoglobin protein do not self-assemble. The morphological and property differences result from amino acid sequence differences that manifest during aggregation in solution and upon drying. Here, FT-IR and Raman spectroscopy analysis techniques are described that highlight the amino acid differences that influence aggregation and final fiber morphological differences. These systems were chosen because they are able to spontaneously assemble into micrometer-sized amyloid fibers at near physiological conditions,[21,22,65] which is 1–3 orders of magnitude greater than previous reports.[5,19,40–42,52,54,55] Furthermore, these spectroscopic methods are capable of discerning the role of different amino acids in the self-assembling peptide mixtures and their contributions that affect the final fiber morphology and modulus. Thus, thorough observation of amyloid formation is possible over many orders of magnitude of scale, including the small scales relevant to disease pathology and the large scales important in "functional" amyloids. The techniques would prove useful to those working in the field of amyloid formation and prion disease, which would better highlight protein features important in β-sheet aggregation.

EXPERIMENTAL

Solutions. We dissolved 25 mg/ml of wheat gluten (WG) (MP Biomedicals, LLC, Solon, OH) in 80 ml of pure water at 37 °C. We then added 30 mg of trypsin (Type I from bovine pancreas, Sigma-Aldrich, St. Louis, MO) to achieve a 1:67 (w/w) enzyme:substrate ratio, and hydrolysis was allowed to occur for 1 day before FT-IR readings were taken. The solutions were monitored and frequently adjusted with 1 M NaOH to maintain a pH of 8 over the first 3 days. After 3 days the hydrolysis was complete, and the solutions remained at constant pH 8. Buffers were not used to prevent any effect that they may have on the self-assembly of large amyloid fibers. Gliadin (Gd, TCI America, Portland, OR, UniProt P04721) was dissolved in 800 ml of pure water at a concentration of 25 mg/ml. Trypsin was added at the same ratio, and the solution was maintained at pH 8 and 37 °C for 3 days to ensure that hydrolysis was complete. The times have been confirmed as the point of complete hydrolysis prior to aggregation.[21,65,78] Gd was poured into Teflon-coated aluminum foil trays and allowed to dry at ambient conditions under a fume hood. The dried, hydrolyzed Gd was combined with myoglobin (My, from equine skeletal muscle, Sigma-Aldrich, UniProt P68082) in 10 ml of pure water at a molar ratio of 0.36:0.64 (Gd:My) and concentration of 25 mg/ml. Solutions were incubated at pH 8 and 37 °C for 20 days. After 20 days the solutions were poured into Teflon-coated aluminum foil trays and dried under a fume hood at ambient conditions, which produces a large amount of micrometer-sized fibers and tapes. The micrometer-sized fibers and tapes were manually collected with tweezers, washed gently with pure water to remove unassembled peptide, and examined with Raman spectroscopy.

Fourier Transform Infrared Spectroscopy. Attenuated total reflection (ATR) FT-IR spectra of the incubating aqueous solutions were recorded daily on a Thermo Nicolet 6700 FT-IR spectrometer (Thermo Fisher Scientific Inc., Waltham, MA) with a 45° ZnSe crystal trough. The spectrum of each protein solution was ratioed against the aqueous solvent background to reveal the protein absorbance spectrum.[75,92–94] Three spectra were acquired at each point in time, and averages ± standard deviations were reported for each condition. The spectra were collected and analyzed with OMNIC v8.1 software.

Fourier Transform Infrared Amide I Analysis. Most proteins are not purely of one secondary structure, and thus the amide I absorbance is formed through contributions from all of the secondary structures present. It is possible to "deconvolute" the amide I absorbance into its secondary structure components by representing it as a sum of peaks assigned to each structure.[77,95–98] The area of each peak is representative of the molar concentration of that particular secondary structure. The spectral region from 1720 to 1580 cm^{-1} was isolated and manually smoothed with the Savitzky–Golay algorithm using 9–13 points. Next, the second derivative of the amide I spectral region was taken without filtering to identify the individual

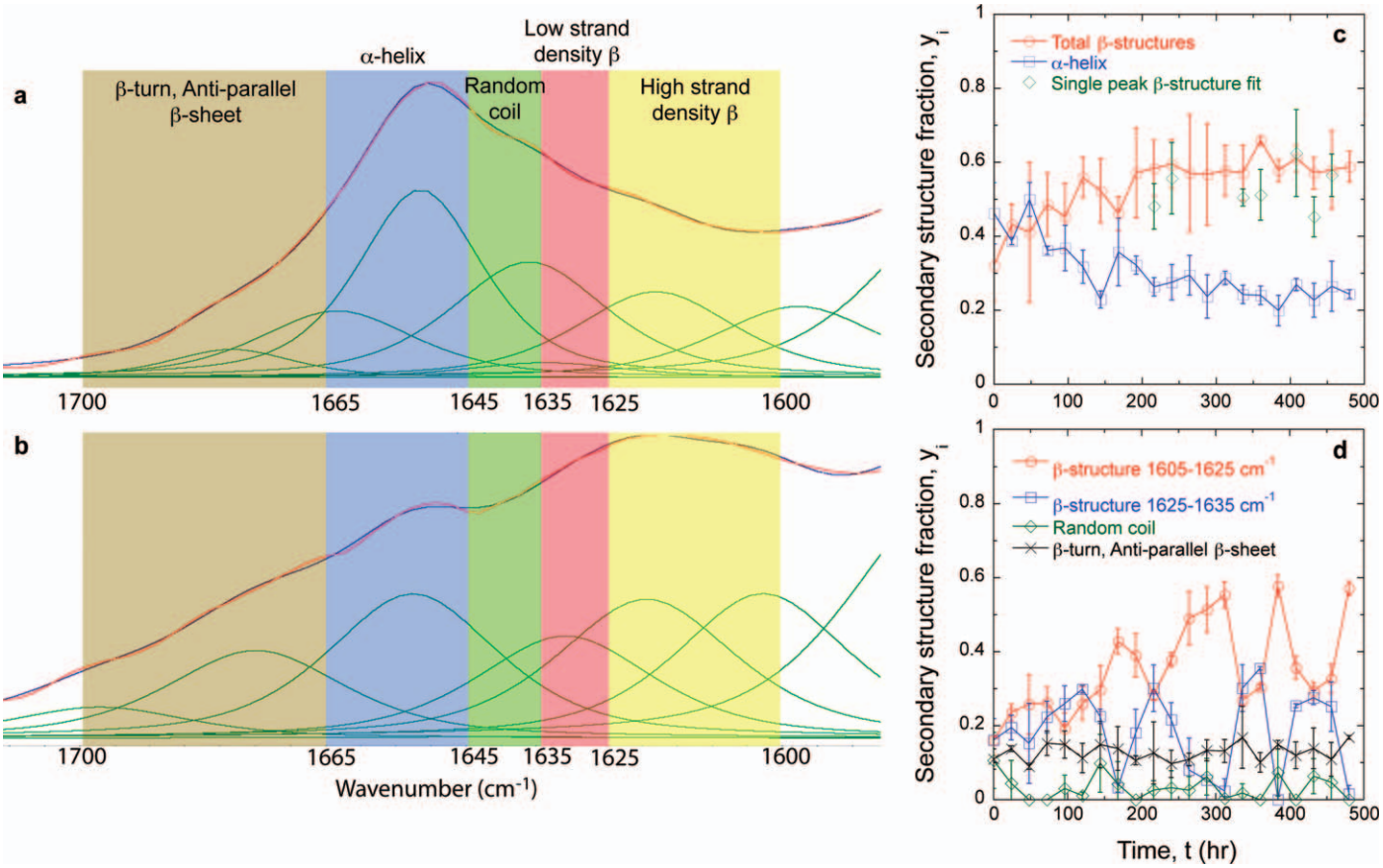

FIG. 1. Gd:My amide I absorbance represented as a sum of Gaussian/Lorentzian peaks (green curves) at (**a**) 0 h and (**b**) 480 h. The fit (red curve) shows good agreement with the actual spectrum (blue curve). Protein secondary structure assignments are high strand density β-sheet (yellow), low strand density β-sheet (red), random coil (green), α-helix (blue), and β-turn, antiparallel β-sheet (brown). (**c, d**) The change in protein secondary structure as amyloid aggregation proceeds can be monitored with time.

amide I components. Fourier self-deconvolution (FSD) was performed with Happ–Genzel apodization by setting enhancement to 2–3 and adjusting the bandwidth until absorbance maxima matched the second derivative minima.[7,70,99] Using the "Peak Resolve" feature of OMNIC version 8.1, the amide I absorbance was fit to a series of Gaussian/Lorentzian peaks matching the FSD. The peak resolve feature uses the Fletcher–Powell–McCormick algorithm to fit the peaks.[100] Amide I fitting was performed with a constant baseline, a target noise of 10.0, and an initial full width at half-height of 3.857. The goodness of fit, in the form of an F-value, was less than 0.5%.

Raman Spectroscopy. Raman spectroscopy was performed on single dried WG and Gd:My fibers and tapes, respectively, with a Senterra dispersive Raman spectrometer and confocal microscope (Bruker Optics, Billerica, MA). WG fibers were analyzed with a 785 nm laser at 100 mW (approximately 20 mW at the fiber), 50× objective, and 1000 × 25 μm aperture. Gd:My tapes were analyzed with a 532 nm laser at 5 mW (approximately 2 mW at the tape), 100× objective, and 50 μm aperture. These conditions produced the least amount of noise and required the least amount of baseline correction. The laser was intrinsically polarized, and polarization experiments were performed on single amyloid fibers or tapes by rotating the amyloid fiber or tape 0°, 45°, and 90° relative to the laser polarization. Multiple measurements were taken at each condition. Raman spectra were cut to exclude the regions below 200 cm^{-1} and above 3200 cm^{-1} because of excess noise. The spectra were then concave rubberband baseline corrected for a small amount of observed fluorescence. Spectra were analyzed with OPUS version 6.5 software.

RESULTS AND DISCUSSION

Fourier Transform Infrared Spectroscopy. Conformation change from random coil and α-helical structures to β-structures is a hallmark of amyloid formation in proteins.[19,45,101,102] Consistent with other amyloid studies, the amide I absorbance maximum shifts from 1640–1650 cm^{-1} (Fig. 1a at 0 h) to 1610–1620 cm^{-1} (Fig. 1b at 480 h) as aggregation proceeds.[21,65] Deconvolution of the amide I absorbance into its principal secondary structure components can quantitatively reveal individual protein secondary structure changes. Figures 1a and 1b show the amide I absorbance as a sum of Gaussian/Lorentzian curves matching the FSD, whose sum presents a good fit to the experimental curve. Based on its position, each curve is assigned to a secondary structure component (Table I). It has been shown that anomalous dispersion (AD) effects can occur from the choice of ATR internal reflective element, sample concentration in solution, or sample thickness in the solid state. These AD effects can cause slight differences in the amide I absorbance position and shape.[103] The dilute solution conditions used, low observed absorbances, and high bandwidths minimize those anomalous effects. Assuming that each protein secondary structure has the same molar absorption coefficient, ε, the area of each

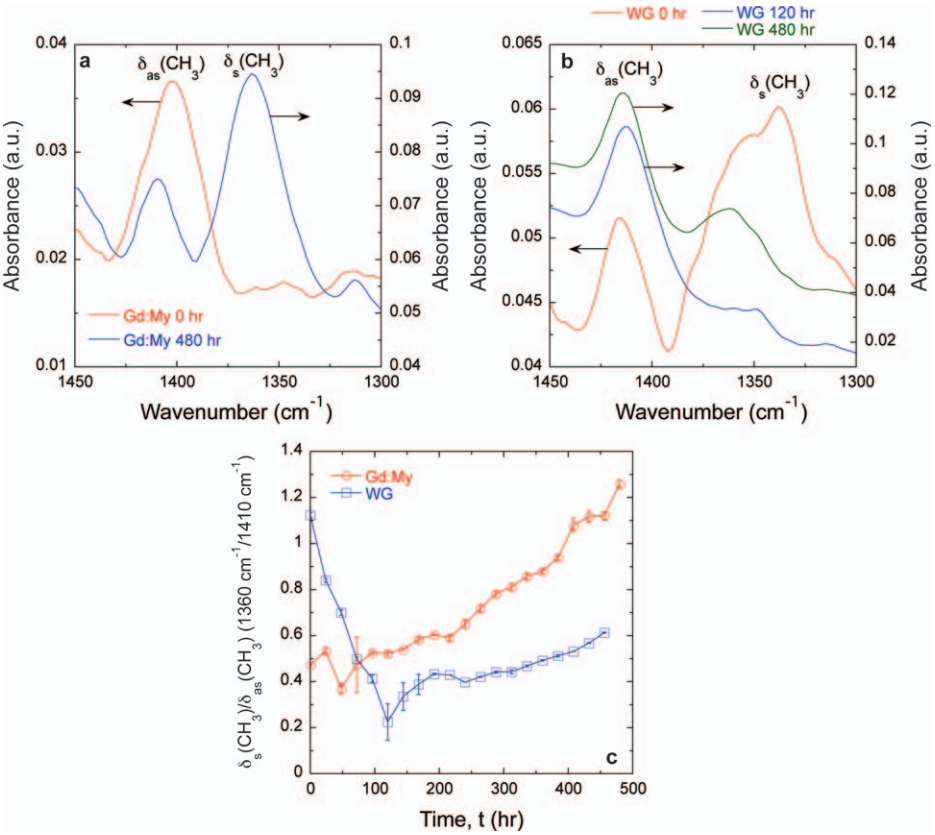

FIG. 2. Spectra of (**a**) Gd:My and (**b**) WG solutions at early and end times illustrating the change in symmetric CH_3 deformation, $\delta_s(CH_3)$, at ~1360 cm^{-1} and asymmetric CH_3 deformation, $\delta_{as}(CH_3)$, at ~1410 cm^{-1}. (**c**) Comparison of hydrophobic packing, $\delta_s(CH_3)/\delta_{as}(CH_3)$, in WG and Gd:My solutions over 480 h.

absorption curve, A_i, can reveal the molar fraction of each secondary structure component, y_i

$$y_i = \frac{A_i}{\sum_{i=1}^{n} A_i} \quad (1)$$

where $\sum_{i=1}^{n} A_i$ is the sum of the areas of n secondary structure components.[104,105] However, it is possible that the molar absorption coefficients of each secondary structure are different, making the analysis only semiquantitative.[106] Here, the gain or loss of each component is monitored with respect to time as amyloid aggregation proceeds (Figs. 1c, 1d). Below 1635 cm^{-1}, two distinct peaks appear in the amide I second derivative and FSD: one in the range of 1605–1625 cm^{-1} and one in the range of 1625–1635 cm^{-1}, consistent with assignments of high strand density and low strand density β-sheets, respectively (Table I and Figs. 1a, 1b shown as Gaussian/Lorentzian peaks used in the fit).[79] However, the relative contribution from each varies at different times. For example, the data collected from 0 to 100 h show the contribution from each is nearly equal, but the data from 260 to 300 h show the higher strand density β-structure dominates (Fig. 1d). Thus, subtleties in the amide I deconvolution require more examination to extract meaningful data. In Fig. 1c, "total β-structures" is the sum of the two β-structure contributions shown individually in Fig. 1d. As a test of the summation, the β-sheet region is manually fit using a single, larger β-structure peak centered in the range 1615–1625 cm^{-1} (Table I; Fig. 1c). There is good agreement between the manual, single peak procedure and the sum of the two individual β-structures for cases when the two individual β-structure peaks are about equal (i.e., 216 h) or when they are disparate (i.e., 240 h). The Gd:My peptide mixture displays a consistent decrease in α-helix with an approximately equal increase in β-structures, which is observed for WG and Gd:My peptide mixtures studied under a variety of conditions, while other secondary structure components remain relatively constant.[21] It can then be concluded that α to β conformational transitions are important in amyloid formation for the peptide mixtures studied here and that properties of the protein α-helices influence the process.[4]

The amide I absorbance primarily originates from the peptide bond carbonyl stretch, ν(C=O) and is commonly used to assign protein secondary structure.[68] As shown above, the overwhelming majority of studies on proteins, and specifically protein aggregation, have involved analysis of the amide I absorbance. However, FT-IR spectroscopy gives information about the state of other chemical groups in proteins and may help to delineate amino acids important in amyloid formation. Part of the problem may originate in a lack of meaningful literature data assigning absorbances to specific amino acid side chains in the region below 1500 cm^{-1}.[107] For WG and Gd:My mixtures, it is also observed that the 1360 cm^{-1} absorbance progressively increases relative to the 1410 cm^{-1} absorbance (Figs. 2a, 2b). The 1360 cm^{-1} absorbance can be assigned to the CH_3 symmetric deformation, $\delta_s(CH_3)$, and the 1410 cm^{-1} absorbance to the asymmetric CH_3 deformation, $\delta_{as}(CH_3)$, on the side groups of the hydrophobic amino acids alanine (A), isoleucine (I), leucine (L), and valine (V) also summarized in Table II.[69,108,109] A, I, L, and V are predominant in the α-helices of WG peptides and myoglobin

TABLE II. FT-IR absorbance assignments for amino acid side groups.

Wavenumber (cm^{-1})[a]	Assignment
1410 s	$\delta_{as}(CH_3)$: CH_3 asymmetric deformation on A, I, L, V
1360 s	$\delta_s(CH_3)$: CH_3 symmetric deformation on A, I, L, V
1103 w	$\gamma_r(NH_2)$: NH_2 rock vibration on Q
1080 m-s	ν(CN): CN stretching vibration on Q, K
1016 s	ν(C–C): C–C stretch on Q, K

[a] s = strong; m = medium; w = weak.

according to secondary structure predictions using PSIPRED.[107,108,110] Considering $\delta_s(CH_3)$ as a measure of up and down movement and $\delta_{as}(CH_3)$ as a measure of side to side movement of the CH_3 amino acid side groups, the increase in the ratio $\delta_s(CH_3)/\delta_{as}(CH_3)$ indicates that A, I, L, and V side groups are laterally constrained in the amyloid structure because they are more able to vibrate up and down relative to side to side (Fig. 2c). Previous reports support this conclusion.[21,65] This would indicate that hydrophobic interactions are an important driving force in protein conformation change and amyloid formation.

While WG and Gd:My systems both display a core aggregated β-sheet amyloid structure and hydrophobic interactions, there are structural differences in their full self-assembled structures that need to be explored.[65] At pH 8 and 37 °C, WG results in 10–20 μm diameter cylindrical fibers, whereas Gd:My results in 10–20 μm wide and 5 μm thick rectangular tapes.[65] Amyloid fibrils of tape and twisted tape morphologies have also been observed.[41,42,44,52] This raises the question of whether there are other amino acid contributions that can differentiate self-assembled protein structures. The FT-IR spectrum reveals changes in the 950–1150 cm^{-1} region (Figs. 3a, 3b). The absorbance around 1080 cm^{-1} can be assigned to the CN stretching absorbance, ν(CN), and the absorbance around 1016 cm^{-1} can be assigned to the C–C stretching absorbance, ν(C–C), both on amino acid side chains.[108,109] Rocking of NH_2, $\gamma_r(NH_2)$, can be assigned around 1103 cm^{-1} (Figs. 3a, 3b).[108] These assignments have also been shown in the Raman spectrum,[111] and the similarities between the Raman and FT-IR spectra for amino acids have been directly shown.[112] Gd:My mixtures of the same molar ratio have been studied under various solution conditions, and the ratio ν(C–C)/ν(CN) could differentiate the final morphology of the amyloid structure early in the self-assembly process (Fig. 3c).[21] Rectangular cross-section tapes show an increase in ν(C–C)/ν(CN) before reaching an asymptote of 0.8–1. Twisted Gd:My tapes, some twisted so tightly that they result in a cylindrical cross-section, show an approximately constant, low value of ν(C–C)/ν(CN) = 0.4. On the other hand, the ratio ν(C–C)/ν(CN) for WG at pH 8 and 37 °C oscillates between 1.5 and 3 over all time and results in a cylindrical fiber (Fig. 3d). The different behavior for ν(C–C)/ν(CN) in each system, especially in describing cylindrical fiber morphologies, intimates these absorbances originate in different amino acids.

Wheat gluten peptides contain a large amount of glutamine repeats or "Q-blocks" and are 38% Q overall, whereas myoglobin contains no Q-blocks and is 4% Q overall. Glutamine contains an amide group at the end of its side group connected to the peptide bond by two CH_2 groups. Myoglobin contains 12.3% lysine (K), while WG proteins, gliadin (1.5% K), low molecular weight glutenin (0.7% K, UniProt P10386), and high molecular weight glutenin (1.2% K, UniProt P10387) contain very little lysine. The lysine side group has a primary amine connected to the peptide bond by four CH_2 groups. Given the amounts in each mixture, ν(C–C)

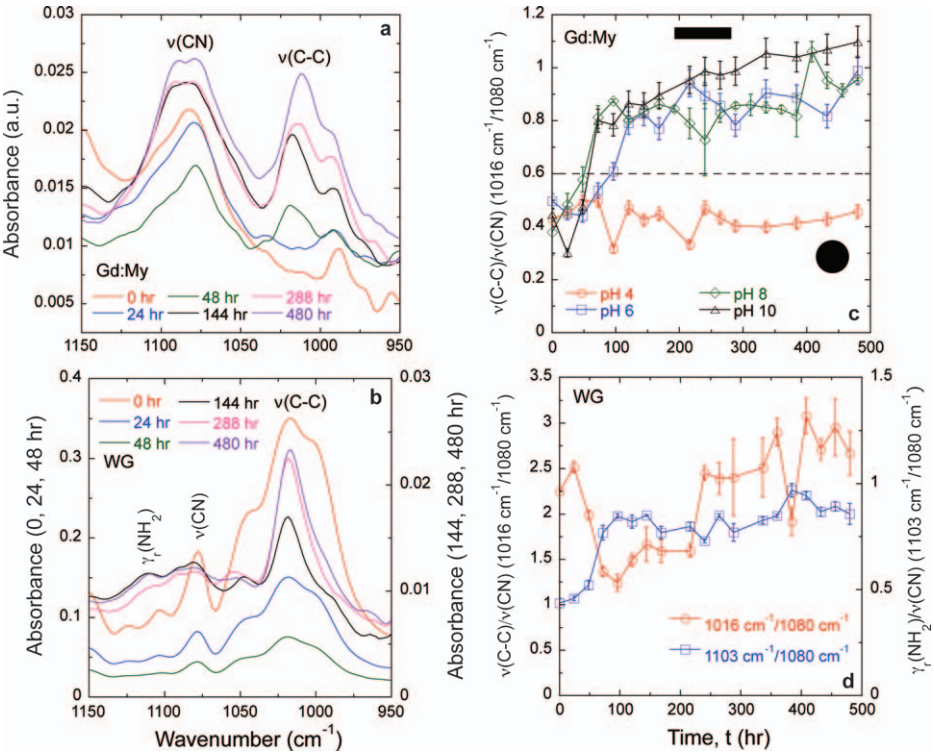

FIG. 3. Spectra of (**a**) Gd:My and (**b**) WG peptide solutions at pH 8 and 37 °C illustrating the change in CN stretching, ν(CN), at ~1080 cm^{-1} and C–C stretching, ν(C–C), at ~1016 cm^{-1}. Rocking vibration of NH_2, $\gamma_r(NH_2)$, at ~1103 cm^{-1} is also observed in this region. (**c**) Comparison of the ν(C–C)/ν(CN) ratio in Gd:My solutions at 37 °C can predict final morphology. (**d**) Glutamine repeat units appear important to WG peptide self-assembly early in the process.

TABLE III. Raman shift assignments.

Raman shift (cm^{-1})[a]	Assignment
~1665 m	Amide I: β-sheet[122]
~1650 m	Amide I: α-helix[82,122]
1614 s	ν(C=C): aromatic C=C stretch on tyrosine (Y)[123]
1610 s	ν(C=C): aromatic C=C stretch on phenylalanine (F)[82,87,123]
1475 s	$\delta(CH_2)$: CH_2 deformation on A, I, L, V side groups[83]
1410 s	$\delta(CH_3)$: CH_3 deformation on A, I, L, V side groups[83]
1230–1280 m-s	Amide III: C–N stretch, ν(CN), and N–H bend, δ(NH), on Q, K side groups[83,104]
~1100 m-s	ν(CN): C–N stretch of Q, K side group[83]

[a] s = strong; m = medium; w = weak.

and ν(CN) originate in lysine and glutamine for Gd:My and WG mixtures, respectively. Rocking of NH_2, $\gamma_r(NH_2)$, is discernible in WG probably because the amide on the Q cannot change its protonation state, but NH_2 on lysine can, and its absorbance position can change. The data in Fig. 3c would suggest that as the NH^+_3 on the lysine side chain is more protonated at decreasing pH, lysine side chains gain enough positive charge to repel each other and twist the self-assembled structure into a cylinder. The charge repulsion mechanism has been shown to twist amyloid tapes into cylinders.[42] Charge repulsion keeps the C–N group at the end of the lysine side chain from hydrogen bonding, so it is able to vibrate more relative to the $(CH_2)_4$ portion of the side chain, resulting in a lower ν(C–C)/ν(CN) ratio. The limited vibration of the $(CH_2)_4$ portion is probably from pH-insensitive hydrophobic interactions, which are important in amyloid self-assembly, as shown here and in previous literature.[21,42,44,65,113] The importance of hydrophobic interactions on lysine in β-sheet formation has been shown for a lysine substituted β_2-microglobulin peptide at near physiological conditions.[114] Screening the positive charge on lysine for a series of KL-containing peptides also shows the importance of lysine hydrophobic interactions in β-sheet aggregation.[115,116] For WG the large ν(C–C)/ν(CN) ratio suggests that the C–N group at the end of the glutamine side chain does not vibrate as much as the $(CH_2)_2$ portion of the side chain (Fig. 3d). The $\gamma_r(NH_2)$/ν(CN) ratio increases for the first 100 h then reaches an asymptote. It is also observed that the $\delta_s(CH_3)/\delta_{as}(CH_3)$ ratio decreases for the first 100 h of WG self-assembly before increasing (Fig. 2c). Taken together, this may suggest that hydrogen bonding of the end of the glutamine side chain is more important than hydrophobic packing in WG self-assembly at early times and that most of the hydrogen bonding is through the carbonyl on the amide because NH_2 is able to vibrate more relative to C–N. The increase of ν(C–C)/ν(CN) and $\delta_s(CH_3)/\delta_{as}(CH_3)$ and constant $\gamma_r(NH_2)$/ν(CN) from 100 to 480 h indicates that hydrophobic packing is more important to self-assembly at long times. Instead of charge repulsion, the amyloid fiber is twisted from Q–Q hydrogen bonding. Indeed, Q–Q hydrogen bonding in Q–blocks has been shown to facilitate amyloid β-sheet formation and is implicated in prion diseases such as Huntington's disease.[24,117–120] An engineered peptide containing Q-blocks has been shown to be highly twisted relative to an engineered peptide of the same length without Q-blocks.[51]

Raman Spectroscopy. After 20 days, incubating peptide and protein mixture solutions are dried and the resulting fibers (WG) and tapes (Gd:My) studied with Raman spectroscopy. The confocal microscope on the dispersive Raman spectrometer allows for focusing along the ~10 μm width of the fibers and tapes. Gd:My tapes display good sensitivity and little noise when excited at 532 nm. However, WG fibers show significant noise at 532 nm. A good signal is obtained at 785 nm. The amide I and III regions are sensitive to protein conformation. However, aromatic groups on amino acids phenylalanine (F), tryptophan (W), and tyrosine (Y) have intense Raman shifts in the region 1600 cm^{-1} to 1620 cm^{-1} that can obscure the amide I signal (Table III).[87,121–123] To more accurately compare protein secondary structure differences between the self-assembled fibers and tapes, amide III between 1200 and 1300 cm^{-1} is used. Historically, the amide III region has not been used to assign protein secondary structure as much as the amide I region.[68,124–128] More recent research has shown that the amide III can be used to accurately assign protein secondary structure changes in silk as it is deformed or processed.[129–132] The DUVRR amide III is very sensitive to the protein structure because of the dihedral angle dependent coupling between $(C)C_\alpha H$ and NH bending vibrations[133] and has been used to study protein secondary structure including that of amyloids.[88–90,134,135] WG fibers show a small peak and Gd:My tapes show a shoulder at ~1216 cm^{-1} indicative of the high strand density β-sheets found in amyloids.[91] Peaks at ~1280 cm^{-1} and 1244 cm^{-1} are assigned to α-helices and random coil structures, respectively.[88,91,129,130] Comparison of the β-sheet Raman intensity at ~1216 cm^{-1} to the α-helix Raman intensity at ~1280 cm^{-1} shows $\beta/\alpha = 0.56$ for Gd:My and 0.12 for WG indicative of more α-helix converting to β-sheet in the Gd:My mixture, which is also observed using FT-IR (Fig. 4).[65] Although the final large structure is not obtained until drying, the final secondary structure can be predicted using the aggregation behavior in solution as characterized using FT-IR. Raman favors covalent bonding and groups of low dipole and high polarizability so more hydrocarbon information is obtainable. The CH_2 deformation, $\delta(CH_2)$, is distinct at ~1475 cm^{-1}, while other CH_2 modes are obscured because of contributions from the aromatic rings on F and Y (Fig. 4).[136] The higher Q content in WG compared with K in

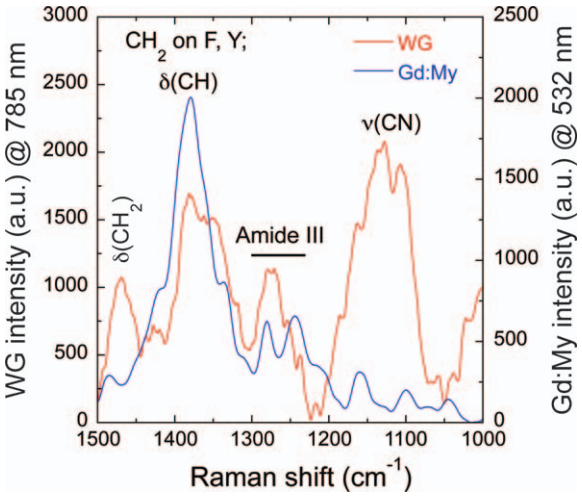

FIG. 4. Raman spectra of WG and Gd:My dried amyloid fibers and tapes with the fiber or tape at 0° to the polarization direction depicting the deformation of CH_2, $\delta(CH_2)$, at ~1475 cm^{-1}, deformation of CH, δ(CH), and CH_2 on F and Y at ~1380 cm^{-1}, vibration of CN, ν(CN), at ~1140 cm^{-1}. The amide III peak is used to determine the secondary structure: α-helix at ~1280 cm^{-1}, random coil at ~1244 cm^{-1}, and β-sheet at ~1216 cm^{-1}.

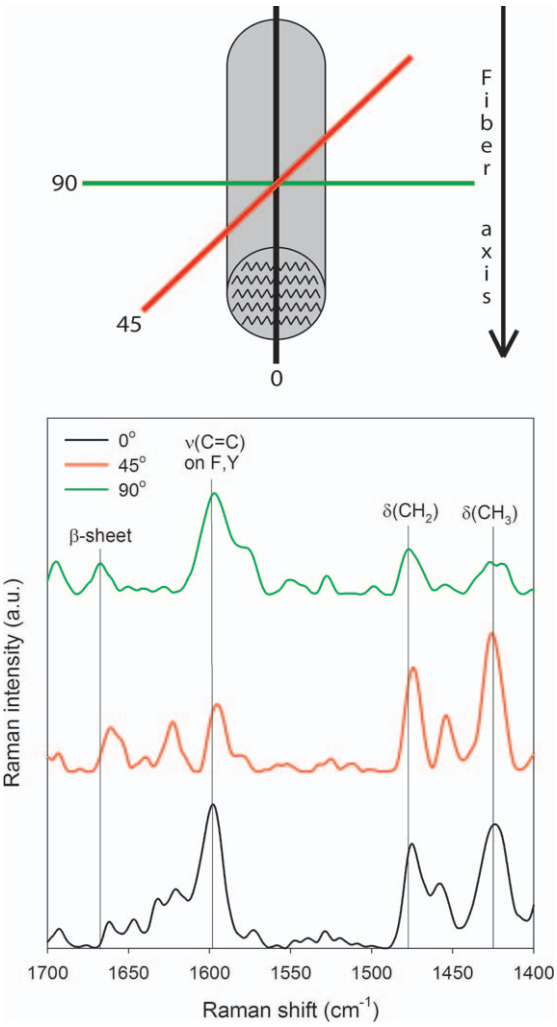

FIG. 5. Raman spectra of a dried WG fiber oriented 0°, 45°, and 90° with respect to laser polarization direction. Laser wavelength is 785 nm.

Gd:My is apparent in the larger ν(CN) intensity relative to other Raman shifts (Fig. 4).

Polarization experiments can be performed with Raman spectroscopy to note the direction of chemical groups and secondary structure in protein fibers.[130,132,137,138] When the amyloid fiber axis is aligned perpendicular to the laser polarization direction (90°) the spectrum shows the highest ratio of β-sheet intensity (~1665 cm^{-1}) relative to CH_3 and CH_2 deformation intensity (1420 cm^{-1} and 1475 cm^{-1}, respectively), which is indicative of the β-sheet or protein chain axis being oriented perpendicular to the fiber axis (Fig. 5). As the polarization direction is rotated 45° and 0° relative to the fiber axis the ratio decreases. This shows that side groups of amino acids A, I, L, and V (CH_3 and CH_2 deformations at 1420 cm^{-1} and 1475 cm^{-1}, respectively, but the 1420 cm^{-1} Raman shift is obscured by F and Y) and phenylalanine and tyrosine (1420, 1610, and 1614 cm^{-1}) are oriented perpendicular to the β-sheet axis (Fig. 5; Table III) revealing that the self-assembled WG and Gd:My fibers and tapes have a cross-β structure.

CONCLUSION

By using FT-IR and Raman spectroscopy, β-sheet formation in self-assembled amyloid structures can be monitored over time in aqueous solution and in the final structure upon drying. Secondary structure change and development can be accomplished through analysis of the amide I region originating from stretching of the carbonyl on the peptide bond. Beyond simple analysis of the amide I region, analysis of the behavior of plentiful amino acids with hydrophobic side groups, A, I, L, and V, illustrates the role of hydrophobic interactions in driving secondary structure change and β-sheet formation. Further, Q in WG mixtures and K in Gd:My mixtures can be isolated in the FT-IR and Raman spectra and their influence on the self-assembled structure delineated. Through polarization of the Raman excitation, the molecular orientation of amino acid side groups relative to the protein chain axis in the β-sheets and fiber axis can be determined. Techniques such as these could be generalized to other amyloid systems to show the effect of hydrophobic interactions and specific amino acids on aggregation behavior.

ACKNOWLEDGMENTS

Generous funding through NSF-CMMI-0856262 and the Virginia Tech Biodesign and Bioprocessing Research Center are greatly appreciated.

1. C.M. Dobson. "Protein Folding and Misfolding". Nature. 2003. 426(6968): 884-890.
2. C.M. Dobson. "Protein Misfolding, Evolution and Disease". Trends Biochem. Sci. 1999. 24(9): 329-332.
3. A. Nayak, A.K. Dutta, G. Belfort. "Surface-Enhanced Nucleation of Insulin Amyloid Fibrillation". Biochem. Biophys. Res. Commun. 2008. 369(2): 303-307.
4. S. Tomaselli, V. Esposito, P. Vangone, N.A.J. van Nuland, A.M.J.J. Bonvin, R. Guerrini, T. Tancredi, P.A. Temussi, D. Picone. "The α-to-β Conformational Transition of Alzheimer's Aβ-(1–42) Peptide in Aqueous Media Is Reversible: A Step by Step Conformational Analysis Suggests the Location of β Conformation Seeding". ChemBioChem. 2006. 7(2): 257-267.
5. T.P.J. Knowles, M.J. Buehler. "Nanomechanics of Functional and Pathological Amyloid Materials". Nat. Nanotechnol. 2011. 6(8): 469-479.
6. F. Chiti, C.M. Dobson. "Protein Misfolding, Functional Amyloid, and Human Disease". Annu. Rev. Biochem. 2006. 75: 333-366.
7. D.E. Barlow, G.H. Dickinson, B. Orihuela, J.L. Kulp, D. Rittschof, K.J. Wahl. "Characterization of the Adhesive Plaque of the Barnacle *Balanus amphitrite*: Amyloid-Like Nanofibrils Are a Major Component". Langmuir. 2010. 26(9): 6549-6556.
8. K. Kamino, K. Inoue, T. Maruyama, N. Takamatsu, S. Harayama, Y. Shizuri. "Barnacle Cement Proteins". J. Biol. Chem. 2000. 275(35): 27360-27365.
9. K. Kamino, S. Odo, T. Maruyama. "Cement Proteins of the Acorn-Barnacle, *Megabalanus rosa*". Biol. Bull. 1996. 190(3): 403-409.
10. P. Fratzl, R. Weinkamer. "Nature's Hierarchical Materials". Prog. Mater. Sci. 2007. 52(8): 1263-1334.
11. M. Bouchard, J. Zurdo, E.J. Nettleton, C.M. Dobson, C.V. Robinson. "Formation of Insulin Amyloid Fibrils Followed by FTIR Simultaneously with CD and Electron Microscopy". Protein Sci. 2000. 9(10): 1960-1967.
12. W. Dzwolak, V. Smirnovas, R. Jansen, R. Winter. "Insulin Forms Amyloid in a Strain-Dependent Manner: An FT-IR Spectroscopic Study". Protein Sci. 2004. 13(7): 1927-1932.
13. S. Guo, B.B. Akhremitchev. "Packing Density and Structural Heterogeneity of Insulin Amyloid Fibrils Measured by AFM Nanoindentation". Biomacromolecules. 2006. 7(5): 1630-1636.
14. J.L. Jimenez. "The Protofilament Structure of Insulin Amyloid Fibrils". Proc. Natl. Acad. Sci. U.S.A. 2002. 99(14): 9196-9201.
15. W.S. Gosal, I.J. Morten, E.W. Hewitt, A. Smith, N.H. Thomson, S.E. Radford. "Competing Pathways Determine Fibril Morphology in the Self-Assembly of β_2-Microglobulin into Amyloid". J. Mol. Biol. 2005. 351(4): 850-864.
16. M.I. Ivanova, M.R. Sawaya, M. Gingery, A. Attinger, D. Eisenberg. "An Amyloid-Forming Segment of β2-Microglobulin Suggests a Molecular Model for the Fibril". Proc. Natl. Acad. Sci. U.S.A. 2004. 101(29): 10584-10589.
17. B. Raman, E. Chatani, M. Kihara, T. Ban, M. Sakai, K. Hasegawa, H. Naiki, C.M. Rao, Y. Goto. "Critical Balance of Electrostatic and Hydrophobic Interactions Is Required for β2-Microglobulin Amyloid Fibril Growth and Stability". Biochemistry. 2005. 44(4): 1288-1299.

18. C.E. Giacomelli, W. Norde. “Influence of Hydrophobic Teflon Particles on the Structure of Amyloid β-Peptide”. Biomacromolecules. 2003. 4(6): 1719-1726.
19. M. Fandrich, M.A. Fletcher, C.M. Dobson. “Amyloid Fibrils from Muscle Myoglobin”. Nature. 2001. 410(6825): 165-166.
20. R.P.W. Davies, A. Aggeli, A.J. Beevers, N. Boden, L.M. Carrick, C.W.G. Fishwick, T.C.B. McLeish, I.A. Nyrkova, A.N. Semenov. “Self-Assembling β-Sheet Tape Forming Peptides”. Supramol. Chem. 2006. 18(5): 435-443.
21. D.M. Ridgley, E.C. Claunch, J.R. Barone. “The Effect of Processing on Large, Self-Assembled Amyloid Fibers”. Soft Matter. 2012. 8(40): 10298-10306.
22. D.M. Ridgley, J.R. Barone. “Evolution of the Amyloid Fiber over Multiple Length Scales”. ACS Nano. 2012. 7(2): 1006-1015.
23. J. Zurdo, J.I. Guijarro, C.M. Dobson. “Preparation and Characterization of Purified Amyloid Fibrils”. J. Am. Chem. Soc. 2001. 123(33): 8141-8142.
24. S. Chen, V. Berthelier, J. Bradley Hamilton, B. O’Nuallain, R. Wetzel. “Amyloid-Like Features of Polyglutamine Aggregates and Their Assembly Kinetics”. Biochemistry. 2002. 41(23): 7391-7399.
25. I. Cherny, E. Gazit. “Amyloids: Not Only Pathological Agents but Also Ordered Nanomaterials”. Angew. Chem. Int. Ed. 2008. 47(22): 4062-4069.
26. A.S. Cohen, E. Calkins. “Electron Microscopic Observations on a Fibrous Component in Amyloid of Diverse Origins”. Nature. 1959. 183(4669): 1202-1203.
27. L.L. del Mercato, G. Maruccio, P.P. Pompa, B. Bochiccio, A.M. Tamburro, R. Cingolani, R. Rinaldi. “Amyloid-Like Fibrils in Elastin-Related Polypeptides: Structural Characterization and Elastic Properties”. Biomacromolecules. 2008. 9(3): 796-803.
28. R. Diaz-Avalos. “Cross-β Order and Diversity in Nanocrystals of an Amyloid-Forming Peptide”. J. Mol. Biol. 2003. 330(5): 1165-1175.
29. E.D. Eanes, G.G. Glenner. “X-Ray Diffraction Studies on Amyloid Filaments”. J. Histochem. Cytochem. 1968. 16(11): 673-677.
30. W.S. Gosal, A.H. Clark, P.D.A. Pudney, S.B. Ross-Murphy. “Novel Amyloid Fibrillar Networks Derived from a Globular Protein: β-Lactoglobulin”. Langmuir. 2002. 18(19): 7174-7181.
31. C.P. Jaroniec, C.E. MacPhee, N.S. Astrof, C.M. Dobson, R.G. Griffin. “Molecular Conformation of a Peptide Fragment of Transthyretin in an Amyloid Fibril”. Proc. Natl. Acad. Sci. U.S.A. 2002. 99(26): 16748-16753.
32. J.L. Jimenez. “Cryo-Electron Microscopy Structure of an SH3 Amyloid Fibril and Model of the Molecular Packing”. EMBO J. 1999. 18(4): 815-821.
33. C.E. MacPhee, C.M. Dobson. “Formation of Mixed Fibrils Demonstrates the Generic Nature and Potential Utility of Amyloid Nanostructures”. J. Am. Chem. Soc. 2000. 122(51): 12707-12713.
34. F.G. Pearce, S.H. Mackintosh, J.A. Gerrard. “Formation of Amyloid-Like Fibrils by Ovalbumin and Related Proteins Under Conditions Relevant to Food Processing”. J. Agric. Food. Chem. 2007. 55(2): 318-322.
35. M.F. Perutz, J.T. Finch, J. Berriman, A. Lesk. “Amyloid Fibers Are Water-Filled Nanotubes”. Proc. Natl. Acad. Sci. U.S.A. 2002. 99(8): 5591-5595.
36. A.T. Petkova. “A Structural Model for Alzheimer’s β-Amyloid Fibrils Based on Experimental Constraints from Solid State NMR”. Proc. Natl. Acad. Sci. U.S.A. 2002. 99(26): 16742-16747.
37. N. Rubin, E. Perugia, M. Goldschmidt, M. Fridkin, L. Addadi. “Chirality of Amyloid Suprastructures”. J. Am. Chem. Soc. 2008. 130(14): 4602-4603.
38. M. Sunde, C.C.F. Blake. “From the Globular to the Fibrous State: Protein Structure and Structural Conversion in Amyloid Formation”. Q. Rev. Biophys. 1998. 31(1): 1-39.
39. M. Torok. “Structural and Dynamic Features of Alzheimer’s Aβ Peptide in Amyloid Fibrils Studied by Site-Directed Spin Labeling”. J. Biol. Chem. 2002. 277(43): 40810-40815.
40. J. Adamcik, A. Berquand, R. Mezzenga. “Single-Step Direct Measurement of Amyloid Fibrils Stiffness by Peak Force Quantitative Nanomechanical Atomic Force Microscopy”. Appl. Phys. Lett. 2011. 98(19): 193701.
41. J. Adamcik, J.M. Jung, J. Flakowski, P. De Los Rios, G. Dietler, R. Mezzenga. “Understanding Amyloid Aggregation by Statistical Analysis of Atomic Force Microscopy Images”. Nat. Nanotechnol. 2010. 5(6): 423-428.
42. J. Adamcik, R. Mezzenga. “Adjustable Twisting Periodic Pitch of Amyloid Fibrils”. Soft Matter. 2011. 7(11): 5437-5443.
43. S.G. Bolder, H. Hendrickx, L.M.C. Sagis, E. van der Linden. “Fibril Assemblies in Aqueous Whey Protein Mixtures”. J. Agric. Food. Chem. 2006. 54: 4229-4234.
44. S. Bolisetty, J. Adamcik, R. Mezzenga. “Snapshots of Fibrillation and Aggregation Kinetics in Multistranded Amyloid β-Lactoglobulin Fibrils”. Soft Matter. 2011. 7: 493-499.
45. M. Fändrich, V. Forge, K. Buder, M. Kittler, C.M. Dobson, S. Diekmann. “Myoglobin Forms Amyloid Fibrils by Association of Unfolded Polypeptide Segments”. Proc. Natl. Acad. Sci. U.S.A. 2003. 100(26): 15463.
46. S. Goda, K. Takano, Y. Yamagata, R. Nagata, H. Akutsu, S. Maki, K. Namba, K. Yutani. “Amyloid Protofilament Formation of Hen Egg Lysozyme in Highly Concentrated Ethanol Solution”. Protein Sci. 2000. 9: 369-375.
47. A. Mostaert, M.J. Higgins, T. Fukuma, F. Rindi, S.P. Jarvis. “Nanoscale Mechanical Characterization of Amyloid Fibrils Discovered in a Natural Adhesive”. J. Biol. Phys. 2006. 32: 393-401.
48. T. Scheibel, R. Parthasarathy, G. Sawicki, X.-M. Lin, H. Jaeger, S.L. Lindquist. “Conducting Nanowires Built by Controlled Self-Assembly of Amyloid Fibers and Selective Metal Deposition”. Proc. Natl. Acad. Sci. U.S.A. 2003. 100(8): 4527-4532.
49. I.A. Nyrkova, A.N. Semenov, A. Aggeli, M. Bell, N. Boden, T.C.B. McLeish. “Self-Assembly and Structure Formation in Living Polymers Forming Fibrils”. Eur. Phys. J. B. 2000. 17(3): 499-513.
50. I.A. Nyrkova, A.N. Semenov, A. Aggeli, N. Boden. “Fibril Stability in Solutions of Twisted β-Sheet Peptides: A New Kind of Micellization in Chiral Systems”. Eur. Phys. J. B. 2000. 17(3): 481-497.
51. A. Aggeli, I.A. Nyrkova, M. Bell, R. Harding, L. Carrick, T.C.B. McLeish, A.N. Semenov, N. Boden. “Hierarchical Self-Assembly of Chiral Rod-Like Molecules as a Model for Peptide β-Sheet Tapes, Ribbons, Fibrils, and Fibers”. Proc. Natl. Acad. Sci. U.S.A. 2001. 98(21): 11857-11862.
52. C. Lara, J. Adamcik, S. Jordens, R. Mezzenga. “General Self-Assembly Mechanism Converting Hydrolyzed Globular Proteins into Giant Multistranded Amyloid Ribbons”. Biomacromolecules. 2011. 12(5): 1868-1875.
53. S. Keten, M.J. Buehler. “Nanostructure and Molecular Mechanics of Spider Dragline Silk Protein Assemblies”. J. R. Soc., Interface. 2010. 7(53): 1709-1721.
54. R. Paparcone, M.J. Buehler. “Microscale Structural Model of Alzheimer Aβ(1-40) Amyloid Fibril”. Appl. Phys. Lett. 2009. 94(24): 243904-243903.
55. R. Paparcone, S. Keten, M.J. Buehler. “Atomistic Simulation of Nanomechanical Properties of Alzheimer’s Aβ(1-40) Amyloid Fibrils Under Compressive and Tensile Loading”. J. Biomech. 2010. 43(6): 1196-1201.
56. K.D. Parker, K.M. Rudall. “Structure of the Silk of *Chrysopa* Egg-Stalks”. Nature. 1957. 179(4566): 905-906.
57. A.J. Geddes, K.D. Parker, E.D. Atkins, E. Beighton. “Cross-β Conformation in Proteins”. J. Mol. Biol. 1968. 32(2): 343-358.
58. W.B. Rippon, J.M. Anderson, A.G. Walton. “Polarized Infrared Studies of a Polytripeptide with Superfolded Cross β Conformation”. J. Mol. Biol. 1971. 56(3): 507-513.
59. R.D.B. Fraser, T.P. MacRae. “Conformation in Fibrous Proteins and Related Synthetic Polypeptides”. New York: Academic Press, 1973.
60. K.M. Rudall. “Silk and Other Cocoon Proteins”. In: M. Florkin, H.S. Mason, editors. Comparative Biochemistry: A Comprehensive Treatise. Constituents of Life Part B. New York: Academic Press, 1962. Vol. IV.
61. H.J. Jin, D.L. Kaplan. “Mechanism of Silk Processing in Insects and Spiders”. Nature. 2003. 424(6952): 1057-1061.
62. V. Villegas, J. Zurdo, V.V. Filimonov, F.X. Avilés, C.M. Dobson, L. Serrano. “Protein Engineering as a Strategy to Avoid Formation of Amyloid Fibrils”. Protein Sci. 2000. 9(9): 1700-1708.
63. M. Krebs, E. Bromley, A. Donald. “The Binding of Thioflavin-T to Amyloid Fibrils: Localisation and Implications”. J. Struct. Biol. 2005. 149(1): 30-37.
64. M. Wakabayashi, K. Matsuzaki. “Formation of Amyloids by Aβ-(1–42) on NGF-Differentiated PC12 Cells: Roles of Gangliosides and Cholesterol”. J. Mol. Biol. 2007. 371(4): 924-933.
65. D.M. Ridgley, K.C. Ebanks, J.R. Barone. “Peptide Mixtures Can Self-Assemble into Large Amyloid Fibers of Varying Size and Morphology”. Biomacromolecules. 2011. 12(10): 3770-3779.
66. M. Balbirnie, R. Grothe, D.S. Eisenberg. “An Amyloid-Forming Peptide from the Yeast Prion Sup35 Reveals a Dehydrated β-Sheet Structure for Amyloid”. Proc. Natl. Acad. Sci. U.S.A. 2001. 98(5): 2375-2380.
67. K. Halverson, P.E. Fraser, D.A. Kirschner, P.T. Lansbury. “Molecular Determinants of Amyloid Deposition in Alzheimer’s Disease: Conformational Studies of Synthetic β-Protein Fragments”. Biochemistry. 1990. 29(11): 2639-2644.

68. S. Krimm, J. Bandekar. "Vibrational Spectroscopy and Conformation of Peptides, Polypeptides, and Proteins". In: C.B. Anfinsen, J.T. Edsall, F.M. Richards, editors. Advances in Protein Chemistry. Orlando: Academic Press, Inc., 1986. Vol. 38, Pp. 181-364.
69. T. Miyazawa, T. Shimanouchi, S.I. Mizushima. "Characteristic Infrared Bands of Monosubstituted Amides". J. Chem. Phys. 1956. 24(2): 408-418.
70. W.K. Surewicz, H.H. Mantsch. "New Insight into Protein Secondary Structure from Resolution-Enhanced Infrared Spectra". Biochim. Biophys. Acta. 1988. 952(2): 115-130.
71. E.R. Blout, M. Idelson. "Polypeptides. VI. Poly-α-L-Glutamic Acid: Preparation and Helix-Coil Conversion". J. Am. Chem. Soc. 1956. 78(2): 497-498.
72. H. Lenormant, A. Baudras, E.R. Blout. "Reversible Configurational Changes in Sodium Poly-α-L-Glutamate Induced by Water". J. Am. Chem. Soc. 1958. 80(23): 6191-6195.
73. R.D.B. Fraser, B.S. Harrap, T.P. MacRae, F.H.C. Stewart, E. Suzuki. "Effect of Glycyl Residues on the Stability of the α-Helix". Biopolymers. 1967. 5(3): 221-257.
74. N.A. Nevskaya, Y.N. Chirgadze. "Infrared Spectra and Resonance Interactions of Amide-I and II Vibrations of α-Helix". Biopolymers. 1976. 15(4): 637-648.
75. G. Vendantham, H.G. Sparks, S.U. Sane, S. Tzannis, T.M. Przybycien. "A Holistic Approach for Protein Secondary Structure Estimation from Infrared Spectra in H_2O Solutions". Anal. Biochem. 2000. 285(1): 33-49.
76. T.F. Kumosinski, J.J. Unruh. "Quantitation of the Global Secondary Structure of Globular Proteins by FTIR Spectroscopy: Comparison with X-Ray Crystallographic Structure". Talanta. 1996. 43(2): 199-219.
77. G. Vecchio, A. Bossi, P. Pasta, G. Carrea. "Fourier-Transform Infrared Conformational Study of Bovine Insulin in Surfactant Solutions". Int. J. Pept. Protein Res. 1996. 48(2): 113-117.
78. A. Athamneh, J.R. Barone. "Enzyme-Mediated Self-Assembly of Highly Ordered Structures from Disordered Proteins". Smart Mater. Struct. 2009. 18(10): 104024-104031.
79. G. Zandomeneghi, M.R.H. Krebs, M.G. McCammon, M. Fandrich. "FTIR Reveals Structural Differences Between Native β-Sheet Proteins and Amyloid Fibrils". Protein Sci. 2004. 13(12): 3314-3321.
80. A. Dong, P. Huang, W.S. Caughey. "Protein Secondary Structures in Water from Second-Derivative Amide I Infrared Spectra". Biochemistry. 1990. 29(13): 3303-3308.
81. J. Kubelka, T.A. Keiderling. "Differentiation of β-Sheet-Forming Structures: Ab Initio-Based Simulations of IR Absorption and Vibrational CD for Model Peptide and Protein β-Sheets". J. Am. Chem. Soc. 2001. 123(48): 12048-12058.
82. U. Böcker, R. Ofstad, Z. Wu, H.C. Bertram, G.D. Sockalingum, M. Manfait, B. Egelandsdal, A. Kohler. "Revealing Covariance Structures in Fourier Transform Infrared and Raman Microspectroscopy Spectra: A Study on Pork Muscle Fiber Tissue Subjected to Different Processing Parameters". Appl. Spectrosc. 2007. 61(10): 1032-1039.
83. H.G.M. Edwards, D.E. Hunt, M.G. Sibley. "FT-Raman Spectroscsopic Study of Keratotic Materials: Horn, Hoof, and Tortoiseshell". Spectrochim. Acta, Part A. 1998. 54(5): 745-757.
84. T.J. Yu, J.L. Lippert, W.L. Peticolas. "Laser Raman Studies of Conformational Variations of Poly-L-Lysine". Biopolymers. 1973. 12(9): 2161-2176.
85. J.F. Rabolt. "Vibrational Analysis of Peptides, Polypeptides, and Proteins. 3. α-Poly(L-Alanine)". Macromolecules. 1977. 10(5): 1065-1074.
86. R.W. Williams. "Determination of the Secondary Structure of Proteins from the Amide I Band of the Laser Raman Spectrum". J. Mol. Biol. 1981. 152(4): 783-813.
87. J.T. Pelton, L.R. McLean. "Spectroscopic Methods for Analysis of Protein Secondary Structure". Anal. Biochem. 2000. 277(2): 167-176.
88. V.A. Shashilov, V. Sikirzhytski, L.A. Popova, I.K. Lednev. "Quantitative Methods for Structural Characterization of Proteins Based on Deep UV Resonance Raman Spectroscopy". Methods. 2010. 52(1): 23-37.
89. M. Xu, V. Shashilov, I.K. Lednev. "Probing the Cross-β Core Structure of Amyloid Fibrils by Hydrogen–Deuterium Exchange Deep Ultraviolet Resonance Raman Spectroscopy". J. Am. Chem. Soc. 2007. 129(36): 11002-11003.
90. V. Sikirzhytski, N.I. Topilina, S. Higashiya, J.T. Welch, I.K. Lednev. "Genetic Engineering Combined with Deep UV Resonance Raman Spectroscopy for Structural Characterization of Amyloid-like Fibrils". J. Am. Chem. Soc. 2008. 130(18): 5852-5853.
91. L.A. Popova, R. Kodali, R. Wetzel, I.K. Lednev. "Structural Variations in the Cross-β Core of Amyloid β Fibrils Revealed by Deep UV Resonance Raman Spectroscopy". J. Am. Chem. Soc. 2010. 132(18): 6324-6328.
92. S. Sivakesava, J. Irudayaraj. "Rapid Determination of Tetracycline in Milk by FT-MIR and FT-NIR Spectroscopy". J. Dairy Sci. 2002. 85(3): 487-493.
93. M.C. Zenobi, C.V. Luengo, M.J. Avena, E.H. Rueda. "An ATR-FTIR Study of Different Phosphonic Acids in Aqueous Solution". Spectrochim. Acta, Part A. 2008. 70(2): 270-276.
94. S. Boyd, J. Kirkwood. "Quantitative Analysis Using ATR-FTIR Spectroscopy". Agilent Technologies Application Note. Santa Clara, CA: Agilent Technologies, Inc., 2011.
95. D.M. Byler, H. Susi. "Examination of the Secondary Structure of Proteins by Deconvolved FTIR Spectra". Biopolymers. 1986. 25(3): 469-487.
96. J.L.R. Arrondo, A. Muga, J. Castresana, F.M. Goñi. "Quantitative Studies of the Structure of Proteins in Solution by Fourier-Transform Infrared Spectroscopy". Prog. Biophys. Mol. Biol. 1993. 59(1): 23-56.
97. W.K. Surewicz, H.H. Mantsch, D. Chapman. "Determination of Protein Secondary Structure by Fourier Transform Infrared Spectroscopy: A Critical Assessment". Biochemistry. 1993. 32(2): 389-394.
98. S. Weisman, H.E. Trueman, S.T. Mudie, J.S. Church, T.D. Sutherland, V.S. Haritos. "An Unlikely Silk: The Composite Material of Green Lacewing Cocoons". Biomacromolecules. 2008. 9(11): 3065-3069.
99. H. Susi, D.M. Byler. "Resolution-Enhanced Fourier Transform Infrared Spectroscopy of Enzymes". Methods Enzymol. 1986. 130: 290-311.
100. M. Bradley. "Curve Fitting in Raman and IR Spectroscopy: Basic Theory of Line Shapes and Applications". In: I. Thermo Fisher Scientific, editor. Madison, WI: Thermo Fisher Scientific, Inc., 2007. Vol. 50733.
101. F. Chiti, C.M. Dobson. "Amyloid Formation by Globular Proteins Under Native Conditions". Nat. Chem. Biol. 2009. 5(1): 15-22.
102. F. Chiti, N. Taddei, M. Bucciantini, P. White, G. Ramponi, C.M. Dobson. "Mutational Analysis of the Propensity for Amyloid Formation by a Globular Protein". EMBO J. 2000. 19(7): 1441-1449.
103. M. Boulet-Audet, T. Buffeteau, S. Boudreault, N. Daugey, M. Peìzolet. "Quantitative Determination of Band Distortions in Diamond Attenuated Total Reflectance Infrared Spectra". J. Phys. Chem. B. 2010. 114(24): 8255-8261.
104. A. Barth, C. Zscherp. "What Vibrations Tell Us About Proteins". Q. Rev. Biophys. 2002. 35(4): 369-430.
105. J. Kong, S. Yu. "Fourier Transform Infrared Spectroscopic Analysis of Protein Secondary Structures". Acta Biochim. Biophys. Sin. 2007. 39(8): 549-559.
106. H.H.J. de Jongh, E. Goormaghtigh, J.M. Ruysschaert. "The Different Molar Absorptivities of the Secondary Structure Types in the Amide I Region: An Attenuated Total Reflection Infrared Study on Globular Proteins". Anal. Biochem. 1996. 242(1): 95-103.
107. Y.N. Chirgadze, O.V. Fedorov, N.P. Trushina. "Estimation of Amino Acid Residue Side-Chain Absorption in the Infrared Spectra of Protein Solutions in Heavy Water". Biopolymers. 1975. 14(4): 679-694.
108. A. Barth. "The Infrared Absorption of Amino Acid Side Chains". Prog. Biophys. Mol. Biol. 2000. 74(3–5): 141-173.
109. H. Gunzler, H.U. Gremlich. "IR Spectroscopy". Weinheim, Germany: Wiley-VCH, 2002.
110. S.Y. Venyaminov, N.N. Kalnin. "Quantitative IR Spectrophotometry of Peptide Compounds in Water (H_2O) Solutions. I. Spectral Parameters of Amino Acid Residue Absorption Bands". Biopolymers. 1990. 30(13–14): 1243-1257.
111. S. Stewart, P.M. Fredericks. "Surface-Enhanced Raman Spectroscopy of Amino Acids Adsorbed on an Electrochemically Prepared Silver Surface". Spectrochim. Acta, Part A. 1999. 55(7–8): 1641-1660.
112. B. Hernandez, F. Pfluger, M. Nsangou, M. Ghomi. "Vibrational Analysis of Amino Acids and Short Peptides in Hydrated Media: IV. Amino Acids with Hydrophobic Side Chains: L-Alaine, L-Valine, and L-Isoleucine". J. Phys. Chem. B. 2009. 113(10): 3169-3178.
113. V. Castelletto, I.W. Hamley, J. Adamcik, R. Mezzenga, J. Gummel. "Modulating Self-Assembly of a Nanotape-Forming Peptide Amphiphile with an Oppositely Charged Surfactant". Soft Matter. 2012. 8(1): 217-226.
114. N.H.H. Heegaard, T.J.D. Jørgensen, N. Rozlosnik, D.B. Corlin, J.S. Pedersen, A.G. Tempesta, P. Roepstorff, R. Bauer, M.H. Nissen. "Unfolding, Aggregation, and Seeded Amyloid Formation of Lysine-58-Cleaved β2-Microglobulin". Biochemistry. 2005. 44(11): 4397-4407.
115. G. Guiffo-Soh, B. Hernández, Y.M. Coïc, F.Z. Boukhalfa Heniche, M. Ghomi. "Vibrational Analysis of Amino Acids and Short Peptides in Hydrated Media. II. Role of KLLL Repeats To Induce Helical Conformations in Minimalist LK-Peptides". J. Phys. Chem. B. 2007. 111(43): 12563-12572.
116. G. Guiffo-Soh, B. Hernandez, Y.M. Coic, F.Z. Boukhalfa-Heniche, G. Fadda, M. Ghomi. "Vibrational Analysis of Amino Acids and Short Peptides in Hydrated Media. 3. Successive KL Repeats Induce Highly

Stable β-Strands Capable of Forming Non-H-Bonded Aggregates". J. Phys. Chem. B. 2008. 112(4): 1282-1289.
117. M.F. Perutz, T. Johnson, M. Suzuki, J.T. Finch. "Glutamine Repeats as Polar Zippers: Their Possible Role in Inherited Neurodegenerative Diseases". Proc. Natl. Acad. Sci. U.S.A. 1994. 91(12): 5355-5358.
118. A.H. DePace, A. Santoso, P. Hillner, J.S. Weissman. "A Critical Role for Amino-Terminal Glutamine/Asparagine Repeats in the Formation and Propagation of a Yeast Prion". Cell. 1998. 93(7): 1241-1252.
119. E. Scherzinger, A. Sittler, K. Schweiger, V. Heiser, R. Lurz, R. Hasenbank, G.P. Bates, H. Lehrach, E.E. Wanker. "Self-Assembly of Polyglutamine-Containing Huntingtin Fragments into Amyloid-Like Fibrils: Implications for Huntington's Disease Pathology". Proc. Natl. Acad. Sci. U.S.A. 1999. 96(8): 4604-4609.
120. P. Sikorski, E. Atkins. "New Model for Crystalline Polyglutamine Assemblies and Their Connection with Amyloid Fibrils". Biomacromolecules. 2005. 6(1): 425-432.
121. R.W. Williams. "Estimation of Protein Secondary Structure from the Laser Raman Amide I Spectrum". J. Mol. Biol. 1983. 166(4): 581.
122. B.G. Frushour. "Raman Spectroscopy of Proteins". Adv. Infrared Raman Spectrosc. 1975. 1: 35.
123. C.Y. Huang, G. Balakrishnan, T.G. Spiro. "Protein Secondary Structure from Deep-UV Resonance Raman Spectroscopy". J. Raman Spectrosc. 2006. 37(1–3): 277-282.
124. W.H. Moore, S. Krimm. "Vibrational Analysis of Peptides, Polypeptides, and Proteins. I. Polyglycine I". Biopolymers. 1976. 15(12): 2439-2464.
125. W.H. Moore, S. Krimm. "Vibrational Analysis of Peptides, Polypeptides, and Proteins. II. β-Poly(L-alanine) and β-Poly(L-alanylglycine)". Biopolymers. 1976. 15(12): 2465-2483.
126. J.L. Lippert, D. Tyminski, P.J. Desmeules. "Determination of the Secondary Structure of Proteins by Laser Raman Spectroscopy". J. Am. Chem. Soc. 1976. 98(22): 7075-7080.
127. R.W. Williams, T. Cutrera, A.K. Dunker, W.L. Peticolas. "The Estimation of Protein Secondary Structure by Laser Raman Spectroscopy from the Amide III′ Intensity Distribution". FEBS Lett. 1980. 115(2): 306-308.
128. R.W. Williams. "Protein Secondary Structure Analysis Using Raman Amide I and Amide III Spectra". Methods Enzymol. 1986. 130: 311-331.
129. J. Sirichaisit, V.L. Brookes, R.J. Young, F. Vollrath. "Analysis of Structure/Property Relationships in Silkworm (*Bombyx mori*) and Spider Dragline (*Nephila edulis*) Silks Using Raman Spectroscopy". Biomacromolecules. 2003. 4(2): 387-394.
130. M.E. Rousseau, T. Lefèvre, L. Beaulieu, T. Asakura, M. Pézolet. "Study of Protein Conformation and Orientation in Silkworm and Spider Silk Fibers Using Raman Microspectroscopy". Biomacromolecules. 2004. 5(6): 2247-2257.
131. M.-E. Rousseau, L. Beaulieu, T. Lefèvre, J. Paradis, T. Asakura, M. Pézolet. "Characterization by Raman Microspectroscopy of the Strain-Induced Conformational Transition in Fibroin Fibers from the Silkworm *Samia cynthia ricini*". Biomacromolecules. 2006. 7(9): 2512-2521.
132. T. Lefèvre, S. Boudreault, C. Cloutier, M. Pézolet. "Conformational and Orientational Transformation of Silk Proteins in the Major Ampullate Gland of *Nephila clavipes* Spiders". Biomacromolecules. 2008. 9(9): 2399-2407.
133. S.A. Asher, A. Ianoul, G. Mix, M.N. Boyden, A. Karnoup, M. Diem, R. Schweitzer-Stenner. "Dihedral ψ Angle Dependence of the Amide III Vibration: A Uniquely Sensitive UV Resonance Raman Secondary Structural Probe". J. Am. Chem. Soc. 2001. 123(47): 11775-11781.
134. A.V. Mikhonin, N.S. Myshakina, S.V. Bykov, S.A. Asher. "UV Resonance Raman Determination of Polyproline II, Extended 2.51-Helix, and β-Sheet Ψ Angle Energy Landscape in Poly-l-Lysine and Poly-l-Glutamic Acid". J. Am. Chem. Soc. 2005. 127(21): 7712-7720.
135. A.V. Mikhonin, S.V. Bykov, N.S. Myshakina, S.A. Asher. "Peptide Secondary Structure Folding Reaction Coordinate: Correlation between UV Raman Amide III Frequency, Ψ Ramachandran Angle, and Hydrogen Bonding". J. Phys. Chem. B. 2006. 110(4): 1928-1943.
136. S. Stewart, P.M. Fredericks. "Surface-Enhanced Raman Spectroscopy of Peptides and Proteins Adsorbed on an Electrochemically Prepared Silver Surface". Spectrochim. Acta, Part A. 1999. 55(7–8): 1615-1640.
137. L. Rintoul, E.A. Carter, S.D. Stewart, P.M. Fredericks. "Keratin Orientation in Wool and Feathers by Polarized Raman Spectroscopy". Biopolymers. 2000. 57(1): 19-28.
138. T. LefeÌvre, M.E. Rousseau, M. Peìzolet. "Protein Secondary Structure and Orientation in Silk as Revealed by Raman Spectromicroscopy". Biophys. J. 2007. 92: 2885-2895.

Chapter 5.

Evolution of the Amyloid Fiber over Multiple Length Scales

Ridgley, D. M., and J. R. Barone. 2013. Evolution of the Amyloid Fiber over Multiple Length Scales. *ACS Nano* 7(2):1006-1015. - Reproduced with generous permission of the America Chemical Society.

Evolution of the Amyloid Fiber over Multiple Length Scales

Devin M. Ridgley and Justin R. Barone*

Biological Systems Engineering Department, Virginia Tech, 303 Seitz Hall, Blacksburg, Virginia 24061, United States

ABSTRACT The amyloid is a natural self-assembled peptide material comparable in specific stiffness to spider silk and steel. Throughout the literature there are many studies of the nanometer-sized amyloid fibril; however, peptide mixtures are capable of self-assembling beyond the nanometer scale into micrometer-sized fibers. Here, atomic force microscopy (AFM) and scanning electron microscopy (SEM) are used to observe the self-assembly of the peptide mixtures in solution for 20 days and the fibers upon drying. Beyond the nanometer scale, self-assembling fibers differentiate into two morphologies, cylindrical or rectangular cross-section, depending on peptide properties. Microscopic observations delineate a four stage self-assembly mechanism: (1) protofibril (2—4 nm high and 15—30 nm wide) formation; (2) protofibril aggregation into fibrils 6—10 nm high and 60—120 nm wide; (3) fibril aggregation into large fibrils and morphological differentiation where large fibrils begin to resemble the final fiber morphology of cylinders (WG peptides) or tapes (Gd:My peptides). WG large fibrils are 50 nm high and 480 nm wide and Gd:My large fibrils are 10 nm high and 150 nm wide; (4) micrometer-sized fiber formation upon drying at 480 h resulting in 18.0 μm diameter cylindrical fibers (WG peptides) and 14.0 μm wide and 6.0 μm thick flat tapes (Gd:My peptides). Evolution of the large fiber morphology can be rationalized on the basis of the peptide properties.

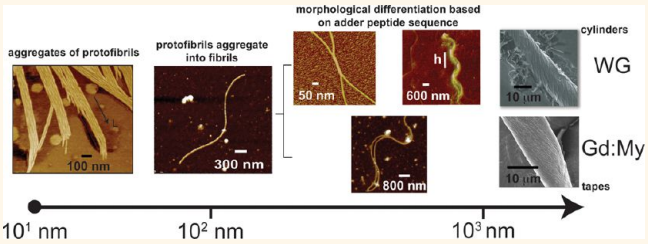

KEYWORDS: self-assembly · protein · cross-β structure · amyloid · fibril · fiber

Amyloids are self-assembled protein materials containing β-sheets.[1−4] There is a large body of work focused on amyloids in pathogenic "prion" diseases such as Alzheimer's, Parkinson's, and Huntington's Diseases.[1,3−5] Self-assembly begins when a protein molecule "misfolds", straightens out, and hydrogen bonds to another misfolded, straight protein molecule to build the β-sheet. Thus these diseases are also termed "protein misfolding diseases". It is now believed that this small β-sheet aggregate is the pathogenic structure in disease pathology. These small β-sheet aggregates can continue to aggregate into protofibrils with diameters of 1−10 nm and lengths of >100 nm. Several protofibrils can then aggregate together into the prion "plaques" observed in advanced prion disease.[6] In amyloid fibrils, the protein chain axis is perpendicular to the fibril axis and thus the β-sheets are termed "cross-β" sheets. In contrast, the protein chain axis and resulting β-sheets in natural silk and β-keratin fibers are aligned along the fiber axis. This is because of the applied deformation required to form the silk or β-keratin fiber, that is, spinning or extrusion. The cross-β structure can be differentiated from β-sheets aligned along the fiber using vibrational spectroscopy or X-ray diffraction.[7,8]

Not all amyloids are detrimental structures. Nature is able to produce a class of beneficial self-assembled structures known as "functional" amyloids meant to proliferate life.[3,9,10] Barnacle cement has been shown to be a rigid, strong, and tough adhesive because it is a composite of insoluble cross-β fibrils in a protein matrix.[11−15] The bacterium *Streptomyces coelicolor* and fungus *Neurospora crassa* self-assemble proteins into extracellular amyloid fibrils and hyphae, respectively, for adhesion and biofilm formation.[10,16] *Escherichia coli* will secrete curli proteins CsgA and CsgB to form fibrous amyloids on the cell surface.[17−21] Cell adhesion proteins on *Candida albicans* form rigid amyloid fibers.[22] Insects of the *Chrysopidae* family form cross-β silks to suspend their eggs for protection.[23,24]

The fibrous amyloid is similar in rigidity to other β-sheet containing protein fibers and the specific modulus approaches that of steel.[25−27] Thus, very rigid materials are

* Address correspondence to jbarone@vt.edu.

Received for review August 2, 2012 and accepted December 23, 2012.

Published online December 26, 2012
10.1021/nn303489a

© 2012 American Chemical Society

formed from a host of weak hydrogen bonds. It has been shown that β-sheets confined to a few nanometers achieve higher modulus, strength, and toughness than larger β-sheets.[28] The smaller β-sheets, about 3 nm in size, give a stick−slip shear response to applied deformation, whereas larger β-sheets, about 7 nm in size, bend. Young's modulus calculated from molecular dynamics and density functional theory yield values of 22.6 and 36.5 GPa, respectively, which agree well with experiment.[26] Thus the size and hierarchy of β-sheet structures in the amyloid influences the properties. Amyloid fibrils have also shown great solvent and temperature resistance, and the fact that no known cure exists for prion disease is a testament to the robustness of the self-assembled β-sheet structure.[29] The outstanding physical properties and observed functional role of amyloids in nature serve as inspiration to use the self-assembled structures as high performance biomaterials in unique nanodevices and nanocomposites.[30−34]

Nanometer-sized amyloid fibrils can spontaneously self-assemble from a host of proteins and peptides.[9,30,35−43] Past studies have documented the growth and morphological development of the nanometer-sized amyloid fibril under various conditions.[34,37,43−69] It is generally accepted that any protein is capable of self-assembling into an amyloid fibril given the right conditions, which are usually extremely denaturing.[3,4] Several studies have implicated a nucleation site or seed in order for amyloid formation to occur.[70,71] Amyloid fibril size is dependent on the peptide or protein used and has been shown to be about 2−10 nm wide with some larger structures forming through aggregation of smaller structures.[40,63,72,73] Solution conditions can also affect the amyloid fibril size and morphology.[74−76] Adamcik *et al.* were able to self-assemble multiple fibrils into twisted tapes with adjustable pitches based on the solution NaCl concentration.[64] The highly studied Aβ(1−40) peptide implicated in prion disease can aggregate into β-structured polymorphs ranging from amorphous aggregates to fibril morphologies by varying NaCl, Zn^{2+}, and SDS concentrations in the incubating solutions.[77]

Fibers larger than nanometer-sized fibrils have been predicted in several studies.[40,78−80] Tapes composed of fibrils can be self-assembled up to approximately 150 nm in width.[81] Recent research has shown that it is possible to self-assemble micrometer-sized amyloid fibers from peptide mixtures.[35,36,75] This mechanism is similar to a previous hypothesis that requires a nucleation site or seed for initiation of cross-β formation and fibril growth.[70,82,83] Extensive research into the self-assembly of fibrils on the nanometer scale has been performed; however, little is understood about the mechanism of self-assembly beyond the nanometer scale, especially in terms of how self-assembling peptide systems can morphologically differentiate beginning at smaller scales and how the morphology persists to higher scales. Here, two peptide mixtures, hydrolyzed wheat gluten (WG) and hydrolyzed gliadin:unhydrolyzed myoglobin (Gd:My), are monitored in solution for 20 days with atomic force microscopy (AFM) and upon drying with scanning electron microscopy (SEM) to elucidate the mechanism for self-assembly of amyloid fibers from the molecular to the micrometer scale. Differences between the peptides in the two mixtures manifest at the nanometer scale and continue through the hierarchy to produce micrometer-sized fibers and tapes with different properties and morphologies. Hierarchical micrometer-sized fibers are the structural material of choice in nature. This research shows that peptide systems can be designed at the molecular level to produce useful, large-scale biomimetic materials that are predictable and controllable.

RESULTS AND DISCUSSION

Trypsin-hydrolyzed wheat gluten and gliadin produce a mixture of peptides that can be used for self-assembly over several orders of magnitude of scale. Wheat gluten is a combination of gliadin and glutenin proteins and replacing the hydrolyzed glutenin fraction with unhydrolyzed myoglobin produces a tape rather than a fiber.[35] Although the hydrolysis produces several peptides, only certain peptides in the mixture have a propensity to self-assemble.[35,75] Those peptides have since been individually synthesized and mixed together and with myoglobin producing similar results to the crude mixture.[35] In the proposed mechanism, a hydrophobic "template" peptide forms a cross-β template to hide hydrophobic amino acid side groups in spaces between β-sheets. The template peptide has hydrophobic amino acids residing next to one another and thus has some hydrophobic groups exposed to the water on the outer faces of the β-sheets (Scheme 1, Stage I). Hydrolyzed gliadin produces the template peptide, Gd20.[35] The "adder" peptide or protein is α-helical and less hydrophobic than the template peptide. A glutenin peptide, GtL75, acts as the adder in the WG system and myoglobin acts as the adder protein in the Gd:My system. The more hydrophilic adder peptide or protein is stable in aqueous solution and does not individually undergo conformation change or aggregate at the experimental conditions as measured with FT-IR spectroscopy.[35,36] However, in the presence of the template, the hydrophobic groups on the α-helices prefer the exposed hydrophobic groups of the template, undergo an α to β transition, and "add" into the template as measured with Fourier transform-infrared (FT-IR) spectroscopy.[35,75] Through AFM and SEM imaging, the progression of large amyloid fiber aggregation can be defined in terms of four morphological stages.

Stage I: Protofibril Formation (*ca.* 0−264 h). WG peptides aggregate into protofibrils $H = 2.5 \pm 0.5$ nm high and

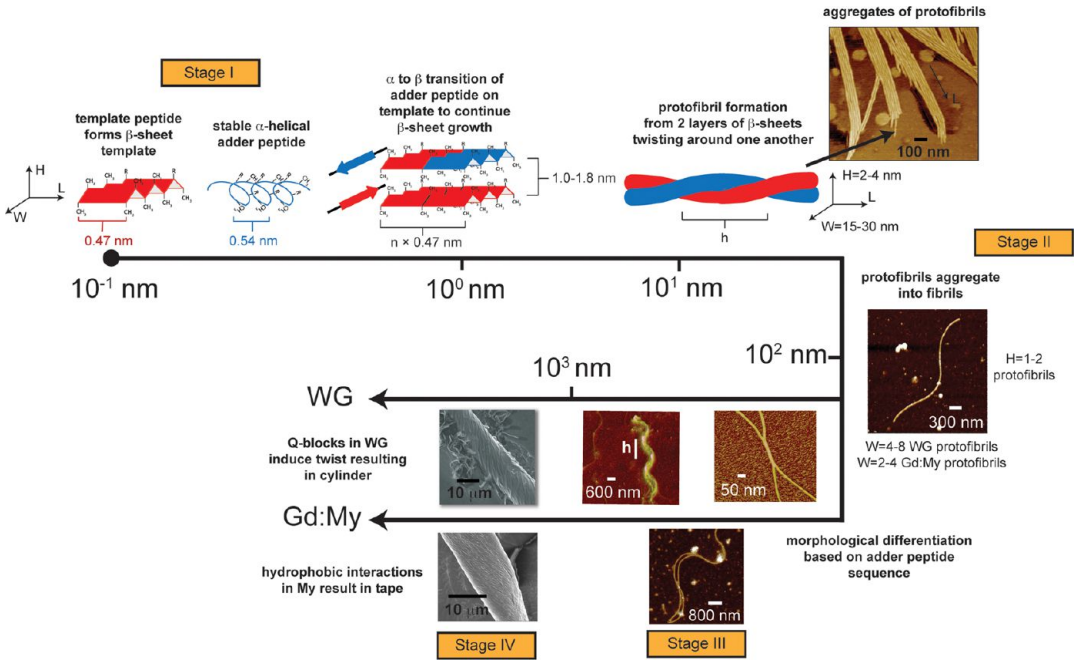

Scheme 1. Four-stage mechanism for peptide mixture aggregation over multiple length scales. In Stage I, the adder peptide is shown adding to the upper β-sheet length and adding to the lower β-sheet height, which are both possible. Morphological differentiation and growth to the micrometer-scale occur in Stages III and IV.

$W = 16.5 \pm 4.5$ nm wide. Gd:My peptides aggregate into protofibrils with $H = 4.3 \pm 1.0$ nm and $W = 31.6 \pm 3.2$ nm with a large protofibril depicted in Figure 1c. X-ray diffraction results show that the protofibril is 2 β-sheet layers high and the distance between sheets is mediated by the largest amino acid side chains.[36] My (17083 g/mol) has a larger molecular weight than GtL75 (8,465 g/mol), and the unassembled chain length also contributes to the observed larger protofibrils.[73] WG protofibrils separate from larger globules while Gd:My protofibrils appear spontaneously (Figure 1c,d). The largest molecular secondary structure transitions occur in Stage I in both WG and Gd:My peptide mixtures.[35]

Stage II: Protofibril Aggregation into Fibrils (*ca.* 240−360 h). Protofibrils aggregate to form larger structures termed fibrils. WG fibrils have $H = 6.7 \pm 2.0$ nm and $W = 82.9 \pm 26.1$ nm (Figure 2a). Gd:My fibrils are $H = 8.6 \pm 2.3$ nm high and $W = 101.0 \pm 28.8$ nm wide (Figures 1c and 2b). FT-IR spectra also reveal an increase in the ratio of the symmetric CH_3 deformation, δ_s, to the asymmetric CH_3 deformation, δ_{as}, throughout the four-stage mechanism. An increase in δ_s/δ_{as} suggests that hydrophobic interactions between peptides play a significant role in conformation change and further self-assembly.[35] Thus, exposed hydrophobic groups on protofibrils continue to hide from water and drive self-assembly. The width of the fibril is composed of 4−8 and 2−4 protofibrils aggregating laterally in the WG and Gd:My systems, respectively. Measured fibril heights are consistent with 1−2 protofibrils aggregating vertically and twisting. Protofibril and fibril formation appear consistent with what has been observed by others where tapes ~2 nm high and 4−10 nm wide form from 2 nm diameter protofibrils aggregating horizontally and twisting[63,64] or "protofilaments" assembling into fibrils in the same manner that protofibrils assemble into fibrils as shown in Figures 1 and 2.[72,73,81,84,85]

The Gd:My fibril structure in Figure 2b resembles the "nanoracket" predicted for Aβ(1−40) fibrils.[6] Gd:My fibrils (also shown in Figure 3) appear to have a lower persistence length, l_p, than WG fibrils and can bend onto themselves. Hydrophobic interactions near the ends of the fibril produce the nanoracket. An estimate of the persistence length for WG and Gd:My Stage II fibrils yields $l_{p,WG} = 1681 \pm 494$ nm and $l_{p,Gd:My} = 1074 \pm 304$ nm. Adamcik *et al.* formed fibrils from the same peptides and found persistence length to scale with the fibril height with thicker fibrils giving a longer persistence length.[63] In Stage II, WG fibrils are narrower and thinner than Gd:My fibrils but possess a longer persistence length, indicating that WG peptides self-assemble into a tighter and more rigid structure. The persistence length is directly proportional to the Young's modulus of the fibril, and thus the Stage II persistence lengths show that property differences between the two systems begin to manifest early in the self-assembly process.

Stage III: Fibril Aggregation into Large Fibrils and Morphological Differentiation (*ca.* 288−480 h). Fibrils aggregate into larger structures termed "large fibrils". WG fibrils twist around each other to form a large fibril with $H = 51.5 \pm 5.8$ nm and $W = 483.5 \pm 30.3$ nm (Figure 3a). The WG large fibril in Figure 2a has $H = 14.0$ nm and $W = 200.0$ nm and shows an intermediate structure

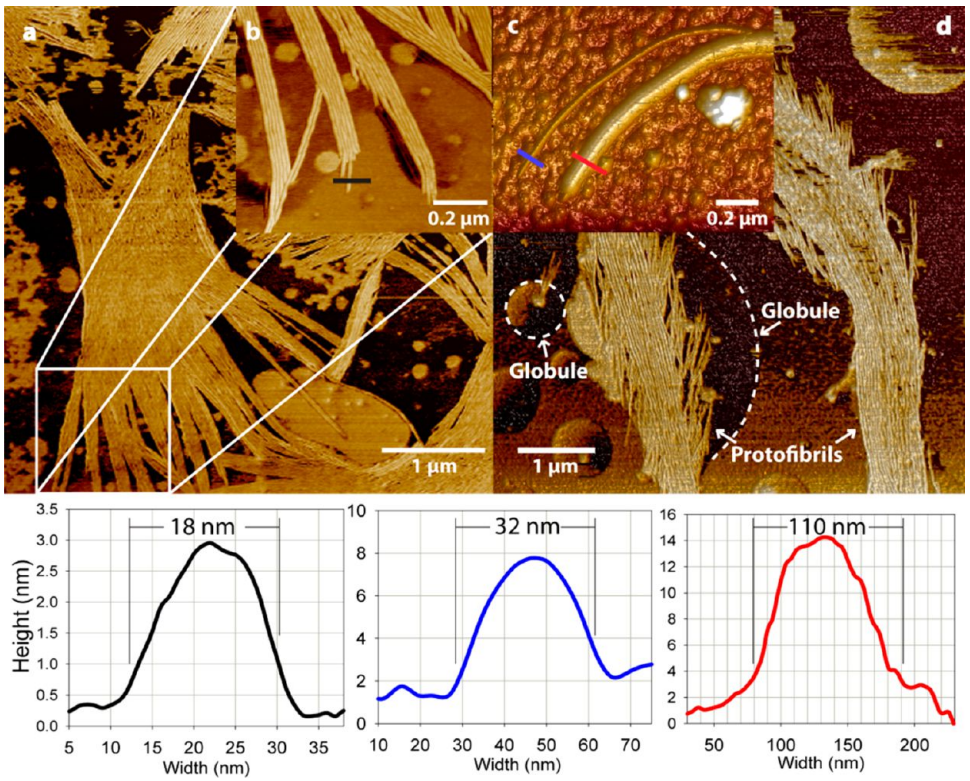

Figure 1. Stage I: (a,b) AFM tapping phase images showing WG aggregated fibrils composed of individual protofibrils of $H = 2.8$ nm and $W = 18.0$ nm (black). (c) AFM topographical image of a large Gd:My protofibril of $H = 6.0$ nm and $W = 32.0$ nm (blue) and fibril of $H = 14.0$ nm and $W = 110.0$ nm (red). (d) AFM tapping phase image of WG fibrils composed of individual protofibrils separating from large globules at very early time.

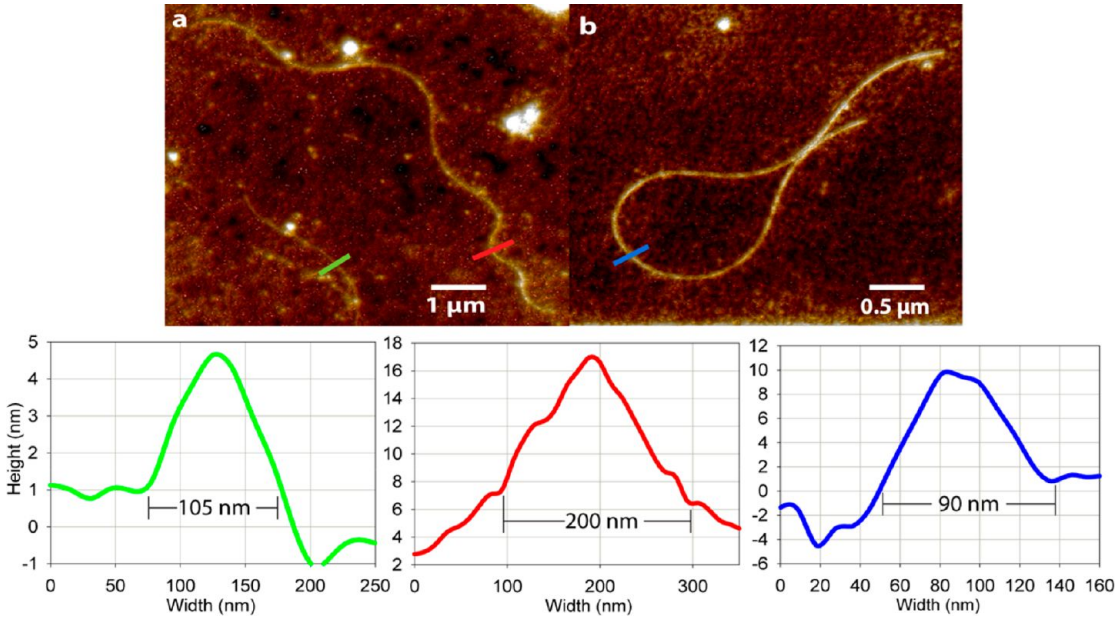

Figure 2. Stage II: AFM topographical images of (a) WG fibril (green) and large fibril (red) and (b) Gd:My fibril (blue).

between Stages II and III. The cross-section is still anisotropic but the beginnings of the final twisted morphology appear in solution at late times. Gd:My fibrils have limited aggregation into large fibrils with $H = 9.8 \pm 1.2$ nm and $W = 155.7 \pm 23.2$ nm (Figure 3b). The final rectangular cross-section of large Gd:My fibers begins in solution and persists upon drying. This is the predominant structure in Stage III.

Morphological differentiation occurs in Stage III where about 4−8 WG fibrils twist into a large fibril

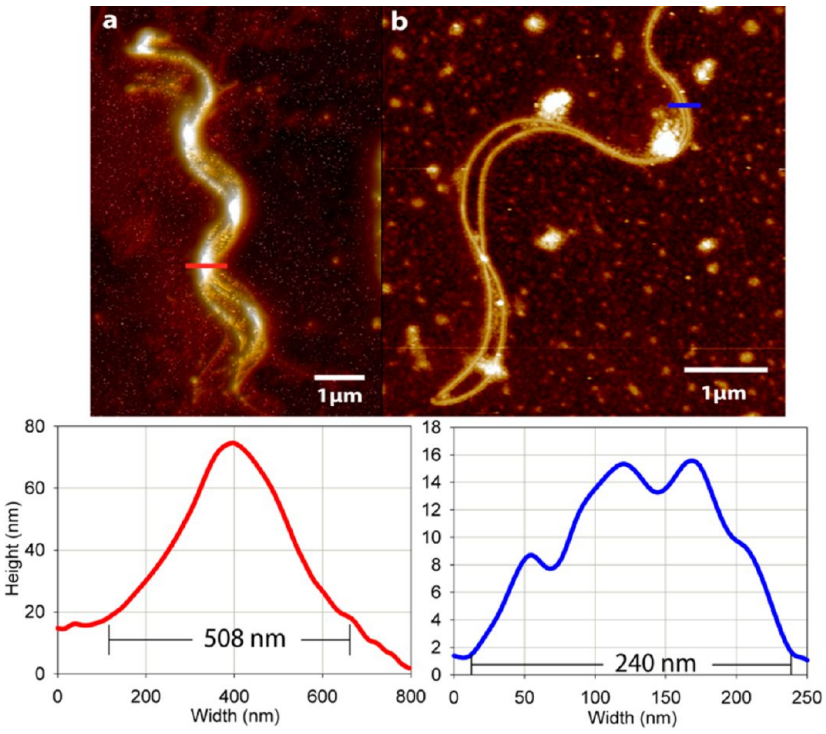

Figure 3. Stage III: AFM topographical images of (a) WG fibrils twisting around each other to form large fibrils and (b) Gd:My fibrils that do not aggregate as frequently or to the same scale as WG fibrils.

with a pitch $h \approx 1410$ nm. The twisting is observable in the AFM image and is confirmed by a large height increase. The WG large fibril is about an order of magnitude smaller than its final fiber dimensions with a pitch about half the length of the final pitch. In Stage III, there is limited Gd:My fibril aggregation into large fibrils resulting in a tape structure with dimensions about an order of magnitude smaller than the final dried tape. Figure 3 shows that Gd:My fibrils have limited lateral aggregation at a stage where WG fibrils begin to twist into a larger structure. Although the morphology of amyloid fibrils at the nanometer scale has been extensively studied, little is known about the continued self-assembly and morphological differentiation at larger scales, which show striking features that can be related to the peptides in the mixtures.[81]

Stage IV: Micrometer-Sized Fiber Formation (>480 h). The final micrometer-sized structure forms upon drying at 480 h. WG peptides form cylindrical fibers of 18.1 ± 9.5 μm in diameter (Figure 4) while Gd:My peptides form flat tapes of $H = 5.7 \pm 0.6$ μm and $W = 14.4 \pm 2.2$ μm (Figure 5). Previous studies using X-ray diffraction and Raman spectroscopy show the WG fibers and Gd:My tapes to contain the cross-β secondary structure.[35,36,75] The final fibers are 10^2-10^3 μm long.[35] Evidence of earlier stage structures exist: WG forms tightly twisted cylindrical cross-section fibers composed of $W = 300-800$ nm wide large fibrils and Gd:My forms rectangular cross-section tapes with $W = 20$ nm protofibrils and $W = 190$ nm large fibrils observed showing the

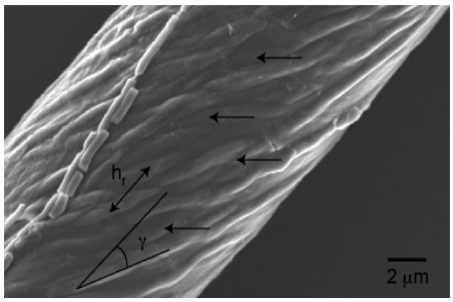

Figure 4. WG fiber of $D = 14.0$ μm composed of twisted large fibrils of 300−800 nm diameter. Arrows indicate where large fibrils twist on top of one another.

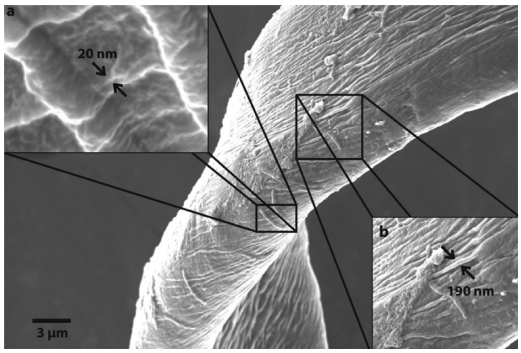

Figure 5. An SEM image of a Gd:My tape ($W = 15$ μm, $H = 6$ μm) where (a) protofibrils and (b) large fibrils are apparent.

micrometer-sized fibers and tapes to be hierarchical. Upon drying the Gd:My solution, large fibrils of $W = 190-900$ nm

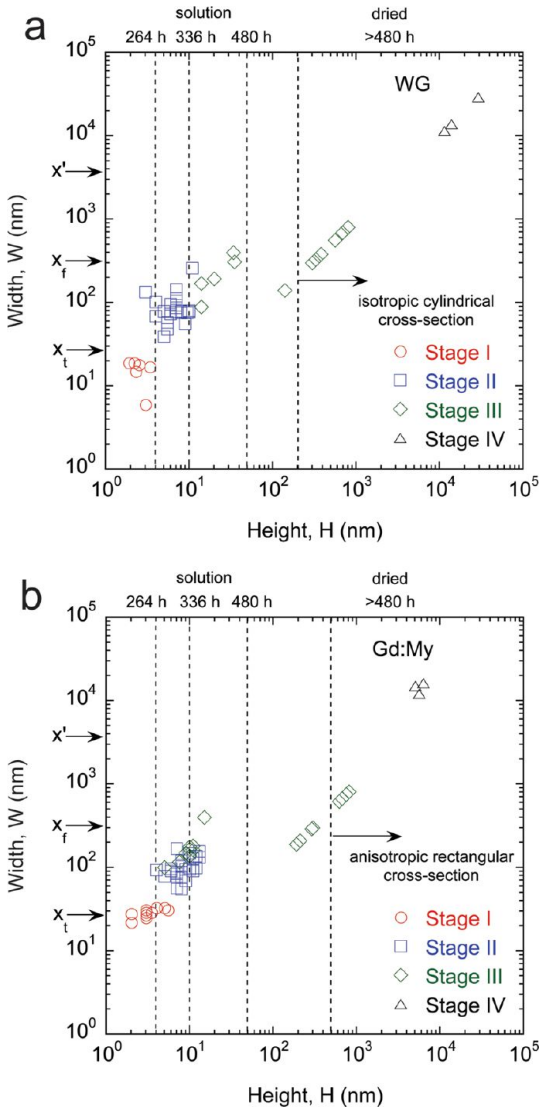

Figure 6. Growth of large self-assembled (a) WG peptide fibers and (b) Gd:My tapes with dimensions measured using AFM and SEM.

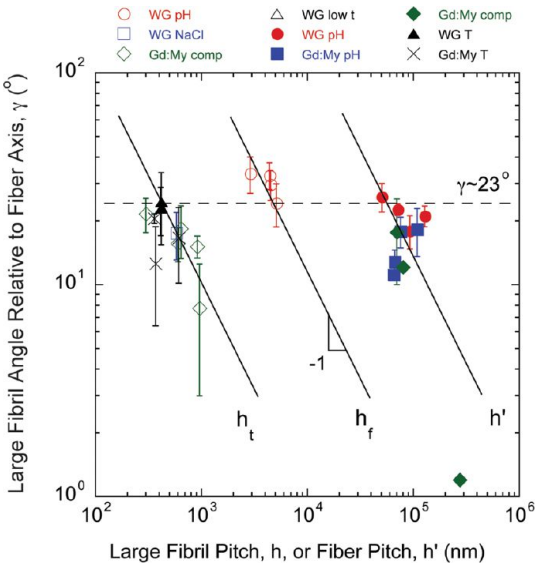

Figure 7. Fibers (h_f) and tapes (h_t) formed from WG and Gd:My peptides under various conditions separate based on morphological characteristics.

are observed in the dried tapes that are not observed in Stage III in solution (Figures 5 and 6b).

Micrometer-Sized Fiber Morphology. It is clear from the SEM images that fibers and tapes form from aggregates of large fibrils formed in Stage III. The large fibrils are oriented at an angle, γ, relative to the fiber or tape axis (Figure 4). At pH 8 and 37 °C, WG has $\gamma = 34°$ and Gd:My has $\gamma = 22°$ showing WG fibers to be more twisted and tightly packed (Figure 4). Therefore, the lateral aggregation of Gd:My fibrils induces a smaller twist than in WG. A transition from a tape to a cylinder morphology occurs at $\gamma \approx 23°$ and WG large fibrils can be prevented from twisting with changes in solution conditions.[75]

Concurrent with the orientation angle of the large fibrils is a pitch, h_f and h_t, for fibers and tapes, respectively.[40,62−64,66,78−80] For WG and Gd:My at pH 8 and 37 °C, $h_f = 2900$ nm and $h_t = 300$ nm, respectively, which defines the distance between large fibrils along the length of the micrometer-sized fiber or tape. Simple geometric considerations relate γ to h, $\gamma(°) = 360x/h$.[40,62−64,66,78−80,86] Measuring γ and h for WG and Gd:My mixtures studied under various experimental conditions shows that a plot of γ *versus* h segregates the resulting fibers and tapes by morphology regardless of peptide type or experimental condition (Figure 7).[35,75] In some cases, micrometer-sized fibers and tapes show very large scale twisting defined by a larger pitch, h'.[75] Fitting the data in Figure 7 to $\gamma(°) = 360x/h$ results in $x_t = 28$ nm, $x_f = 320$ nm, and $x' = 3.9$ μm. The length x_t is approximately equal to the protofibril width, which is the smallest discernible feature in the Gd:My tapes (Figure 5). x_f is approximately equal to the large fibril width, which is the smallest discernible feature in the WG fibers (Figure 4). It has been shown for protofibrils that the distance, x, is the distance between two peptides in the cross-β structure.[28,64,78,86] The peptides extend lengthwise across the width of the protofibril and when stacked side-by-side comprise the length of the protofibril. Protofibrils (in Gd:My) and large fibrils (in WG) organize side by side at an angle, γ, relative to the tape or fiber axis, respectively, thus x describes the smallest discernible feature comprising the tape or fiber length. x' is approximately equal to the final micrometer-sized fiber diameter and tape width. The x values span 2 orders of magnitude of scale (10^1−10^3 nm) and are length scales characteristic of the hierarchical nature of the self-assembly of micrometer-sized fibers and tapes.

In the simplest incarnation of the proposed multiscale self-assembly mechanism, hydrophobic interactions initiate template formation, the adder peptide addition, and aggregation of protofibrils into larger structures.[35,75] This is the path followed by Gd:My.

Myoglobin has large sequences of hydrophobic groups in its α-helices producing an α-helix hydrophobic content of 76%. Myoglobin only aggregates through hydrophobic interactions in certain portions of the protein which limits its solution phase aggregation to fibrils/large fibrils of dimensions H = 8−10 nm and W = 100−150 nm. Loosely bound protofibrils and fibrils are observed in the final dried Gd:My tapes, which have a Young's modulus of only $E_t \approx 0.15$ GPa. Lara *et al.* observe fibril aggregation similar to Stage III aggregation.[81] These "giant amyloid ribbons" resemble the Gd:My structures observed here and form from hydrolysates of hen egg white lysozyme and β-lactoglobulin with peptide molecular weights less than 6500 g/mol.[81] It is entirely possible that these hydrolysates contain peptides that meet "template" and "adder" definitions. That study also highlights the role of hydrophobic interactions in the lateral growth of the large tape.[66]

Myoglobin and GtL75 have similar aliphatic indices (AI), a measure of the molecular hydrophobicity.[35] However, glutenin peptides, specifically GtL75, contain glutamine repeat units or "Q-blocks" that are known facilitators of cross-β formation.[44,87−90] Myoglobin contains 4% Q without any Q-blocks. At short time, more protofibrils and fibrils form from WG globules than spontaneously form in Gd:My solution (Figure 1). Q-blocks appear to facilitate more early stage aggregation in WG through amide−amide hydrogen bonding on the amino acid side groups as measured with FT-IR spectroscopy.[35,75] This results in the more compact structure with smaller protofibril and fibril dimensions and higher rigidity manifesting as a longer persistence length in early stages. Experiments with short peptides containing Q-blocks have shown the resulting amyloid protofibrils to be more twisted than protofibrils formed from peptides of the same length without Q-blocks.[78] The Q-blocks facilitate twisting of the WG structures as seen in the AFM and SEM results and are responsible for morphological differentiation and a much higher Young's modulus of $E_f \approx 2.5$ GPa.[35,75] WG fibers have a longer pitch than Gd:My tapes. This appears to result from the more extensive formation of wider and thicker large fibrils in WG compared to Gd:My in Stage III and upon drying. Protofibrils and fibrils are assembled and twisted tightly in the WG large fibrils and are thus not the smallest discernible feature in WG fibers, unlike Gd:My tapes. The weaker hydrophobic interactions and lack of Q-Q bonding in Q-blocks do not allow twisting in the Gd:My system producing soft tapes rather than stiff cylinders.

CONCLUSION

Peptide mixtures can self-assemble into the often-studied nanometer scale amyloid protofibril and fibril. However, peptide mixtures with "template" and "adder" properties continue to assemble to the micrometer scale in a four-stage mechanism (Scheme 1). Hydrophobic adder proteins lacking Q-blocks, like My, have delayed and less extensive aggregation that rarely progresses past W = 150 nm in solution. Adder peptides with Q-blocks, like GtL75, facilitate aggregation through all four stages and cause twisting of the aggregating structure most notably at lengths greater than 100 nm. Most interestingly, the two peptide mixtures differentiate into two different morphologies. Differences in protofibril size and fibril persistence length appear in Stages I and II while stark morphological differences appear in Stages III and IV: a twisted cylindrical morphology for WG, containing GtL75, and a flat tape morphology for Gd:My. The twisted morphology from Q-blocks results in a fiber with a modulus 1 order of magnitude higher than that of the flat Gd:My tapes, which are built through weaker hydrophobic interactions only. An understanding of the peptide properties that dictate the progression and morphology of the large amyloid fiber indicates that it is possible to design a robust structure tailored to a specific function that exists on a length scale that lends itself to pragmatic engineering applications.

METHODS

Wheat Gluten (WG) and Gliadin (Gd) Hydrolysis and Self-Assembly. WG and Gd solutions were prepared in the same manner as previously described.[75] WG solution conditions were maintained at pH 8 and 37 °C for 20 days with samples collected periodically for AFM analysis.

Gd:My Solution. Gd:My solutions were made in the same manner as previously described.[75] Solution conditions were maintained at pH 8 and 37 °C with samples collected periodically for AFM analysis.

Atomic Force Microscopy (AFM). An amount of 50 μL of each solution was spin-coated on freshly cleaved mica at 4000 rpm for 1 min. Other studies have dried and washed their samples to reveal the amyloid fibrils on the mica surface. Spin-coating was used to immediately stop the self-assembly process and reveal the resulting amyloid structures to avoid a finite drying time that could have affected results.[64,66,81] Images were obtained with an Innova AFM (Bruker, Santa Barbara, CA) with a 0.01−0.025 Ohm-cm antimony-doped Si probe (Bruker, Part: MPP-1123-10) in tapping mode with a scan rate of 0.3 Hz. Images and measurements were evaluated using NanoScope Analysis v1.40 software. For dimensional measurements, the same image processing was performed for each figure. However, image contrast and clarity were enhanced with NanoScope Analysis v1.40 and Adobe Photoshop CS4 for the purposes of presentation. Dimension measurements of protofibrils (WG = 8, Gd:My = 11), fibrils (WG = 10, Gd:My = 18), large fibrils (WG = 5, Gd:My = 3) and fibers (WG, Gd:My = 3) were taken, and the averages ± standard deviations were reported. Multiple (at least 3) measurements were made on completely and partially separated protofibrils, fibrils, and large fibrils so that accurate heights and widths were reported. Fibers were measured once because of the uniformity of the cross-section and consistency with a more extensive previous study of fiber dimensions.[35]

Persistence length measurements were made as described previously.[63] Contour length and the angle between the tangents to both ends of the contour length were measured from the AFM images using ImageJ v1.46. The persistence length estimates were made on 17 WG and 13 Gd:My Stage II fibrils with averages ± standard deviations reported.

Scanning Electron Microscopy (SEM). WG and Gd:My solutions were dried on Teflon-coated aluminum foil under the fume hood at ambient conditions after 20 days. Fibers and tapes formed from dried solution were mounted onto aluminum SEM stubs with double-sided tape. Scanning electron micrographs were obtained using a LEO 1550 field-emission SEM (Zeiss, Peabody, MA) with a 4−6 mm working distance, 5 kV accelerating voltage, and an In-lens SE-detector.

Conflict of Interest: The authors declare no competing financial interest.

Acknowledgment. Generous funding through NSF-CMMI-0856262 and the USDA funded Virginia Tech Biodesign and Bioprocessing Research Center is gratefully acknowledged.

REFERENCES AND NOTES

1. Dobson, C. M. Protein Misfolding, Evolution and Disease. *Trends Biochem. Sci.* **1999**, *24*, 329–332.
2. Dobson, C. M.; Sali, A.; Darplus, M. Protein Folding: A Perspective from Theory and Experiment. *Angew. Chem., Int. Ed.* **1998**, *37*, 868–893.
3. Chiti, F.; Dobson, C. M. Protein Misfolding, Functional Amyloid, and Human Disease. *Annu. Rev. Biochem.* **2006**, *75*, 333–366.
4. Dobson, C. M. Protein Folding and Misfolding. *Nature* **2003**, *426*, 884–890.
5. Prusiner, S. B. Prions. *Proc. Natl. Acad. Sci. U.S.A.* **1998**, *95*, 13363–13383.
6. Paparcone, R.; Cranford, S. W.; Buehler, M. J. Self-Folding and Aggregation of Amyloid Nanofibrils. *Nanoscale* **2011**, *3*, 1748–1755.
7. Sunde, M. Common Core Structure of Amyloid Fibrils by Synchrotron X-ray Diffraction. *J. Mol. Biol.* **1997**, *273*, 729–739.
8. Hiramatsu, H.; Kitagawa, T. FT-IR Approaches on Amyloid Fibril Structure. *BBA-Proteins Proteom.* **2005**, *1753*, 100–107.
9. Knowles, T. P. J.; Buehler, M. J. Nanomechanics of Functional and Pathological Amyloid Materials. *Nat. Nanotechnol.* **2011**, *6*, 469–479.
10. Fowler, D. M.; Koulov, A. V.; Balch, W. E.; Kelly, J. W. Functional Amyloid—From Bacteria to Humans. *Trends Biochem. Sci.* **2007**, *32*, 217–224.
11. Kamino, K.; Odo, S.; Maruyama, T. Cement Proteins of the Acorn-Barnacle. *Megabalanus rosa. Biol. Bull.* **1996**, *190*, 403–409.
12. Kamino, K.; Inoue, K.; Maruyama, T.; Takamatsu, N.; Harayama, S.; Shizuri, Y. Barnacle Cement Proteins. *J. Biol. Chem.* **2000**, *275*, 27360–27365.
13. Kamino, K. Underwater Adhesive of Marine Organisms as the Vital Link between Biological Science and Material Science. *Mar. Biotechnol.* **2008**, *10*, 111–121.
14. Sullan, R. M. A.; Gunari, N.; Tanur, A. E.; Chan, Y.; Dickinson, G. H.; Orihuela, B.; Rittschof, D.; Walker, G. C. Nanoscale Structures and Mechanics of Barnacle Cement. *Biofouling* **2009**, *25*, 263–275.
15. Barlow, D. E.; Dickinson, G. H.; Orihuela, B.; Kulp, J. L., III; Rittschof, D.; Wahl, K. J. Characterization of the Adhesive Plaque of the Barnacle *Balanus amphitrite*: Amyloid-Like Nanofibrils are a Major Component. *Langmuir* **2010**, *26*, 6549–6556.
16. Gebbink, M. F. B. G.; Claessen, D.; Bouma, B.; Dijkhuizen, L.; Wosten, H. A. B. Amyloids—A Functional Coat for Microorganisms. *Nat. Rev. Microbiol.* **2005**, *3*, 333–341.
17. Ben Nasr, A.; Olsen, A.; Sjobring, U.; Muller-Esterl, W.; Bjorck, L. Assembly of Human Contact Phase Proteins and Release of Bradykinin at the Surface of Curli-Expressing *Escheria coli*. *Mol. Microbiol.* **1996**, *20*, 927–935.
18. Hammer, N. D.; Schmidt, J. C.; Chapman, M. R. The Curli Nucleator Protein, CsgB, Contains an Amyloidogenic Domain that Directs CsgA Polymerization. *Proc. Natl. Acad. Sci. U.S.A.* **2007**, *104*, 12494–12499.
19. Wang, X.; Chapman, M. R. Curli Provide the Template for Understanding Controlled Amyloid Propagation. *Prion* **2008**, *2*, 57–60.
20. Wang, X.; Hammer, N. D.; Chapman, M. R. The Molecular Basis of Functional Bacterial Amyloid Polymerization and Nucleation. *J. Biol. Chem.* **2008**, *283*, 21530–21539.
21. Chapman, M. R.; Robinson, L. S.; Pinkner, J. S.; Roth, R.; Heuser, J.; Hammar, M.; Normark, S.; Hultgren, S. J. Role of *Escherichia coli* Curli Operons in Directing Amyloid Fiber Formation. *Science* **2002**, *295*, 851–855.
22. Alsteens, D.; Ramsook, C. B.; Lipke, P. N.; Dufrêne, Y. F. Unzipping a Functional Microbial Amyloid. *ACS Nano* **2012**, *6*, 7703–7711.
23. Parker, K. D.; Rudall, K. M. The Silk of the Egg-Stalk of the Green Lace-Wing Fly. *Nature* **1957**, *179*, 905–906.
24. Weisman, S.; Trueman, H. E.; Mudie, S. T.; Church, J. S.; Sutherland, T. D.; Haritos, V. S. An Unlikely Silk: The Composite Material of Green Lacewing Cocoons. *Biomacromolecules* **2008**, *9*, 3065–3069.
25. Seidel, A.; Liivak, O.; Calve, S.; Adaska, J.; Ji, G.; Yang, Z.; Grubb, D.; Zax, D. B.; Jelinski, L. W. Regenerated Spider Silk: Processing, Properties, and Structure. *Macromolecules* **2000**, *33*, 775–780.
26. Keten, S.; Xu, Z.; Ihle, B.; Buehler, M. J. Nanoconfinement Controls Stiffness, Strength and Mechanical Toughness of β-Sheet Crystals in Silk. *Nat. Mater.* **2010**, *9*, 359–367.
27. Xu, Z.; Paparcone, R.; Buehler, M. J. Alzheimer's Aβ(1−40) Amyloid Fibrils Feature Size-Dependent Mechanical Properties. *Biophys. J.* **2010**, *98*, 2053–2062.
28. Paparcone, R.; Keten, S.; Buehler, M. J. Atomistic Simulation of Nanomechanical Properties of Alzheimer's Aβ(1−40) Amyloid Fibrils under Compressive and Tensile Loading. *J. Biomech.* **2010**, *43*, 1196–1201.
29. Fukuma, T.; Mostaert, A.; Jarvis, S. Explanation for the Mechanical Strength of Amyloid Fibrils. *Tribol. Lett.* **2006**, *22*, 233–237.
30. Knowles, T. P. J.; Oppenheim, T. W.; Buell, A. K.; Chirgadze, D. Y.; Welland, M. E. Nanostructured Films from Hierarchical Self-Assembly of Amyloidogenic Proteins. *Nat. Nanotechnol.* **2010**, *5*, 204–207.
31. Li, C.; Adamcik, J.; Mezzenga, R. Biodegradable Nanocomposites of Amyloid Fibrils and Graphene with Shape-Memory and Enzyme-Sensing Properties. *Nat. Nanotechnol.* **2012**, *7*, 421–427.
32. Gazit, E. Self-Assembled Peptide Nanostructures: The Design of Molecular Building Blocks and Their Technological Utilization. *Chem. Soc. Rev.* **2007**, *32*, 1263–1269.
33. Reches, M.; Gazit, E. Casting Metal Nanowires within Discrete Self-Assembled Peptide Nanotubes. *Science* **2003**, *300*, 625–627.
34. Scheibel, T.; Parthasarathy, R.; Sawicki, G.; Lin, X. M.; Jaeger, H.; Lindquist, S. L. Conducting Nanowires Built by Controlled Self-Assembly of Amyloid Fibers and Selective Metal Deposition. *Proc. Natl. Acad. Sci. U.S.A.* **2003**, *100*, 4527–4532.
35. Ridgley, D. M.; Ebanks, K. C.; Barone, J. R. Peptide Mixtures Can Self-Assemble into Large Amyloid Fibers of Varying Size and Morphology. *Biomacromolecules* **2011**, *12*, 3770–3779.
36. Athamneh, A.; Barone, J. R. Enzyme-Mediated Self-Assembly of Highly Ordered Structures from Disordered Proteins. *Smart Mater. Struct.* **2009**, *18*, 104024.
37. Bouchard, M.; Zurdo, J.; Nettleton, E. J.; Dobson, C. M.; Robinson, C. V. Formation of Insulin Amyloid Fibrils followed by FT-IR Simultaneously with CD and Electron Microscopy. *Protein Sci.* **2000**, *9*, 1960–1967.
38. Gosal, W. S.; Morten, I. J.; Hewitt, E. W.; Smith, A.; Thomson, N. H.; Radford, S. E. Competing Pathways Determine Fibril Morphology in the Self-Assembly of β_2-Microglobulin into Amyloid. *J. Mol. Biol.* **2005**, *351*, 850–864.

39. Fandrich, M.; Fletcher, M. A.; Dobson, C. M. Amyloid Fibrils from Muscle Myoglobin. *Nature* **2001**, *410*, 165–166.
40. Davies, R. P. W.; Aggeli, A.; Beevers, A. J.; Boden, N.; Carrick, L. M.; Fishwick, C. W. G.; McLeish, T. C. B.; Nyrkova, I. A.; Semenov, A. N. Self-Assembling β-sheet Tape Forming Peptides. *Supramol. Chem.* **2006**, *18*, 435–443.
41. Barghorn, S.; Davies, P.; Mandelkow, E. Tau Paired Helical Filaments from Alzheimer's Disease Brain and Assembled *in Vitro* Are Based on β-Structure in the Core Domain. *Biochemistry U.S.* **2004**, *43*, 1694–1703.
42. Hasegawa, K.; Yamaguchi, I.; Omata, S.; Gejyo, F.; Naiki, H. Interaction between Aβ(1−42) and Aβ(1−40) in Alzheimer's β-Amyloid Fibril Formation *in Vitro*. *Biochemistry U.S.* **1999**, *38*, 15514–15521.
43. Ivanova, M. I.; Sawaya, M. R.; Gingery, M.; Attinger, A.; Eisenberg, D. An Amyloid-Forming Segment of β2-Microglobulin Suggests a Molecular Model for the Fibril. *Proc. Natl. Acad. Sci. U.S.A.* **2004**, *101*, 10584–10589.
44. Chen, S.; Berthelier, V.; Bradley Hamilton, J.; O'Nuallain, B.; Wetzel, R. Amyloid-like Features of Polyglutamine Aggregates and Their Assembly Kinetics. *Biochemistry U.S.* **2002**, *41*, 7391–7399.
45. Cherny, I.; Gazit, E. Amyloids: Not Only Pathological Agents but Also Ordered Nanomaterials. *Angew. Chem., Int. Ed.* **2008**, *47*, 4062–4069.
46. Cohen, A. S.; Calkins, E. Electron Microscopic Observations on a Fibrous Component in Amyloid of Diverse Origins. *Nature* **1959**, *183*, 1202–1203.
47. del Mercato, L. L.; Maruccio, G.; Pompa, P. P.; Bochiccio, B.; Tamburro, A. M.; Cingolani, R.; Rinaldi, R. Amyloid-like Fibrils in Elastin-Related Polypeptides: Structural Characterization and Elastic Properties. *Biomacromolecules* **2008**, *9*, 796–803.
48. Diaz-Avalos, R. Cross-β Order and Diversity in Nanocrystals of an Amyloid-Forming Peptide. *J. Mol. Biol.* **2003**, *330*, 1165–1175.
49. Eanes, E. D.; Glenner, G. G. X-ray Diffraction Studies on Amyloid Filaments. *J. Histochem. Cytochem.* **1968**, *16*, 673–677.
50. Gosal, W. S.; Clark, A. H.; Pudney, P. D. A.; Ross-Murphy, S. B. Novel Amyloid Fibrillar Networks Derived from a Globular Protein: β-Lactoglobulin. *Langmuir* **2002**, *18*, 7174–7181.
51. Jaroniec, C. P.; MacPhee, C. E.; Astrof, N. S.; Dobson, C. M.; Griffin, R. G. Molecular Conformation of a Peptide Fragment of Transthyretin in an Amyloid Fibril. *Proc. Natl. Acad. Sci. U.S.A.* **2002**, *99*, 16748–16753.
52. Jimenez, J. L. Cryo-electron Microscopy Structure of an SH3 Amyloid Fibril and Model of the Molecular Packing. *EMBO J.* **1999**, *18*, 815–821.
53. Jimenez, J. L. The Protofilament Structure of Insulin Amyloid Fibrils. *Proc. Natl Acad. Sci. U.S.A.* **2002**, *99*, 9196–9201.
54. MacPhee, C. E.; Dobson, C. M. Formation of Mixed Fibrils Demonstrates the Generic Nature and Potential Utility of Amyloid Nanostructures. *J. Am. Chem. Soc.* **2000**, *122*, 12707–12713.
55. Pearce, F. G.; Mackintosh, S. H.; Gerrard, J. A. Formation of Amyloid-like Fibrils by Ovalbumin and Related Proteins under Conditions Relevant to Food Processing. *J. Agric. Food Chem.* **2007**, *55*, 318–322.
56. Perutz, M. F.; Finch, J. T.; Berriman, J.; Lesk, A. Amyloid Fibers Are Water-Filled Nanotubes. *Proc. Natl. Acad. Sci. U.S.A.* **2002**, *99*, 5591–5595.
57. Petkova, A. T. A Structural Model for Alzheimer's β-Amyloid Fibrils based on Experimental Constraints from Solid State NMR. *Proc. Natl. Acad. Sci. U.S.A.* **2002**, *99*, 16742–16747.
58. Rubin, N.; Perugia, E.; Goldschmidt, M.; Fridkin, M.; Addadi, L. Chirality of Amyloid Suprastructures. *J. Am. Chem. Soc.* **2008**, *130*, 4602–4603.
59. Sunde, M.; Blake, C. C. F. From the Globular to the Fibrous State: Protein Structure and Structural Conversion in Amyloid Formation. *Q. Rev. Biophys.* **1998**, *31*, 1–39.
60. Torok, M. Structural and Dynamic Features of Alzheimer's Aβ Peptide in Amyloid Fibrils Studied by Site-Directed Spin Labeling. *J. Biol. Chem.* **2002**, *277*, 40810–40815.
61. Zurdo, J.; Guijarro, J. I.; Dobson, C. M. Preparation and Characterization of Purified Amyloid Fibrils. *J. Am. Chem. Soc.* **2001**, *123*, 8141–8142.
62. Adamcik, J.; Berquand, A.; Mezzenga, R. Single-Step Direct Measurement of Amyloid Fibrils Stiffness by Peak Force Quantitative Nanomechanical Atomic Force Microscopy. *Appl. Phys. Lett.* **2011**, *98*, 193701.
63. Adamcik, J.; Jung, J. M.; Flakowski, J.; De Los Rios, P.; Dietler, G.; Mezzenga, R. Understanding Amyloid Aggregation by Statistical Analysis of Atomic Force Microscopy Images. *Nat. Nanotechnol.* **2010**, *5*, 423–428.
64. Adamcik, J.; Mezzenga, R. Adjustable Twisting Periodic Pitch of Amyloid Fibrils. *Soft Matter* **2011**, *7*, 5437–5443.
65. Bolder, S. G.; Hendrickx, H.; Sagis, L. M. C.; van der Linden, E. Fibril Assemblies in Aqueous Whey Protein Mixtures. *J. Agric. Food Chem.* **2006**, *54*, 4229–4234.
66. Bolisetty, S.; Adamcik, J.; Mezzenga, R. Snapshots of Fibrillation and Aggregation Kinetics in Multistranded Amyloid β-Lactoglobulin Fibrils. *Soft Matter* **2011**, *7*, 493–499.
67. Fandrich, M.; Forge, V.; Buder, K.; Kittler, M.; Dobson, C. M.; Diekmann, S. Myoglobin forms Amyloid Fibrils by Association of Unfolded Polypeptide Segments. *Proc. Natl. Acad. Sci. U.S.A.* **2003**, *100*, 15463–15468.
68. Goda, S.; Takano, K.; Yamagata, Y.; Nagata, R.; Akutsu, H.; Maki, S.; Namba, K.; Yutani, K. Amyloid Protofilament Formation of Hen Egg Lysozyme in Highly Concentrated Ethanol Solution. *Protein Sci.* **2000**, *9*, 369–375.
69. Mostaert, A.; Higgins, M. J.; Fukuma, T.; Rindi, F.; Jarvis, S. P. Nanoscale Mechanical Characterization of Amyloid Fibrils Discovered in a Natural Adhesive. *J. Biol. Phys.* **2006**, *32*, 393–401.
70. Tomaselli, S.; Esposito, V.; Vangone, P.; van Nuland, N. A. J.; Bonvin, A. M. J. J.; Guerrini, R.; Tancredi, T.; Temussi, P. A.; Picone, D. The α-to-β Conformational Transition of Alzheimer's Aβ-(1−42) Peptide in Aqueous Media is Reversible: A Step by Step Conformational Analysis Suggests the Location of β Conformation Seeding. *ChemBioChem* **2006**, *7*, 257–267.
71. Jarrett, J. T.; Lansbury, P. T. Amyloid Fibril Formation Requires a Chemically Discriminating Nucleation Event: Studies of an Amyloidogenic Sequence from the Bacterial Protein OsmB. *Biochemistry* **1992**, *31*, 12345–12352.
72. Ionescu-Zanetti, C.; Khurana, R.; Gillespie, J. R.; Petrick, J. S.; Trabachino, L. C.; Minert, L. J.; Carter, S. A.; Fink, A. L. Monitoring the Assembly of Ig Light-Chain Amyloid Fibrils by Atomic Force Microscopy. *Proc. Natl. Acad. Sci. U.S.A.* **1999**, *96*, 13175–13179.
73. Chamberlain, A. K.; MacPhee, C. E.; Zurdo, J.; Morozova-Roche, L. A.; Hill, H. A. O.; Dobson, C. M.; Davis, J. J. Ultrastructural Organization of Amyloid Fibrils by Atomic Force Microscopy. *Biophys. J.* **2000**, *79*, 3282–3293.
74. Sweers, K. K. M.; van der Werf, K. O.; Bennink, M. L.; Subramaniam, V. Atomic Force Microscopy under Controlled Conditions Reveals Structure of C-Terminal Region of α-Synuclein in Amyloid Fibrils. *ACS Nano* **2012**, *6*, 5952–5960.
75. Ridgley, D. M.; Claunch, E. C.; Barone, J. R. The Effect of Processing on Large, Self-Assembled Amyloid Fibers. *Soft Matter* **2012**, *8*, 10298–10306.
76. Raman, B.; Chatani, E.; Kihara, M.; Ban, T.; Sakai, M.; Hasegawa, K.; Naiki, H.; Rao, C. M.; Goto, Y. Critical Balance of Electrostatic and Hydrophobic Interactions Is Required for β2-Microglobulin Amyloid Fibril Growth and Stability. *Biochemistry* **2005**, *44*, 1288–1299.
77. Kodali, R.; Williams, A. D.; Chemuru, S.; Wetzel, R. Aβ(1−40) Forms Five Distinct Amyloid Structures Whose β-Sheet Contents and Fibril Stabilities Are Correlated. *J. Mol. Biol.* **2010**, *401*, 503–517.
78. Aggeli, A.; Nyrkova, I. A.; Bell, M.; Harding, R.; Carrick, L.; McLeish, T. C. B.; Semenov, A. N.; Boden, N. Hierarchical Self-Assembly of Chiral Rod-like Molecules as a Model for Peptide β-Sheet Tapes, Ribbons, Fibrils, and Fibers. *Proc. Natl. Acad. Sci. U.S.A.* **2001**, *98*, 11857–11862.
79. Nyrkova, I. A.; Semenov, A. N.; Aggeli, A.; Bell, M.; Boden, N.; McLeish, T. C. B. Self-Assembly and Structure Formation in

Living Polymers Forming Fibrils. *Euro. Phys. J. B* **2000**, *17*, 499–513.
80. Nyrkova, I. A.; Semenov, A. N.; Aggeli, A.; Boden, N. Fibril Stability in Solutions of Twisted β-Sheet Peptides: A New Kind of Micellization in Chiral Systems. *Euro. Phys. J. B* **2000**, *17*, 481–497.
81. Lara, C.; Adamcik, J.; Jordens, S.; Mezzenga, R. General Self-Assembly Mechanism Converting Hydrolyzed Globular Proteins Into Giant Multistranded Amyloid Ribbons. *Biomacromolecules* **2011**, *12*, 1868–1875.
82. Ban, T.; Yamaguchi, K.; Goto, Y. Direct Observation of Amyloid Fibril Growth, Propagation, and Adaptation. *Acc. Chem. Res.* **2006**, *39*, 663–670.
83. Jarrett, J. T.; Lansbury, P. T. Seeding "One-Dimensional Crystallization" of Amyloid: A Pathogenic Mechanism in Alzheimer's Disease and Scrapie? *Cell* **1993**, *73*, 1055–1058.
84. Keller, A.; Fritzsche, M.; Yu, Y. P.; Liu, Q.; Li, Y. M.; Dong, M.; Besenbacher, F. Influence of Hydrophobicity on the Surface-Catalyzed Assembly of the Islet Amyloid Polypeptide. *ACS Nano* **2011**, *5*, 2770–2778.
85. Lashuel, H. A.; LaBrenz, S. R.; Woo, L.; Serpell, L. C.; Kelly, J. W. Protofilaments, Filaments, Ribbons, and Fibrils from Peptidomimetic Self-Assembly: Implications for Amyloid Fibril Formation and Materials Science. *J. Am. Chem. Soc.* **2000**, *122*, 5262–5277.
86. Paparcone, R.; Buehler, M. J. Microscale Structural Model of Alzheimer Aβ(1−40) Amyloid Fibril. *Appl. Phys. Lett.* **2009**, *94*, 243904–3.
87. Perutz, M. F.; Johnson, T.; Suzuki, M.; Finch, J. T. Glutamine Repeats as Polar Zippers: Their Possible Role in Inherited Neurodegenerative Diseases. *Proc. Natl. Acad. Sci. U.S.A.* **1994**, *91*, 5355–5358.
88. DePace, A. H.; Santoso, A.; Hillner, P.; Weissman, J. S. A Critical Role for Amino-Terminal Glutamine/Asparagine Repeats in the Formation and Propagation of a Yeast Prion. *Cell* **1998**, *93*, 1241–1252.
89. Scherzinger, E.; Sittler, A.; Schweiger, K.; Heiser, V.; Lurz, R.; Hasenbank, R.; Bates, G. P.; Lehrach, H.; Wanker, E. E. Self-Assembly of Polyglutamine-Containing Huntingtin Fragments into Amyloid-like Fibrils: Implications for Huntington's Disease Pathology. *Proc. Natl. Acad. Sci. U.S.A.* **1999**, *96*, 4604–4609.
90. Sikorski, P.; Atkins, E. New Model for Crystalline Polyglutamine Assemblies and Their Connection with Amyloid Fibrils. *Biomacromolecules* **2005**, *6*, 425–432.

Chapter 6.

The Role of Protein Hydrophobicity in Conformation Change and Self-Assembly into Large Amyloid Fibers

Ridgley, D. M., E. C. Claunch, P. W. Lee, and J. R. Barone. 2014. The Role of Protein Hydrophobicity in Conformation Change and Self-Assembly into Large Amyloid Fibers. *Biomacromolecules*, DOI: 10.1021/bm401815u. - Reproduced with the generous permission of the American Chemical Society.

Note: The Supporting Information referred to in Chapter 6 is located in Appendix A.

Article

pubs.acs.org/Biomac

The Role of Protein Hydrophobicity in Conformation Change and Self-Assembly into Large Amyloid Fibers

Devin M. Ridgley, Elizabeth C. Claunch, Parker W. Lee, and Justin R. Barone*

Biological Systems Engineering Department, Virginia Tech, 301D HABB1, Blacksburg, Virginia 24061, United States

Supporting Information

ABSTRACT: It has been found that a short hydrophobic "template" peptide and a larger α-helical "adder" protein cooperatively self-assemble into micrometer sized amyloid fibers. Here, a common template of trypsin hydrolyzed gliadin is combined with six adder proteins (α-casein, α-lactalbumin, amylase, hemoglobin, insulin, and myoglobin) to determine what properties of the adder protein drive amyloid self-assembly. Utilizing Fourier Transform-Infrared (FT-IR) spectroscopy, the Amide I absorbance reveals that the observed decrease in α-helix with time is approximately equal to the increase in high strand density β-sheet, which is indicative of amyloid formation. The results show that the hydrophobic moment is a good predictor of conformation change but the fraction of aliphatic amino acids within the α-helices is a better predictor. Upon drying, the protein mixtures form large amyloid fibers. The fiber twist is dependent on the aliphatic index and molecular weight of the adder protein. Here we demonstrate that it is possible to predict the propensity of an adder protein to unfold into an amyloid structure and to predict the fiber morphology, both from adder protein molecular features, which can be applied to the pragmatic engineering of large amyloid fibers.

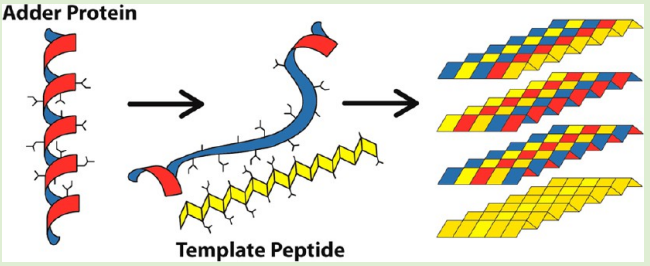

INTRODUCTION

Over the last few decades there has been extensive research focused on understanding the cause and mechanism of a debilitating class of neurodegenerative diseases termed "prion" diseases.[1−7] Prions are formed from the spontaneous misfolding of a protein into β-sheets that in some cases can further self-assemble into an amyloid fibril.[1,6] Amyloid fibrils are characterized by a high strand density β-sheet secondary structure oriented perpendicular to the fibril axis.[8] High strand density β-sheets typical of amyloids have a lower twist and more protein strands per β-sheet compared to native β-sheets found in silk or β-keratin.[9] As a result, the Amide I absorbance of high strand density β-sheets as measured using Fourier transform infrared (FT-IR) spectroscopy appears at lower wavenumbers, <1625 cm^{-1}, than native β-sheets, 1625−1635 cm^{-1}.[10] Prior to misfolding these proteins are stable and serve a variety of biological functions. Some unknown event initiates misfolding and in some cases the proteins undergo an α-helix to β-sheet secondary structure transition.[10−16] It is generally accepted that any protein is capable of misfolding into an amyloid fibril given the right conditions, which are usually denaturing.[2,7] Indeed, a host of proteins and peptides such as myoglobin, β_2-microglobulin, and insulin have formed amyloid fibrils at primarily denaturing conditions.[1,17−29]

While the accidental misfolding of proteins can have debilitating effects in disease, certain organisms in nature produce "functional" amyloids as materials to sustain life.[1] Acorn barnacle *Megabalanus rosa* cement contains amyloid fibers that make it one of the most robust adhesives in nature.[30−35] *Escherichia coli* and *Streptomyces coelicolor* bacteria produce amyloid fibrils for surface-to-surface adhesion to create a matrix that can lead to bacterial biofilms.[36−38] Hydrophobin protein secreted from the fungus *Magnaporthe grisea* produces an amyloid hyphae that allows the fungus to attach to hydrophobic surfaces.[39−41] Atomic force microscopy (AFM) can be used to measure nanofibril cross-section and topography to calculate bending rigidity and moment of inertia. Using this technique, Knowles et al. found elastic moduli of E = 2−14 GPa for nanofibrils of "regular" morphology and E = 0.14−0.40 GPa for nanofibrils of "irregular" morphology.[42] AFM force spectroscopy yielded E = 3.3 ± 0.14 GPa for insulin amyloid fibrils.[45] Peak force quantitative nanomechanical AFM found E = 3.7 ± 1.1 GPa for β-lactoglobulin amyloid fibrils.[43,44] Molecular simulations predict amyloids to have E = 2.34 GPa at small strains and E = 12.43 GPa and 18.05 at large compressive and tensile strains, respectively.[18,46] These values approach the moduli of silk fibers but silk requires spinning to form the fiber while amyloid fibrils form spontaneously.[11,45,47−51] The functional role, high modulus, and easier production compared to other fibers like silk make amyloids an interesting motif for high performance biomaterials.[19,52−54]

Recent studies have focused on using the amyloid fibril as an engineered biomaterial. Adamcik et al. produced β-lactoglobulin amyloid tapes of approximately 20 nm wide with adjustable

Received: December 10, 2013
Revised: February 19, 2014

 © XXXX American Chemical Society

pitches based on the solution ionic strength.[55] Later studies produced large ribbons of approximately 150 nm wide with hen egg white lyzozyme and β-lactoglobulin.[56] Li et al. synthesized amyloid fibril reinforced graphene composites that were conductive, biodegradable, and inexpensive.[57] Previous research demonstrated that it was possible to form micrometer-sized amyloid fibers at near physiological conditions with hydrolyzed wheat gluten (WG) or hydrolyzed gliadin (Gd) combined with myoglobin (My) or amylase (Am).[11,58] The morphology and structural properties of the fibers could be manipulated as a function of solution conditions and the composition of the protein mixtures.[11,14] A four stage hierarchical mechanism of assembly from the nanometer to the micrometer scale was reported where (1) proteins self-assembled into protofibrils 10−30 nm wide, (2) protofibrils self-assembled into "fibrils" 60−120 nm wide, (3) fibrils self-assembled into "large fibrils" 150−480 nm wide, and (4) large fibrils assembled into "large amyloid fibers" 10−20 μm wide.[51] Further *in vivo* studies have shown that proteins expressed extracellularly self-assembled into large amyloid fibers demonstrating that the assembly of amyloid fibers can be genetically encoded.[59]

The key to hierarchical self-assembly of large amyloid fibers is to create mixtures of "template" and "adder" proteins.[11,58] Template proteins are high in aliphatic amino acids alanine (A), isoleucine (I), leucine (L), and valine (V), which makes the protein very hydrophobic and unstable in an aqueous environment. When using trypsin-hydrolyzed gliadin as the template, the template peptide, Gd20, is enzymatically released from the soluble full protein and is in very high concentration so that it quickly finds other template peptides.[59] The template peptides stabilize themselves by forming a β-sheet elementary unit where hydrophobic groups hide within the layers between the sheets.[51] So two template peptides each with two predominantly hydrophobic faces minimize surface energy by forming a sheet so that the number of exposed hydrophobic faces is reduced to two, three template peptides hide four faces with two remaining exposed, and so forth. This stacked β-sheet structure is termed the "template" and still has some hydrophobic groups exposed to the hydrophilic environment. The exposed faces of the template can minimize surface energy by interacting with another protein termed the "adder" protein. An adder protein is soluble in water, highly α-helical, and will not undergo conformation change unless perturbed. When brought into contact with one another, the α-helix on the adder protein will unravel on the template surface and "add" into the β-sheet structure and this addition seems to be crucial to self-assembly over several orders of magnitude of scale.[11] Indeed, it has been shown that α-helical proteins will readily undergo α to β transitions on hydrophobic surfaces and Aβ_{42} has been shown to do the same on cell surfaces.[60−62] FT-IR spectroscopy shows that the decrease in α-helix is approximately equal to the increase in high strand density β-sheets.[10,11,14,63,64] However, the change in α-helix content is always observed to be lower than the total α-helix content of the protein.[11] In addition, changing the adder protein will send the self-assembly down different paths resulting in large amyloid fibers of different morphology and properties and this seems to be related to the hydrophobicity of the adder protein.[14,51] It is hypothesized that the change in the α-helical content is related to the hydrophobic character of the α-helices on the adder protein and in turn this affects the conformation change and larger scale self-assembly. In this paper, adder proteins of varying α-helix content and hydrophobicity are mixed with a common template to explore the role of adder protein α-helix hydrophobicity in conformation change and self-assembly.

EXPERIMENTAL SECTION

Materials and Methods. *Calculation of Protein Parameters.* Adder protein secondary structures were found using PSIPRED.[65−67] From the secondary structure, the α-helical fraction of the protein, n_α, and the A, I, L, and V fraction of the α-helices, ϕ_α, was calculated. Protein molecular weight (MW) and aliphatic index (AI)[68] were computed with the ProtParam tool of the ExPASy Bioinformatics Resource Portal.[69] The mean relative hydrophobic moment, m$\mu_{H,rel}$, of each α-helix was calculated with the Peptide Sequence Analysis Tool created by Alex Tossi and Luca Sandri using the Kyte-Doolittle hydrophobicity scale.[70−72] Table 1 and Supporting Information Table S2 list the adder protein properties.

Table 1. The UniProt ID, Number of Amino Acids (#aa), α-Helix Fraction (n_α), Fraction of Aliphatic Amino Acids within the α-Helices (ϕ_α), and Mean Relative Hydrophobic Moment (m$\mu_{H,rel}$) for the Six Adder Proteins Used in This Study

adder protein	UniProt ID	#aa	n_α	ϕ_α	mu$_{H,rel}$
α-casein (Ac)	P02662	214	0.45	0.35	0.38
α-lactalbumin (Al)	P00711	142	0.38	0.38	0.41
amylase (Am)	P06278	512	0.25	0.36	0.41
hemoglobin (Hm)	P01958	142	0.69	0.41	0.34
insulin (In)	P01308	110	0.44	0.55	0.31
myoglobin (My)	P68082	154	0.76	0.36	0.39

Protein Mixtures. Hydrolyzed Gliadin (Gd, UniProt P04721, 30 403 g/mol) was prepared as previously reported and is used as the template.[11] To achieve a Gd/adder molar ratio of 0.36:0.64, 4.11 μmoles of Gd was mixed with 7.31 μmoles of the adder protein (Ac, Al, Am, Hm, In, or My) in 10 mL of pure water, which was consistent with previous studies.[11,14,51] Amylase was mixed at a 0.39:0.61 (Gd/Am) molar ratio to be consistent with a previous study but is very similar to the other molar ratios.[11] In order to reduce the stabilizing disulfide bonds within insulin and α-lactalbumin, a 1:1 molar ratio of β-mercaptoethanol (β-ME)/disulfide bond was used. For instance, insulin contained six cysteine amino acids that form three intramolecular disulfide bonds. Thus, 7.31 μmol of insulin*3 = 21.93 μmol of β-ME needed. β-ME is 78.13 g/mol and 1.114 g/cm^3, thus 1.5 μL of β-ME was added to the solution. Control solutions were made in the same manner without the addition of Gd. All solutions were well mixed and maintained at pH 8 and 37 °C for twenty days. FT-IR scans were taken daily as previously described.[11] The solutions were vortexed before each FT-IR scan to ensure the solution was homogeneous. Otherwise the solutions were maintained at pH 8 and 37 °C for twenty days without stirring. At the end of twenty days, the solutions were poured into Teflon-coated aluminum foil trays and allowed to fully dry at ambient conditions under a fume hood, which takes about one day. Amyloid fibers were manually collected with tweezers and scanning electron microscope (SEM) images were acquired as previously described.[11,51]

Analysis. Secondary structure fractions were determined through deconvolution of the FT-IR Amide I absorbance using Omnic v7.3 software and the procedure is described elsewhere.[10] The overall change in α-helix, Δ(α-helix), and high strand density β-sheet, $\Delta(\beta\text{-sheet})_{HD}$, were determined by the Amide I regions around 1650 cm^{-1} and <1625 cm^{-1}, respectively, as previously reported, and the values are represented as the maximum change over a 20 day period.[10,73] Multiple repeats of each solution were performed to get averages ± standard errors: Gd/Ac (6), Gd/Al (5), Gd/Am (6), Gd/Hm (6), Gd/In (5), Gd/My (4). Statistical analysis was performed with JMP v10.0 software.

dx.doi.org/10.1021/bm401815u | *Biomacromolecules* XXXX, XXX, XXX−XXX

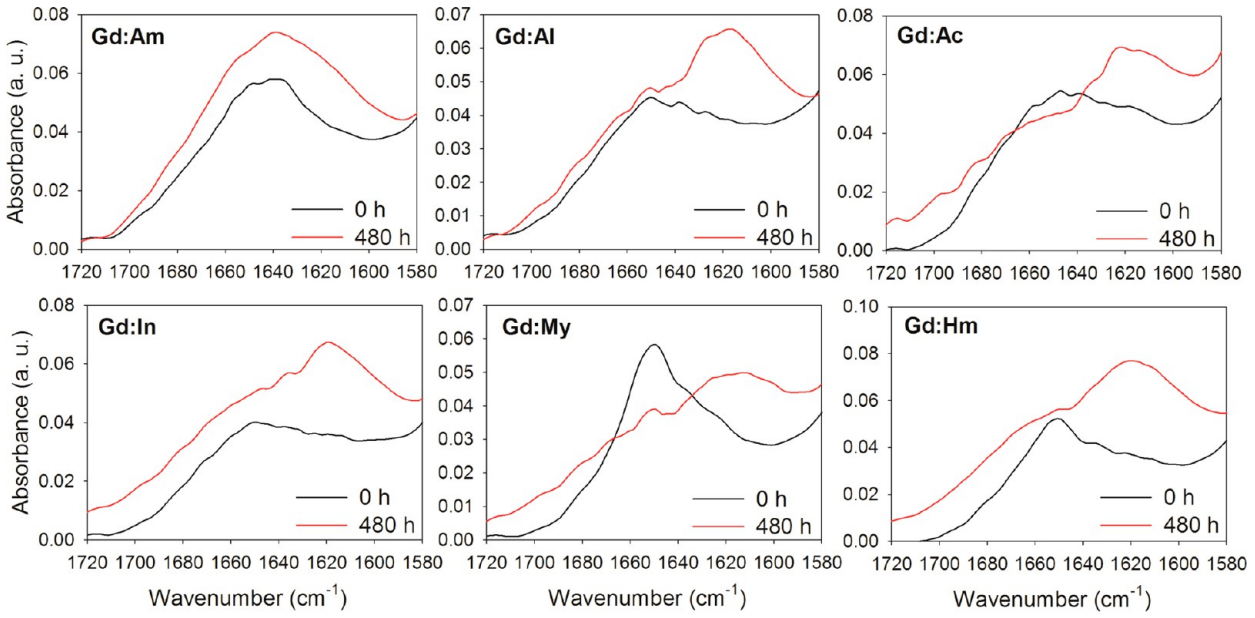

Figure 1. FT-IR spectra of the six protein mixtures (Gd/Am, Gd/Al, Gd/Ac, Gd/In, Gd/My and Gd/Hm) at early and late times showing the secondary structure transition from α-helix at ~1650 cm^{-1} to $(\beta\text{-sheet})_{HD}$ at <1625 cm^{-1} over 20 days.

RESULTS

Fourier Transform-Infrared Spectroscopy (FT-IR). FT-IR spectroscopy is a common method to characterize amyloids.[11,14,73−76] The Amide I absorbance region (1600−1700 cm^{-1}) has been used to characterize the secondary structure of proteins.[77] In earlier work on the template and adder protein mechanism, a clear trend was noticed where the loss in α-helix was approximately equal to the gain in $(\beta\text{-sheet})_{HD}$ upon deconvolution of the Amide I absorbance.[11] It was hypothesized that this conformation change largely occurred in the adder protein because the template protein is highly hydrophobic, unstable, and likely to undergo any conformation change quickly as it assembled into the template. To prove this hypothesis, the conformation change of a series of adder proteins with a common template, trypsin-hydrolyzed gliadin (Gd), were studied. Early and late time spectra reveal an Amide I absorbance shift from ~1650 to ~1620 cm^{-1} for five of the six protein mixtures, which clearly indicates an α to β conformational change (Figure 1). Gd/Am has an increased absorbance at 1620 cm^{-1} at 480 h compared to 0 h indicating that there is increased high density β-sheet content within the protein mixture while the α-helix fraction remains constant. This indicates that Am undergoes minimal α to β conformation change and the high density β-sheet gain is coming at the expense of other secondary structures.

In an effort to quantify the conformational changes within the protein mixtures, the Amide I absorbance was deconvoluted into Gaussian−Lorentzian peaks assigned to each of the secondary structure components.[10] Using the typical assumption for the Amide I deconvolution, which is equal molar absorptivity of each secondary structure component, each peak represents the approximate secondary structure molar fraction (random coil, α-helix, low density β-sheet, and high density β-sheet).[75,78,79] The decrease in α-helix and the increase in $(\beta\text{-sheet})_{HD}$ with respect to time can be observed and quantified in the same manner as previously reported.[10] This method was utilized to assess the maximum secondary structure change of the 6 protein mixtures over a 20 day period. It is observed that $\Delta(\beta\text{-sheet})_{HD}$ is approximately equal to $-\Delta(\alpha\text{-helix})$ (Table 2). This is consistent with previous reports.[11,14,51] The control solutions (identical to the mixtures without Gd) showed some conformational change, however the magnitudes were less than the protein mixtures (Figure 2).

Table 2. The Maximum Secondary Structure Change over a 20 Day Period for the 6 Protein Mixtures[a]

protein mixture	$-\Delta(\alpha\text{-helix})$	$\Delta(\beta\text{-sheet})_{HD}$
Gd/Ac	0.17 ± 0.022	0.21 ± 0.028
Gd/Al	0.15 ± 0.054	0.20 ± 0.120
Gd/Am	0.002 ± 0.021	0.10 ± 0.011
Gd/Hm	0.32 ± 0.022	0.39 ± 0.016
Gd/In	0.23 ± 0.022	0.25 ± 0.015
Gd/My	0.29 ± 0.011	0.36 ± 0.006

[a]The averages ± standard errors are reported.

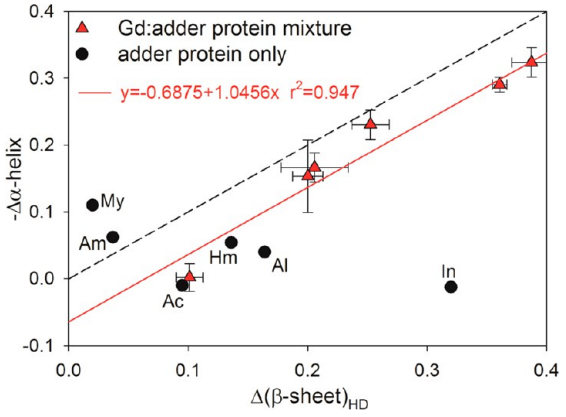

Figure 2. The average $\Delta(\beta\text{-sheet})_{HD}$ and $\Delta(\alpha\text{-helix})$ of the six protein mixtures and control solutions plotted with respect to each other. The error bars represent the standard error.

dx.doi.org/10.1021/bm401815u | Biomacromolecules XXXX, XXX, XXX−XXX

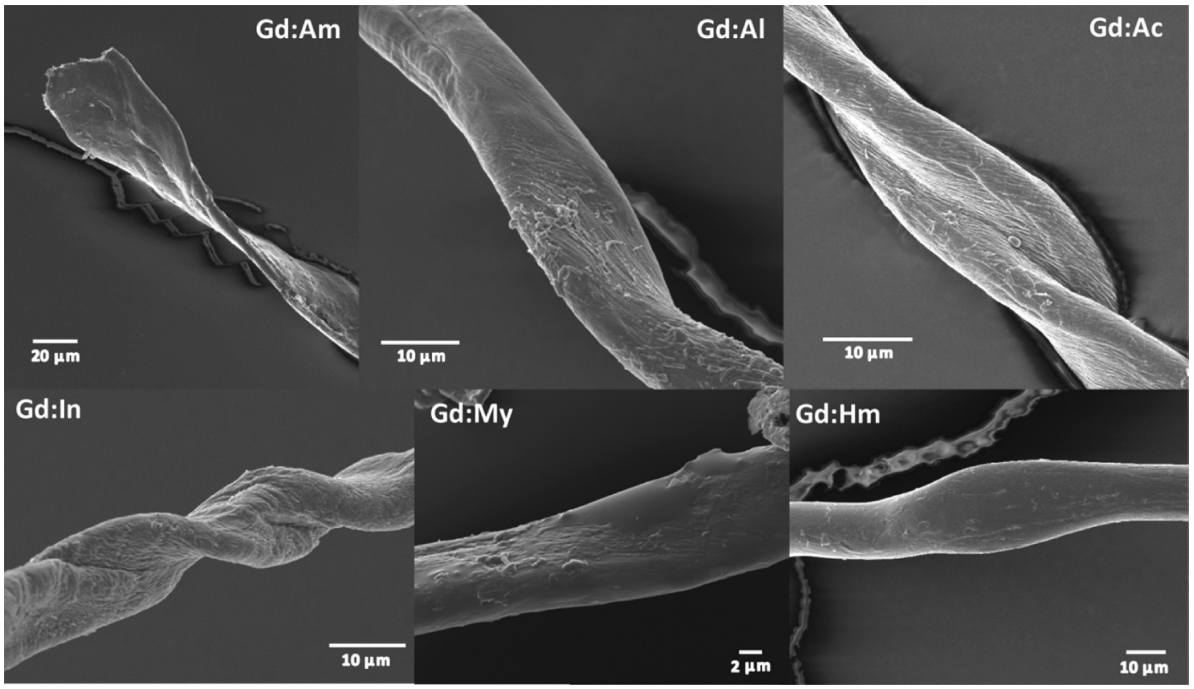

Figure 3. Scanning electron microscope (SEM) images of micrometer sized amyloid fibers formed from the 6 Gd/adder solutions upon drying after 20 days of incubation at pH 8 and 37 °C.

Scanning Electron Microscopy (SEM). Each of the protein mixtures self-assembled into micrometer-sized amyloid fibers upon drying (Figure 3). The fiber morphologies varied depending on the adder protein used. Solutions containing insulin and α-lactalbumin had intramolecular disulfide bonds reduced by β-mercaptoethanol. The loss of the disulfide bonds made it easier for the insulin and α-lactalbumin control solutions to form high density β-sheets (Figure 2) and these proteins have been shown to form amyloids under denaturing conditions.[73,80,81]

DISCUSSION

Adder Protein Conformation Change. Many proteins have shown the ability to self-assemble into amyloid fibrils but usually under the denaturing conditions necessary to destabilize protein molecules and allow them to form β-sheets.[1−4,82] Natural "functional" amyloids and pathogenic prion proteins must take advantage of their surroundings to do the same.[34,35,60,62,83] At the relatively mild solution conditions of pH 8 and 37 °C, peptides from hydrolyzed gliadin, Gd, initiate protein misfolding within six adder proteins (Ac, Al, Am, Hm, In, and My) resulting in self-assembly of large amyloid fibers. Five of the six protein mixtures undergo an α-helix to β-sheet conformational change (Figures 1 and 2). However, not all of the α-helix in the adder protein converts to β-sheet. Figure 4a shows that for any given adder protein, less than half of the total protein α-helix fraction (n_α) converts to β-sheet. Thus, portions of the α-helix must unravel into β-sheets. Previous research has shown that hydrophobic interactions between template and adder proteins appear to be important in self-assembly.[11,14] This has been observed in the FT-IR spectrum as an increase in the ratio of the symmetric CH_3 deformation to the asymmetric CH_3 deformation, $\delta_s(CH_3)/\delta_{as}(CH_3)$, during self-assembly, which indicates "hydrophobic packing" or interdigitation of CH_3 groups on A, I, L, and V.[10] Each protein mixture shows an increase in $\delta_s(CH_3)/\delta_{as}(CH_3)$ and the increase correlates to the loss of α-helix in 5 of the 6 mixtures (Figure 4b, Am is omitted from the linear fit and this is discussed below). Thus a second hypothesis is that hydrophobic portions of the α-helices are the most likely to unravel onto the partially hydrophobic surface of the template.

One way to describe the hydrophobic character of an α-helix is using the "hydrophobic moment."[84,85] Hydrophobic moment measures the asymmetry of the hydrophobicity of the α-helix. A large hydrophobic moment means that the α-helix is predominantly hydrophobic on one side or face and predominantly hydrophilic on the other side or face. Two α-helices in a soluble protein usually have their hydrophobic moments pointing toward each other (and away from water) to stabilize the protein. Similarly, α-helices in surface proteins will have high hydrophobic moments so that the hydrophobic side faces an apolar phase while the hydrophilic side faces a polar phase. If adder protein α-helices unravel onto hydrophobic template surfaces and convert to β-sheets, then the extent of the α to β conversion should correlate with the hydrophobic moment of the α-helix. The relative mean hydrophobic moment for each α-helix in the protein, $m\mu_{H,rel,i}$, is the mean hydrophobic moment normalized to a perfectly amphiphilic protein made up of isoleucine and arginine, the most hydrophobic and hydrophilic amino acids, respectively, in the Kyte-Doolittle scale.[86] Multiplying the relative mean hydrophobic moment for each α-helix in the protein by the fraction of the adder protein that the particular α-helix comprises, $n_{\alpha,i}$ (note $n_\alpha=\sum n_{\alpha,i}$) will yield the fraction of hydrophobic "faces" in the adder protein, $\sum(m\mu_{H,rel,i}*n_{\alpha,i})$, where the hydrophobic moment contribution of each α-helix is summed over the entire protein. There is a good correlation (r^2 = 0.65) between the loss in α-helix and the fraction of hydrophobic faces (Figure 5a) suggesting that the hydrophobic regions of the α-helix are the portions that change conformation.

Hydrophobic moment considers the directionality or spatial variation of the hydrophobicity of the α-helix and takes into

dx.doi.org/10.1021/bm401815u | Biomacromolecules XXXX, XXX, XXX−XXX

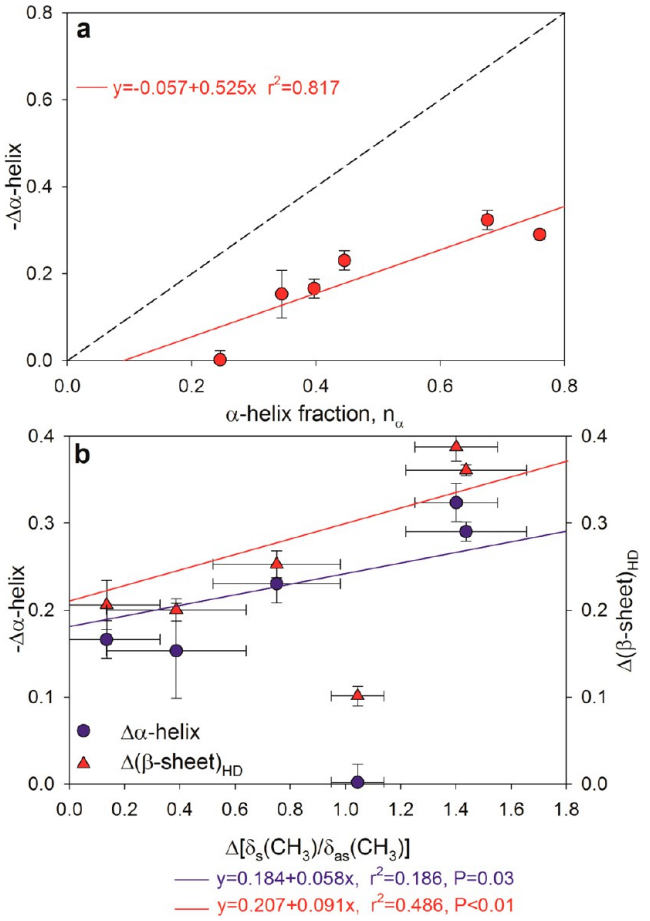

Figure 4. (a) The average decrease of α-helix plotted with respect to the total protein α-helix fraction, n_α, of the adder proteins within the six protein mixtures. (b) The average decrease of α-helix and increase of $(\beta\text{-sheet})_{HD}$ plotted against the observed hydrophobic packing, $\delta_s(CH_3)/\delta_{as}(CH_3)$, for the six protein mixtures. The error bars represent the standard error.

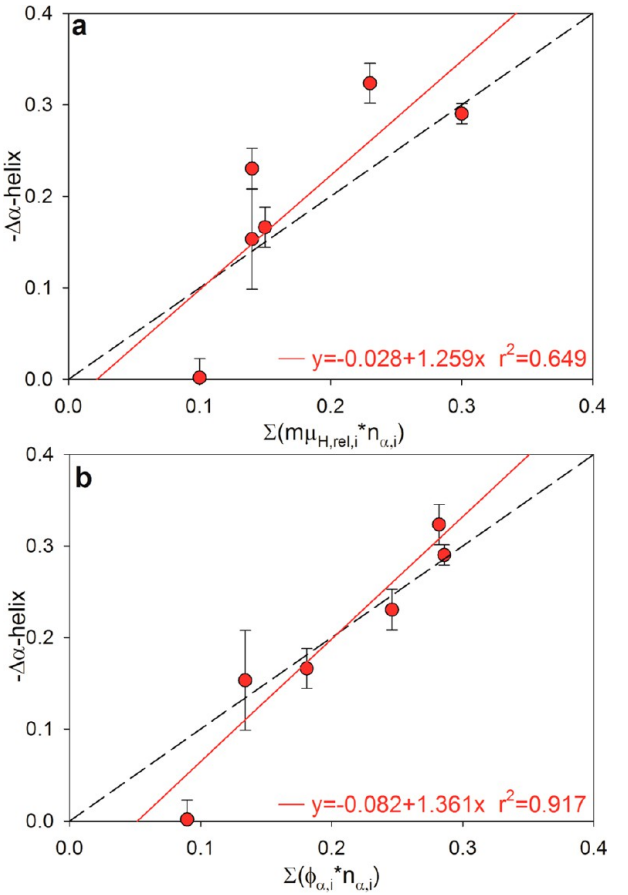

Figure 5. (a) The average decrease of α-helix plotted against the fraction of hydrophobic "faces" in the adder protein, $\sum(m\mu_{H,rel,i}{}^*n_{\alpha,i})$, for the six protein mixtures. (b) The average decrease of α-helix plotted with respect to the α-helix fraction, $n_{\alpha,i}$, multiplied by the fraction of A, I, L, and V, $\phi_{\alpha,i}$, within the α-helices of each adder protein. The error bars represent the standard error.

account all of the amino acids in the helix. However, not all of the helix fraction in each adder protein unravels so either a portion of each helix unravels or only some of the helices completely unravel. It is possible to argue for either happening. First, consider a portion of each helix in the adder protein unraveling. The amino acids that would contribute the most to the adder protein conformation change would be those with the most accessible hydrophobic groups to the template's surface exposed hydrophobic groups, which are rigidly held in place as part of the β-sheet template structure. The thermodynamic impetus to unravel the α-helix would be

$$G_H \approx \sum_i H_i\left(\frac{A_i}{A_0} - \frac{1}{2}\right) \quad (1)$$

where G_H is the hydrophobic contribution to the free energy of the α-helix, H_i is the hydrophobicity of the ith amino acid (approximately in kcal/mol) for transfer from a hydrophobic to a hydrophilic phase, and A_i/A_0 is the fraction of the surface of the ith amino acid available to solvent or the surrounding environment.[84,85] The free energy to unravel the α-helix is favorable, that is, G_H is negative, when the hydrophobic amino acid side chains in the adder protein α-helix are high accessible to the template and transfer from a hydrophilic to a hydrophobic environment, that is, from water to the β-sheet template surface. A correlation has been established between conformation change and the change in CH_3 groups on A, I, L, and V (Figure 4b).[10,11,14] When presented with a hydrophobic environment, it appears most likely that CH_3 groups on the end of amino acid side chains would be the most likely to prefer the template because H_i and (A_i/A_0) would both be high in eq 1. For other amino acid side groups, for instance, lysine, there is a long hydrophobic chain capped by a very hydrophilic primary amine. Spatially, the hydrophobic portion of the side chain is not very accessible to the template surface relative to the primary amine. Taking $\phi_{\alpha,i}$ as the fraction of A, I, L, and V in each α-helix and multiplying by $n_{\alpha,i}$, the total α-helix fraction in the protein, yields the fraction of the α-helices capable of undergoing conformation change based on the preceding argument.[11] A strong ($r^2 = 0.92$), nearly 1:1 correlation is found suggesting that not just hydrophobic regions but those containing template accessible CH_3 groups in the α-helices of adder proteins drive conformation change (Figure 4b).

Next, consider the case of some of the α-helices in each protein completely unraveling. PSIPRED predicts multiple α-helices in each adder protein (Supporting Information Table S1). Each has a different hydrophobic moment so some α-helices would be more likely to prefer the exposed hydrophobic groups on the template over others. Taking the number of amino acids in the α-helices of each protein, N_α and

dx.doi.org/10.1021/bm401815u | Biomacromolecules XXXX, XXX, XXX–XXX

multiplying by the overall change in the molar fraction of α-helix, $\Delta(\alpha\text{-helix})$, yields the number of amino acids that undergo conformation change in the protein, $\Delta\alpha^{*}N_{\alpha}$ (Table 3).

Table 3. Number of Amino Acids Undergoing Conformation Change in Each Adder Protein

protein	N_{α}	$\Delta(\alpha\text{-helix})$	$\Delta\alpha^{*}N_{\alpha}$
Ac	85	0.17	14.45
Al	49	0.15	7.35
Am	126	0.002	0.25
Hm	96	0.32	30.72
In	49	0.23	11.27
My	117	0.29	33.93

Highlighted in Supporting Information Table S1 are the highest mean relative hydrophobic moment α-helices, $m\mu_{H,rel,i}$, (and by definition the highest $m\mu_{H,i}$ α-helices) for each adder protein discounting the 2 amino acid α-helices predicted by PSIPRED. Comparing $\Delta\alpha^{*}N_{\alpha}$ to the length of each α-helix, L_i, italicized in Supporting Information Table S1 shows that perhaps some of the individual α-helices completely unravel. For instance, the eighth α-helix, α_8, of Ac is 15 amino acids long, has the highest hydrophobic moment, and $\Delta\alpha^{*}N_{\alpha}$ = 14.45 for Ac. Thus it is highly probably that α_8 of Ac is the α-helix that completely unravels. Similarly, α_2 of Al, $\alpha_4 + \alpha_7$ of Hm, α_3 or α_6 of In, and $\alpha_3 + \alpha_5 + \alpha_7$ of My are the most likely to unravel based on a similar comparison. The lack of conformation change is curious in Am because it contains 10 α-helices and several with a high hydrophobic moment. However, it has the lowest α-helix molar fraction at n_{α} = 0.25 and the highest molecular weight, 58 549 Da (512 amino acids) suggesting that hydrophobic groups within α-helices are not easily accessible at the solution conditions in the study and are buried within the protein. Am shows a gain in high-density β-sheet and a gain in $\delta_s(CH_3)/\delta_{as}(CH_3)$ and results of the Amide I deconvolution show the loss in random coil structures to be 0.11 ± 0.02, which is very close to the measured gain in high-density β-sheet. Thus, conformation change in Am occurs at hydrophobic amino acids residing in more easily accessible random coil regions. It would be interesting to study amylase at various solution conditions to see if the α-helices can be coaxed to unravel onto a β-sheet template.

The six adder proteins tested have different molecular weights, α-helix molar fractions (n_{α}), A, I, L, and V compositions (ϕ_{α}), mean relative hydrophobic moments ($m\mu_{rel,H,i}$), and isoelectric points (pI). But, when combined with a template (Gd) adder proteins tend to undergo a near 1:1 α-helix to $(\beta\text{-sheet})_{HD}$ conformational change as long as hydrophobic regions on the α-helices are accessible. The extent of conformational change within the adder proteins can be predicted by utilizing the mean relative hydrophobic moment or the fraction of A, I, L, and V within the α-helices, multiplied by n_{α} or by comparing $\Delta\alpha^{*}N_{\alpha}$ to the α-helices in the adder protein with the highest hydrophobic moments. Therefore, it is possible to predict the propensity of an adder protein to unfold onto a template into an amyloid structure utilizing the intrinsic properties of the adder α-helices and to note spatially within the protein where conformation change is happening. Thus, proteins could be designed to unfold and self-assemble into β-sheets of very specific size with unassembled portions in between. The size of the β-sheets has been shown theoretically to influence the properties of the material and controlling unassembled portions in between would portend a further level of control in protein materials design.[87,88]

Fiber Morphology. Each template/adder protein mixture self-assembles to the micrometer scale and obtains a different fibrous morphology (Figure 3). Previous research has shown that different adder proteins alter the morphology of the large amyloid fibers.[11,14,51] To determine which factors contribute to each morphology, fiber morphological features are quantified (see Figure 1 in Ridgley et al.).[14] The pitch of the large fibrils (ca. 100−200 nm wide), h_t, that self-assemble into and wrap around the fiber is found to be dependent on the overall pitch of the fiber, h' (Figure 6a). In addition, h_t is dependent on the

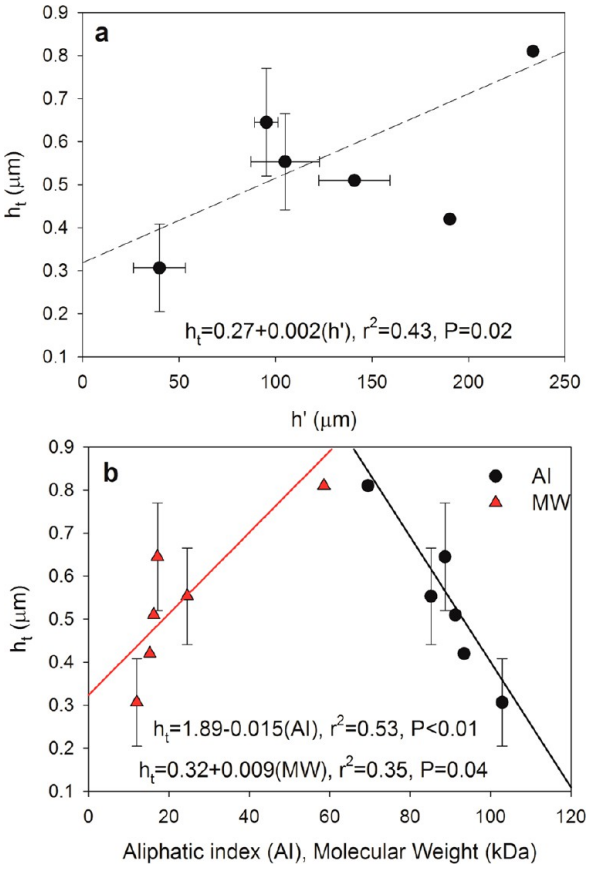

Figure 6. Measurements of morphological features of self-assembled Gd/adder protein amyloid fibers showing (a) correlation between h_t and h' and (b) h_t and the AI and MW. All fitted lines are statistically significant, $P < 0.05$.

AI and MW (Figure 6b). The relationship between h_t and h' shows a self-similarity between the two largest scales of the self-assembly. The pitch observed at the large fibril stage (h_t) influences the pitch at the highest scale, which is the large fiber (h').[14,51,59] This is a strong indication that the molecular interactions that drive large fibril wrapping on the nanometer scale are conserved to fiber wrapping on the micrometer scale. On the molecular level, overall hydrophobicity appears to be important to how smaller scale structures, like large fibrils, self-assemble into the final large fiber. A higher AI results in large fibrils assembling with a tighter twist as measured by a lower h_t showing hydrophobic interactions not only influence conformation change but higher scale self-assembly and morphology development (Figure 6b). h_t is inversely proportional to the

dx.doi.org/10.1021/bm401815u | Biomacromolecules XXXX, XXX, XXX−XXX

MW, which supports a previous model that shows an adder protein of higher molecular weight has portions of the protein that remain unassembled and hinder the twisting of a fiber.[11] These results demonstrate that it is possible to predict the morphology of a large amyloid fiber based on molecular features of the adder protein.

CONCLUSION

This study compared six diverse adder proteins to discern what properties of an adder protein drive conformation change and self-assembly into large amyloid fibers in the presence of a hydrophobic and highly unstable template. The results showed that for 5 of the 6 proteins studied, the loss of α-helix is nearly equal to the increase of high-density β-sheet content, which was indicative of amyloid formation. However, not all of the α-helix unfolded into β-sheets. It was observed that adder protein conformation change correlated with changes in hydrophobic amino acids during self-assembly. The adder protein α-helix fraction, n_α, fraction of A, I, L, and V within the α-helices, ϕ_α, and the mean relative hydrophobic moment of the α-helices, $m\mu_{H,rel}$, were capable of predicting the conformation change. Adder protein hydrophobicity, as measured by AI and MW, could predict large scale fiber morphology features. This study demonstrates that it is possible to engineer large amyloid fibers utilizing the template and adder mechanism of amyloid self-assembly by controlling the intrinsic properties of the adder protein. Furthermore, this study may offer some insight into a common mechanism of amyloid self-assembly in nature.

ASSOCIATED CONTENT

Supporting Information

A table listing the individual α-helix hydrophobic moments within each adder protein, a table of the aliphatic index, molecular weight, grand average hydropathicity, isoelectric point, and the fiber morphology of the adder proteins. This material is available free of charge via the Internet at http://pubs.acs.org.

AUTHOR INFORMATION

Corresponding Author

*E-mail: jbarone@vt.edu. Phone: (540) 231-0680.

Notes

The authors declare no competing financial interest.

ACKNOWLEDGMENTS

Generous funding through NSF-CMMI-0856262, USDA-NIFA #2010-65504-20429 and the Virginia Tech Biodesign and Bioprocessing Research Center are greatly appreciated.

REFERENCES

(1) Chiti, F.; Dobson, C. M. *Annu. Rev. Biochem.* **2006**, *75*, 333−366.
(2) Dobson, C. M. *Nature* **2003**, *426*, 884−890.
(3) Dobson, C. M. *Philos. Trans. R. Soc. London, Ser. B* **2001**, *356*, 133−145.
(4) Dobson, C. M.; Šali, A.; Karplus, M. *Angew. Chem., Int. Ed.* **1998**, *37*, 868−893.
(5) Prusiner, S. B. *Cell* **1983**, *35*, 349−358.
(6) Prusiner, S. B. *N. Engl. J. Med.* **2001**, *344*, 1516−1526.
(7) Prusiner, S. B. *Proc. Natl. Acad. Sci. U.S.A.* **1998**, *95*, 13363−13383.
(8) Sunde, M.; Blake, C. C. *Q. Rev. Biophys.* **1998**, *31*, 1−39.
(9) Kubelka, J.; Keiderling, T. A. *J. Am. Chem. Soc.* **2001**, *123*, 12048−12058.
(10) Ridgley, D. M.; Claunch, E. C.; Barone, J. R. *Appl. Spectrosc.* **2013**, *57*, 1417−1426.
(11) Ridgley, D. M.; Ebanks, K. C.; Barone, J. R. *Biomacromolecules* **2011**, *12*, 3770−3779.
(12) Safar, J.; Roller, P. P.; Gajdusek, D. C.; Gibbs, C. J. *J. Biol. Chem.* **1993**, *268*, 20276−20284.
(13) Soto, C.; Castaño, E. M.; Frangione, B.; Inestrosa, N. C. *J. Biol. Chem.* **1995**, *270*, 3063−3067.
(14) Ridgley, D. M.; Claunch, E. C.; Barone, J. R. *Soft Matter* **2012**, *8*, 10298−10306.
(15) Pan, K.-M.; Baldwin, M.; Nguyen, J.; Gasset, M.; Serban, A.; Groth, D.; Mehlhorn, I.; Huang, Z.; Fletterick, R. J.; Cohen, F. E. *Proc. Natl. Acad. Sci. U.S.A.* **1993**, *90*, 10962−10966.
(16) Nguyen, J.; Baldwin, M. A.; Cohen, F. E.; Prusiner, S. B. *Biochemistry* **1995**, *34*, 4186−4192.
(17) Heegaard, N. H. H.; Jørgensen, T. J. D.; Rozlosnik, N.; Corlin, D. B.; Pedersen, J. S.; Tempesta, A. G.; Roepstorff, P.; Bauer, R.; Nissen, M. H. *Biochemistry* **2005**, *44*, 4397−4407.
(18) Knowles, T. P. J.; Buehler, M. J. *Nat. Nanotechnol.* **2011**, *6*, 469−479.
(19) Knowles, T. P. J.; Oppenheim, T. W.; Buell, A. K.; Chirgadze, D. Y.; Welland, M. E. *Nat. Nanotechnol.* **2010**, *5*, 204−207.
(20) Bouchard, M.; Zurdo, J.; Nettleton, E. J.; Dobson, C. M.; Robinson, C. V. *Protein Sci.* **2000**, *9*, 1960−1967.
(21) Fandrich, M.; Fletcher, M. A.; Dobson, C. M. *Nature* **2001**, *410*, 165−166.
(22) Gosal, W. S.; Morten, I. J.; Hewitt, E. W.; Smith, D. A.; Thomson, N. H.; Radford, S. E. *J. Mol. Biol.* **2005**, *351*, 850−864.
(23) Hasegawa, K.; Yamaguchi, I.; Omata, S.; Gejyo, F.; Naiki, H. *Biochemistry* **1999**, *38*, 15514−15521.
(24) Knowles, T. P.; Fitzpatrick, A. W.; Meehan, S.; Mott, H. R.; Vendruscolo, M.; Dobson, C. M.; Welland, M. E. *Science* **2007**, *318*, 1900−1903.
(25) Raman, B.; Chatani, E.; Kihara, M.; Ban, T.; Sakai, M.; Hasegawa, K.; Naiki, H.; Rao, C. M.; Goto, Y. *Biochemistry* **2005**, *44*, 1288−1299.
(26) Aggeli, A.; Nyrkova, I. A.; Bell, M.; Harding, R.; Carrick, L.; McLeish, T. C. B.; Semenov, A. N.; Boden, N. *Proc. Natl. Acad. Sci. U.S.A.* **2001**, *98*, 11857−11862.
(27) Davies, R. P. W.; Aggeli, A.; Beevers, A. J.; Boden, N.; Carrick, L. M.; Fishwick, C. W. G.; McLeish, T. C. B.; Nyrkova, I.; Semenov, A. N. *Supramol. Chem.* **2006**, *18*, 435−443.
(28) Fändrich, M.; Forge, V.; Buder, K.; Kittler, M.; Dobson, C. M.; Diekmann, S. *Proc. Natl. Acad. Sci. U.S.A.* **2003**, *100*, 15463−15468.
(29) Xue, W. F.; Homans, S. W.; Radford, S. E. *Proc. Natl. Acad. Sci. U.S.A.* **2008**, *105*, 8926−8931.
(30) Kamino, K. *Mar. Biotechnol.* **2008**, *10*, 111−121.
(31) Nakano, M.; Shen, J.-R.; Kamino, K. *Biomacromolecules* **2007**, *8*, 1830−1835.
(32) Kamino, K.; Inoue, K.; Maruyama, T.; Takamatsu, N.; Harayama, S.; Shizuri, Y. *J. Biol. Chem.* **2000**, *275*, 27360−27365.
(33) Kamino, K. *J. Biol. Chem.* **2000**, *275*, 27360−27365.
(34) Kamino, K. *Biol. Bull.* **1996**, *190*, 403−409.
(35) Barlow, D. E.; Dickinson, G. H.; Orihuela, B.; Kulp, J. L., III; Rittschof, D.; Wahl, K. J. *Langmuir* **2010**, *26*, 6549−6556.
(36) Fowler, D. M.; Koulov, A. V.; Balch, W. E.; Kelly, J. W. *Trends Biochem. Sci.* **2007**, *32*, 217−224.
(37) Larsen, P. *Environ. Microbiol.* **2007**, *9*, 3077−3090.
(38) Claessen, D.; Rink, R.; de Jong, W.; Siebring, J.; de Vreugd, P.; Hidde Boersma, F. G.; Dijkhuizen, L.; Wosten, H. A. B. *Genes Dev.* **2003**, *17*, 1714−1726.
(39) Gebbink, M. F. B. G.; Claessen, D.; Bouma, B.; Dijkhuizen, L.; Wosten, H. A. B. *Nat. Rev. Microbiol.* **2005**, *3*, 333−341.
(40) Wösten, H. A. *EMBO J.* **1994**, *13*, 5848−5854.
(41) Talbot, N. J. *Plant Cell* **1993**, *5*, 1575−1590.
(42) Knowles, T. P.; Fitzpatrick, A. W.; Meehan, S.; Mott, H. R.; Vendruscolo, M.; Dobson, C. M.; Welland, M. E. *Science* **2007**, *318*, 1900−1903.

(43) Adamcik, J.; Berquand, A.; Mezzenga, R. *Applied Physics Letters* **2011**, *98*, 193701.
(44) Adamcik, J.; Lara, C.; Usov, I.; Jeong, J. S.; Ruggeri, F. S.; Dietler, G.; Lashuel, H. A.; Hamely, I. W.; Mezzenga, R. *Nanoscale* **2012**, *4*, 4426−4429.
(45) Smith, J. F.; Knowles, T. P. J.; Dobson, C. M.; MacPhee, C. E.; Welland, M. E. *Proc. Natl. Acad. Sci. U.S.A.* **2006**, *103*, 15806−15811.
(46) Paparcone, R.; Keten, S.; Buehler, M. J. *J. Biomech.* **2010**, *43*, 1196−1201.
(47) Nova, A.; Keten, S.; Pugno, N. M.; Redaelli, A.; Buehler, M. J. *Nano Lett.* **2010**, *10*, 2626−2634.
(48) Qin, Z.; Buehler, M. J. *Nat. Mater.* **2013**, *12*, 185−187.
(49) Vehoff, T.; Glišović, A.; Schollmeyer, H.; Zippelius, A.; Salditt, T. *Biophys. J.* **2007**, *93*, 4425−4432.
(50) Kaplan, D. L. *Nat. Biotechnol.* **2002**, *20*, 239−240.
(51) Ridgley, D. M.; Barone, J. R. *ACS Nano* **2013**, *7*, 1006−1015.
(52) Paparcone, R. *J. Biomech.* **2010**, *43*, 1196−1201.
(53) Gazit, E. *Chem. Soc. Rev.* **2007**, *36*, 1263−1269.
(54) Reches, M.; Gazit, E. *Science* **2003**, *300*, 625−627.
(55) Adamcik, J.; Mezzenga, R. *Soft Matter* **2011**, *7*, 5437−5443.
(56) Lara, C. c.; Adamcik, J.; Jordens, S.; Mezzenga, R. *Biomacromolecules* **2011**, *12*, 1868−1875.
(57) Li, C.; Adamcik, J.; Mezzenga, R. *Nat. Nanotechnol.* **2012**, *7*, 421−427.
(58) Athamneh, A.; Barone, J. R. *Smart Mater. Struct.* **2009**, *18*, 104024−104031.
(59) Ridgley, D. M.; Freedman, B. G.; Lee, P. W.; Barone, J. R. *Biomater. Sci.* **2014**, DOI: 10.1039/C3BM60223K.
(60) Fink, A. L. *Folding Des.* **1998**, *3*, R9−R23.
(61) Zhu, M.; Souillac, P. O.; Ionescu-Zanetti, C.; Carter, S. A.; Fink, A. L. *J. Biol. Chem.* **2002**, *277*, 50914−50922.
(62) Bokvist, M.; Lindström, F.; Watts, A.; Gröbner, G. *J. Mol. Biol.* **2004**, *335*, 1039−1049.
(63) Zandomeneghi, G.; Krebs, M. R. H.; McCammon, M. G.; Fandrich, M. *Protein Sci.* **2004**, *13*, 3314−3321.
(64) Dong, A.; Huang, P.; Caughey, W. S. *Biochemistry* **1990**, *29*, 3303−3308.
(65) Buchan, D. W. A.; Ward, S. M.; Lobley, A. E.; Nugent, T. C. O.; Bryson, K.; Jones, D. T. *Nucleic Acids Res.* **2010**, *38*, W563−W568.
(66) Jones, D. T. *J. Mol. Biol.* **1999**, *292*, 195−202.
(67) Jones, D. T.; Buchan, D.; Nugent, T.; Minneci, F.; Bryson, K. *The PSIPRED Protein Sequence Analysis Workbench*; 2013, http://bioinf.cs.ucl.ac.uk/psipred/. Accessed December 18, 2012.
(68) Atsushi, I. *J. Biochem.* **1980**, *88*, 1895−1898.
(69) Gasteiger, E.; Hoogland, C.; Gattiker, A.; Duvaud, S. E.; Wilkins, M. R.; Appel, R. D.; Bairoch, A. In *Protein Identification and Analysis Tools on the ExPASy Server, The Proteomics Protocols Handbook*; Walker, J. M., Ed.; Humana Press: Totowa, NJ, 2005; p 571−607.
(70) Tossi, A.; Sandri, L.; Giangaspero, A. *Peptides* **2002**, 416−417.
(71) Kyte, J. *J. Mol. Biol.* **1982**, *157*, 105−132.
(72) Tossi, A.; Saundri, L. *Peptide Sequence Analysis Tool*; 2002.http://www.bbcm.univ.trieste.it/~tossi/HydroCalc/HydroMCalc.html. Accessed October 17, 2013.
(73) Dzwolak, W.; Loksztejn, A.; Smirnovas, V. *Biochemistry* **2006**, *45*, 8143−8151.
(74) Zurdo, J.; Guijarro, J. I.; Dobson, C. M. *J. Am. Chem. Soc.* **2001**, *123*, 8141−8142.
(75) Hiramatsu, H.; Kitagawa, T. *Biochim. Biophys. Acta* **2005**, *1753*, 100−107.
(76) Szabo, Z.; Klement, E.; Jost, K.; Zarandi, M.; Soos, K.; Penke, B. *Biochem. Biophys. Res. Commun.* **1999**, *265*, 297−300.
(77) Krimm, S.; Bandekar, J. In *Advances in Protein Chemistry*; Anfinsen, C. B., Edsall, J. T., Richards, F. M., Eds.; Academic Press, Inc.: New York, 1986; Vol. *38*, pp 181−364.
(78) Jackson, M.; Haris, P. I.; Chapman, D. *Biochim. Biophys. Acta* **1989**, *998*, 75−79.
(79) Fabian, H.; Naumann, D.; Misselwitz, R.; Ristau, O.; Gerlach, D.; Welfle, H. *Biochemistry* **1992**, *31*, 6532−6538.
(80) Dzwolak, W.; Smirnovas, V.; Jansen, R.; Winter, R. *Protein Sci.* **2004**, *13*, 1927−1932.
(81) Goers, J.; Permyakov, S. E.; Permyakov, E. A.; Uversky, V. N.; Fink, A. L. *Biochemistry* **2002**, *41*, 12546−12551.
(82) Bucciantini, M.; Giannoni, E.; Chiti, F.; Baroni, F.; Formigli, L.; Zurdo, J.; Taddei, N.; Ramponi, G.; Dobson, C. M.; Stefani, M. *Nature* **2002**, *416*, 507−511.
(83) Chernoff, Y.; Lindquist, S.; Ono, B.; Inge-Vechtomov, S.; Liebman, S. *Science* **1995**, *268*, 880−884.
(84) Eisenberg, D.; Weiss, R. M.; Terwilliger, T. C.; Wilcox, W. *Faraday Symp. Chem. Soc.* **1982**, *17*, 109−120.
(85) Eisenberg, D.; Wilcox, W.; McLachlan, A. D. *J. Cell. Biochem.* **1986**, *31*, 11−17.
(86) Kyte, J.; Doolittle, R. F. *J. Mol. Biol.* **1982**, *157*, 105−132.
(87) Xu, Z.; Paparcone, R.; Buehler, M. J. *Biophys. J.* **2010**, *98*, 2053−2062.
(88) Paparcone, R.; Buehler, M. J. *Appl. Phys. Lett.* **2009**, *94*, 243904−3.

Chapter 7.

Genetically Encoded Self-Assembly of Large Amyloid Fibers

Ridgley, D. M., B. G. Freedman, P. W. Lee, and J. R. Barone. 2014. Genetically Encoded Self-Assembly of Large Amyloid Fibers. *Biomater. Sci.* 2(4):560-566. - Reproduced with generous permission of the Royal Society of Chemistry.

Note: The Supporting Information referred to in Chapter 7 is located in Appendix B.

Biomaterials Science

PAPER

View Article Online
View Journal | View Issue

Genetically encoded self-assembly of large amyloid fibers†

Cite this: *Biomater. Sci.*, 2014, **2**, 560

D. M. Ridgley, B. G. Freedman, P. W. Lee and J. R. Barone*

Received 23rd September 2013,
Accepted 21st December 2013

DOI: 10.1039/c3bm60223k

www.rsc.org/biomaterialsscience

"Functional" amyloids are found throughout nature as robust materials. We have discovered that "template" and "adder" proteins cooperatively self-assemble into micrometer-sized amyloid fibers with a controllable, hierarchical structure. Here, *Escherichia coli* is genetically engineered to express a template protein, Gd20, that can initiate self-assembly of large amyloid fibrils and fibers. Through atomic force microscopy (AFM) we found that expression of Gd20 produces large amyloid fibrils of 490 nm diameter and 2–15 μm length. Addition of an extracellular adder protein, myoglobin, continues self-assembly to form amyloid tapes with widths of ~7.5 μm, heights of ~400 nm, and lengths exceeding 100 μm. Without myoglobin the amyloid fibrils are metastable over time. When myoglobin is present, the amyloid fiber continues self-assembling to a width of ~18 μm and height of ~1 μm. Experimental results demonstrate that large amyloid fibers with a tailored stiffness and morphology can be engineered at the DNA level, spanning four orders of magnitude.

Published on 14 January 2014. Downloaded on 04/03/2014 16:54:39.

Introduction

Amyloid fibrils are usually studied in the context of neurodegenerative diseases.[1] "Functional" amyloids used by organisms for survival are being discovered, such as in the barnacle cement of *Megabalanus rosa*.[2–4] The functional nature, high specific modulus, and ability to be self-assembled from a variety of proteins make amyloids interesting designer nanomaterials.[5–7] There are many studies of the nanometer-sized amyloid fibril, which displays consistent morphology and properties when produced from a variety of proteins.[8–10] The amyloid fibril is composed of high strand density β-sheets that are oriented perpendicular to the fibril axis.[11,12] Recent research has demonstrated that it is possible to grow large amyloid fibers with tailored morphology (circular or rectangular cross-sections) and modulus (0.1–2.5 GPa) *in vitro* by utilizing a "template" and "adder" protein mixture.[13] The large amyloid fibers form from nanometer fibrils that continue to interact to the micrometer scale.[14] Different amyloid fibers can be self-assembled by altering solution conditions, template to adder protein molar ratios, or adder protein length and sequence.[13,15] Template proteins are capable of conformation change on their own but adder proteins are not. The predominantly hydrophobic template protein assumes the β-sheet as the lowest energy state to hide most hydrophobic groups between the sheets. For a population of template proteins, most hydrophobic groups are hidden inside the β-sheets but the template still has hydrophobic faces. Hydrophobic groups on the α-helices of predominantly hydrophilic adder proteins prefer the exposed hydrophobic groups on the template, undergo an α to β transition, and "add" into the structure to form larger β-sheets and fibrils. It is the "addition" event that allows further self-assembly beyond the stable nanometer template scale and is what makes this system unique. The conformational changes resulting from addition allow a large entropy gain by the water relative to template formation alone. Further assembly involves a competition between hydrophobic and hydrogen bonding interactions that differentiates morphology and properties based on adder protein properties.

Observation of a controllable, hierarchical protein self-assembly process fostered the notion that large structures of varying shape and modulus could be encoded at the genetic level. For instance, a cylindrical fiber 20 μm across and 10^4 μm long with a 1 GPa modulus could be built simply by inserting the DNA of the correct template and adder proteins into a cellular expression system. The fiber could be constructed into a composite by expressing a third, non-assembling protein or polymer to act as a matrix. Silk-like copolymers and recombinant collagen have been produced by expressing the desired protein(s) in *E. coli* or *P. pastoris*.[16,17] Unfortunately, the target protein(s) must undergo substantial post-expression processing to assemble the protein fiber.[18,19] Scheibel *et al.* used *Saccharomyces cerevisiae* to express the Sup35p prion determinant

Biological Systems Engineering, Virginia Tech, 203 Seitz Hall, Blacksburg, VA 24061, USA. E-mail: jbarone@vt.edu; Tel: (+1 540) 231-0680

†Electronic supplementary information (ESI) available: A table of the intrinsic properties of Gd20 and myoglobin as well as their respective amino acid sequences, cross-sectional measurements of the X fibril and XMy fiber at 72 hours. See DOI: 10.1039/c3bm60223k

This journal is © The Royal Society of Chemistry 2014

Published on 14 January 2014. Downloaded on 04/03/2014 16:54:39.

protein that self-assembled into amyloid fibril templates to form conducting nanowires.[20] Here we investigate the potential for genetically encoded self-assembly through the expression of our template protein, Gd20, in *E. coli* with and without the extracellular addition of the My adder protein.

Materials and methods

DNA insertion

All chemicals were obtained from Thermo Fisher Scientific unless otherwise specified. All bacteria were grown on LB media supplemented with 100 mg L^{-1} ampicillin or 15 g L^{-1} agar where appropriate.[21] All *Escherichia coli* strains, plasmids, and enzymes were purchased from New England BioLabs (Ipswich, MA, USA). The oligopeptide sequence of Gd20 (Start-TFLILALLAIVATTATTAVR-Stop-Stop) was optimized for expression in *E. coli* strain K12 using the JCat program[22] and the resulting double-stranded DNA was ordered from Integrated DNA Technologies (Coralville, IA). The gene fragment was amplified by PCR (Eppendorf, Hauppauge, NY) with oligonucleotide primers Forward (5′-GGTGGTCATATGAC CTTCC-TGATCCTGGC-3′) and Reverse (5′-GTGGTTGCTCTTCCGCA-TTATTAACGAACA GCGGTGGT-3′) which included NdeI and SapI restriction sites for entry into vector pTXB1 (New England BioLabs). The resulting plasmid, pTXGd20, was transformed into *E. coli* NEB5-alpha by standard protocols[21] and verified by PCR. The plasmid DNA was purified by miniprep (Gerard BioTec, Oxford, OH, USA) and transformed into the protein expression *E. coli* cell line ER2566.

Gd20 expression

Cells containing the Gd20 plasmid were grown up in LB-Amp to an optical density at 600 nm ($0D_{600}$) of 0.5. Isopropyl β-D-1-thiogalactopyranoside (IPTG) was added at a concentration of 0.4 mM to X and XMy to induce expression of Gd20. Myoglobin (My, from equine skeletal muscle, Sigma-Aldrich, St. Louis, MO, UniProt P68082) was added to NXMy and XMy at a concentration of 12.5 mg ml^{-1}, which was simply the concentration used previously and was expected to be sufficient to allow addition into any Gd20 template produced.[13]

Fourier-transform infrared (FT-IR) spectroscopy

The four cell cultures were dried on Teflon coated aluminum foil after 43 and 72 hours of incubation. Spectra of the dried cultures were acquired on a Thermo Fisher Scientific, Inc. (Waltham, MA) 6700 FT-IR with a Smart Orbit diamond attenuated total reflectance (ATR) accessory. Spectra were acquired using Omnic v8.0 software in the same manner as previously reported.[13,15] The spectral region from 1720–1580 cm^{-1} was isolated and manually smoothed with the Savitzky–Golay algorithm using 9–13 points. The second derivative of the Amide I spectral region was taken without filtering to identify the individual Amide I components.

Atomic force microscopy (AFM)

AFM was performed on an Innova AFM (Bruker, Santa Barbara, CA) after 37 hours (X, NX, XMy) and 72 hours (X, NX, XMy and NXMy) with samples prepared, imaged, and enhanced in the same manner as previously reported.[14] Nanoindentation of the large fibrils (X) and fibers (XMy) was performed in contact mode with a 0.01–0.025 Ohm cm antimony-doped Si probe (Bruker, part: MPP-31123-10, R: 8 nm and k: 0.9 N m^{-1}). The deflection-displacement curves were obtained with NanoDrive v8.01 software using the Point Spectroscopy mode with 512 points taken at a 0.5 μm s^{-1} approach/retreat rate. The curves were converted to a force-displacement curve utilizing the probe's spring constant according to the manufacturer.[23] Young's modulus was extrapolated according to Guo *et al.* with Poisson's ratio taken as 0.3, which has been used in previous amyloid studies.[24,25] 11 indentations were performed on 2 XMy fibers (XMy) and 6 X large fibrils (X) each at 37 hours. 7 indentations were performed on 1 XMy fiber and 4 X large fibrils each at 72 hours. The averages ± the standard errors are reported.

Results and discussion

Four cell cultures are analyzed with atomic force microscopy (AFM) and Fourier transform-infrared (FT-IR) spectroscopy to determine the presence of amyloid fibrils or fibers and their structure: (1) cells without expression of Gd20 (NX), (2) cells without expression of Gd20 but My addition (NXMy), (3) cells with expression of Gd20 (X), and (4) cells with expression of Gd20 and My addition (XMy).

The four cell cultures (NX, NXMy, X, XMy) are analyzed with AFM to assess fiber formation in the presence or absence of Gd20 or My. The NX culture shows coalesced, partially lysed *E. coli* with no fibrous structures (Fig. 1a). When Gd20 is expressed in the X culture several fibrous structures appear throughout the solution. X produces large amyloid fibrils of 490 nm diameter and 2–15 μm length (Fig. 1b–d) similar to the large fibrils observed *in vitro* previously.[14] Closer examination of the fibrils reveals that *E. coli* is attached to the surface (Fig. 1c). The small molecular weight and high hydrophobicity of Gd20 (ESI Table 1† and Fig. 1) may cause some of it to embed in the cell lipid bilayer and become partially exposed outside the cell surface, acting as a bridge between the cell and the self-assembled amyloid fibril (Scheme 1).

Previous studies have indicated that a template and an adder protein are necessary for the formation of large amyloid fibers at near physiological conditions.[13] Extracellular My is added to the cultures to determine how a proven adder protein affects the formation of amyloid fibers. The NXMy culture tests how My interacts with *E. coli* in the absence of Gd20. NXMy does not form fibrous structures and the My appears to coalesce along with *E. coli*, similar to what is observed in the NX culture upon spin coating (Fig. 1e). On the other hand, XMy self-assembles into large amyloid tapes with width of ~7.5 μm, height of ~400 nm, and lengths exceeding 100 μm

Published on 14 January 2014. Downloaded on 04/03/2014 16:54:39.

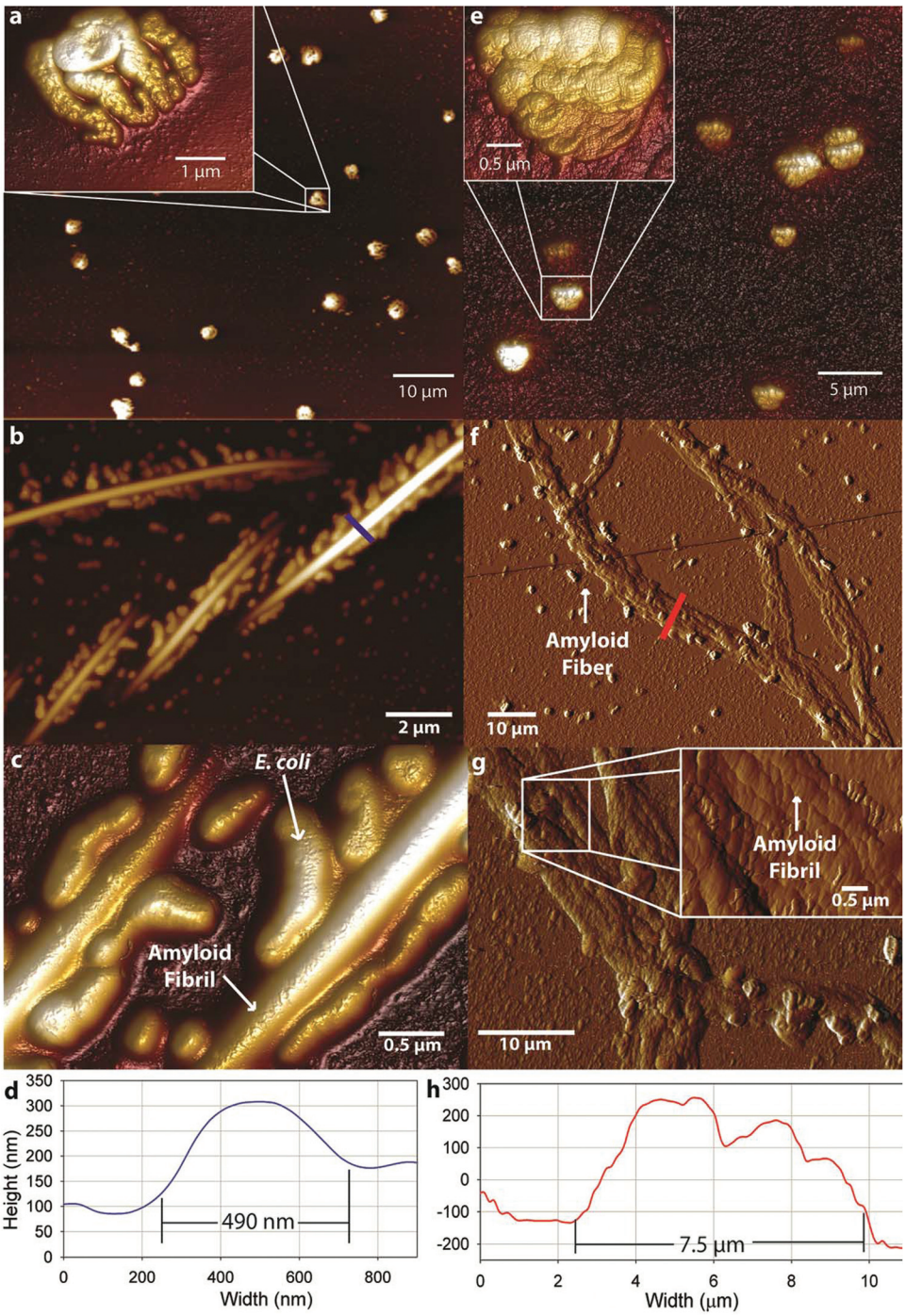

Fig. 1 AFM topographical images and cross section graphs of (a) NX cell culture showing coalescence of *E. coli* cells, (b,c,d) X cell culture showing *E. coli* cells attached to the surface of large amyloid fibrils with a diameter of 490 nm, (e) NXMy cell culture showing My coalescence in the absence of a template protein and (f,g) AFM tapping amplitude images of XMy amyloid fibers of W = 7.5 μm and H = 0.4 μm with (h) the corresponding cross section. All solutions are imaged after 37 hours of incubation with the exception of NXMy (72 hours).

(Fig. 1f–h). The tape is composed of large fibrils of widths 400–900 nm (Fig. 1g) that resemble those in Fig. 1b and c from the X culture and previous studies.[14] This process largely mimics the self-assembly of protein mixtures *in vitro* where Gd20 and My aggregate into (a) ~30 nm wide protofibrils, (b) protofibrils aggregate into ~100 nm wide fibrils, (c) fibrils aggregate into 400–900 nm wide large fibrils of elliptical cross-section that then (d) aggregate extensively laterally and limitedly vertically into ~7.5 μm wide tapes of rectangular cross-section.[13–15] Protofibrils have been shown to have an intrinsic twist due to the left-handed chirality of the amino acids within the high density β-sheet core.[26] This was confirmed with WG and Gd:My template and adder systems *in vitro* with AFM.[14] Spectroscopic studies have indicated that hydrophobic

This journal is © The Royal Society of Chemistry 2014

Published on 14 January 2014. Downloaded on 04/03/2014 16:54:39.

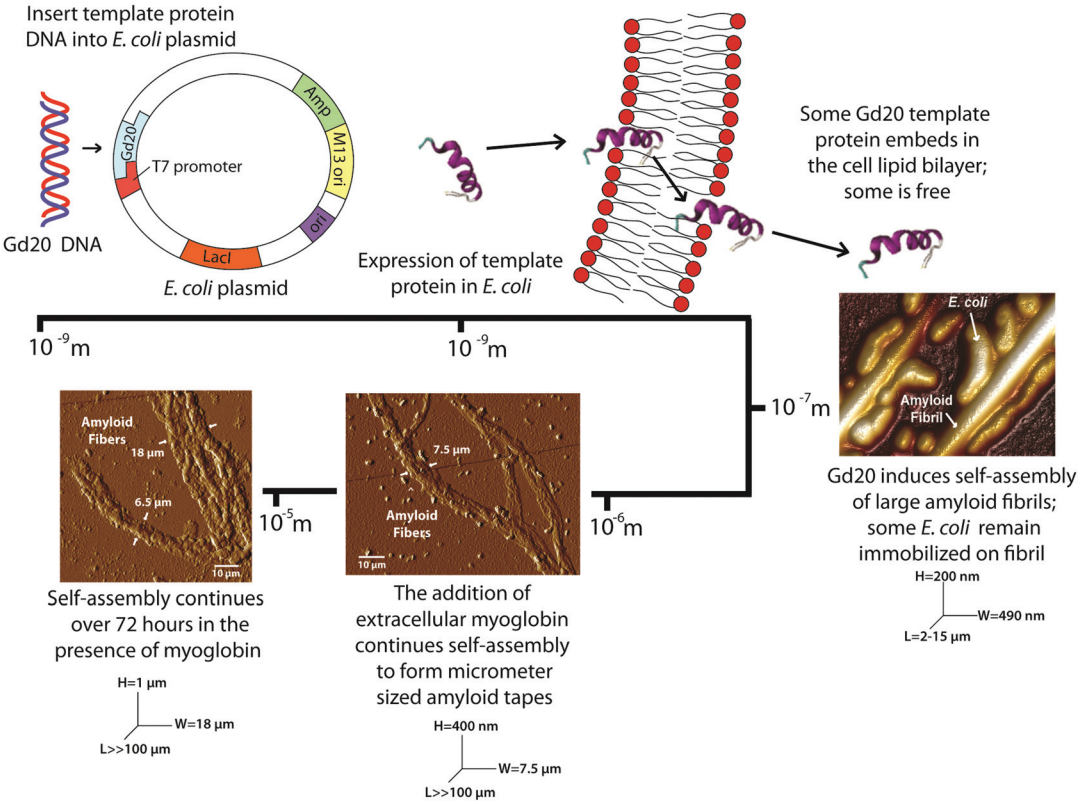

Scheme 1 Genetic encoding of the Gd20 template protein into an *E. coli* plasmid results in the self-assembly of amyloid fibrils and fibers spanning four orders of magnitude.

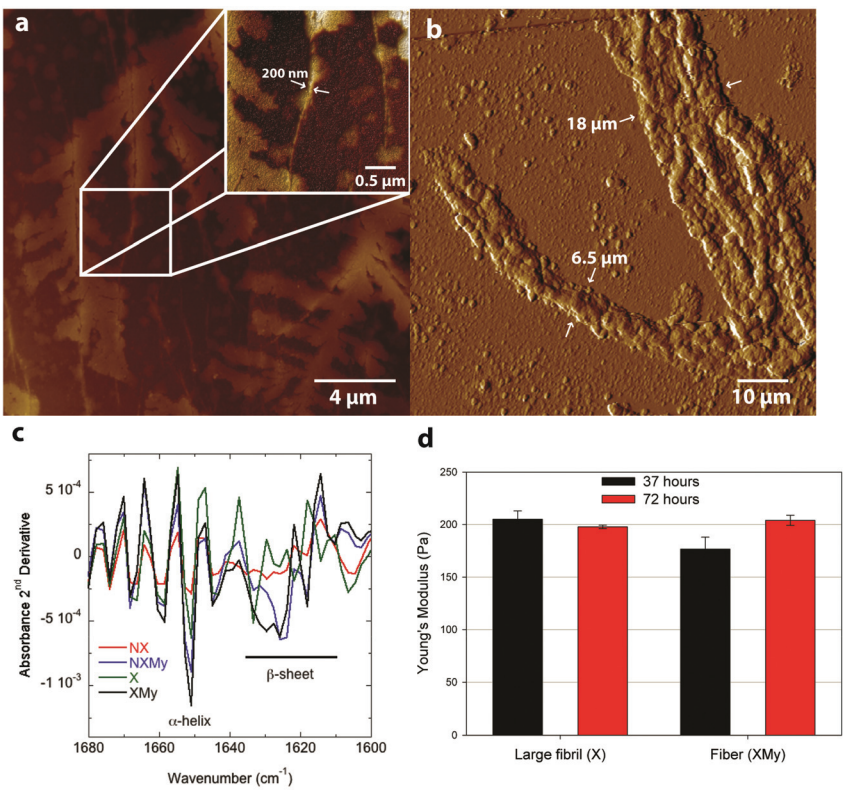

Fig. 2 (a) AFM topographical image of X after 72 h and (b) AFM tapping amplitude image of XMy after 72 hours. (c) FT-IR Amide I 2nd derivative spectra of the four cell cultures (X, NX, XMy, and NXMy) at 43 hours. (d) Young's modulus of large fibrils (X) and fibers (XMy) indented at 37 and 72 hours.

Published on 14 January 2014. Downloaded on 04/03/2014 16:54:39.

interactions promote self-assembly of smaller structures into larger structures, which is what drives aggregation to higher scales here as well (Scheme 1 and Fig. 3).[13,27] For Gd:My, the twist at the protofibril stage does not persist to higher stages.

X and XMy cultures are imaged after 72 hours to determine if the amyloid structures continue to self-assemble over time. Fibrils from the X culture are of smaller width, ~200 nm (Fig. 2a and ESI Fig. 2†), than at 37 hours, ~490 nm (Fig. 1b–d). The decrease in width suggests that the 490 nm large fibril is metastable or not fully compacted at early times. Indeed, few studies have been able to surpass the ~100 nm width barrier for amyloid fibrils or tapes formed after long incubation times.[28,29] So the metastability of a larger structure may be intrinsic to certain amyloid forming proteins, especially systems that have only 1 assembling protein. After 72 hours XMy assembles into a tape similar to early times but with a larger width of ~18 μm and height of ~1 μm (Fig. 2b and ESI Fig. 2†) suggesting that unassembled proteins in a mixture of template and adder proteins continue to interact as time progresses to grow toward an equilibrium structure.

Analysis of the Amide I absorbance obtained from Fourier transform-infrared (FT-IR) spectroscopy can be used to determine protein secondary structure.[30,31] NX does not contain any significant structure (Fig. 2c and 3a). Expression of Gd20 (X) shows the presence of α-helices (~1650 cm^{-1}), the predominant structure of Gd20 as predicted with PSIPRED,[32] and β-sheets (1610–1630 cm^{-1}) as the template forms, including high strand density β-sheets found in amyloids at <1625 cm^{-1}.[33] X β-sheets appear metastable as the ratio of the area of the β-sheet region to the α-helix region decreases from 2.1 at 43 hours to 1.8 at 72 hours (Fig. 3a). The addition of My is evident from increased α-helical content, the predominant My secondary structure. β-sheet formation occurs when My is exposed to *E. coli* (NXMy) or *E. coli* that express Gd20 (XMy) at times coincident with the AFM data in Fig. 1. Native My is 79% α-helix with no β-sheet content. We have observed consistent α to β transitions in our *in vitro* fiber-forming systems with My as the adder protein and this would appear to be the case with NXMy and XMy. NXMy does not show fibril or fiber formation but My can self-assemble into amyloid fibrils under the right conditions.[34] Here, My forms β-sheets, the

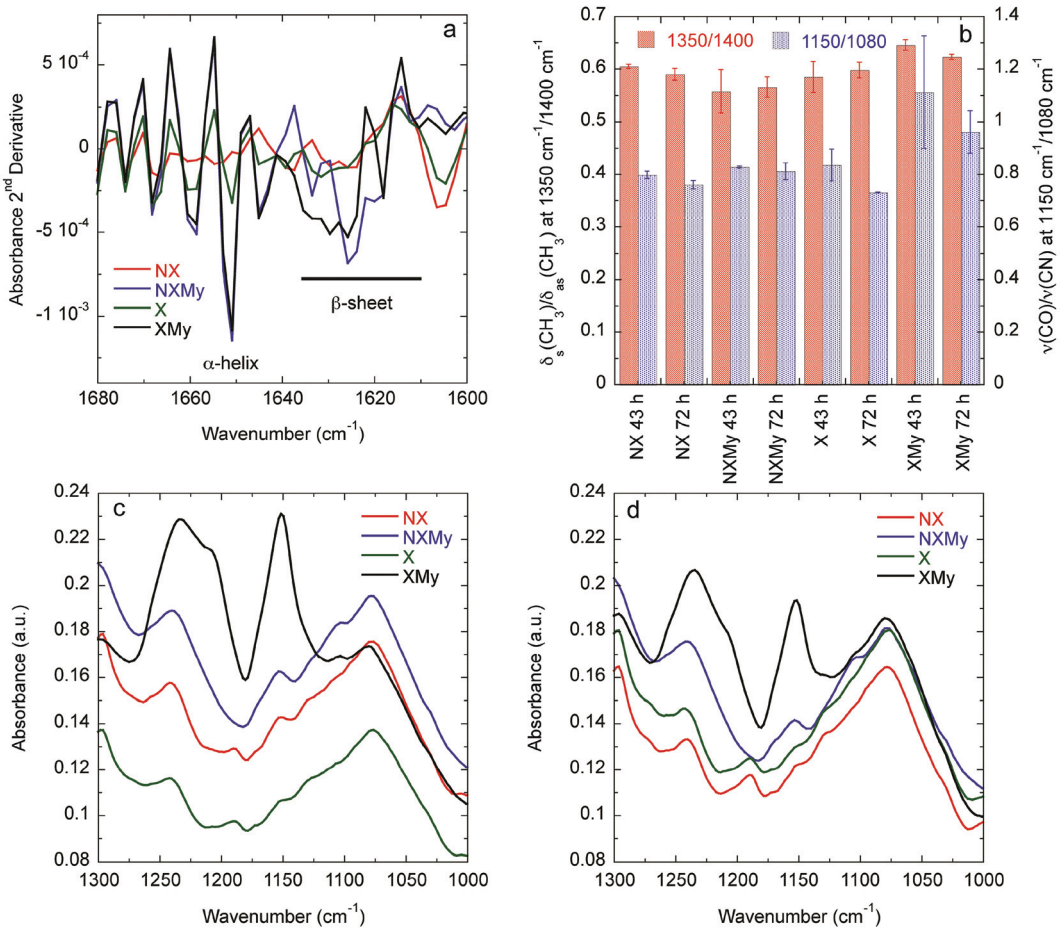

Fig. 3 (a) Amide I absorbance 2nd derivative at 72 h. (b) Ratios describing interdigitation of CH_3 groups on A, I, L, and V (1350 cm^{-1}/1400 cm^{-1}) and exposure and interaction of C–O and C–N groups (1150 cm^{-1}/1080 cm^{-1}) during self-assembly. FT-IR 1000–1300 cm^{-1} spectral region for (c) 43 and (d) 72 h.

This journal is © The Royal Society of Chemistry 2014

Published on 14 January 2014. Downloaded on 04/03/2014 16:54:39.

elementary amyloid structure, probably on the hydrophobic cell surface, which mimics our template protein characteristics to allow the α to β transition but not fibril formation. Proteins have been shown to undergo α to β transitions on hydrophobic surfaces.[13,35] XMy displays the largest β-sheet content and consistent large fiber formation indicating that the Gd20 template can influence β-sheet formation and is important to fiber formation. XMy has the highest ratio of $\delta_s(CH_3)/\delta_{as}(CH_3)$ at 1350 cm^{-1}/1400 cm^{-1}, which we term "hydrophobic packing" and describes the interdigitation of alanine (A), isoleucine (I), leucine (L), and valine (V) amino acid side groups as one driving force for self-assembly of large amyloid fibrils and fibers (Fig. 3b).[15] More importantly, XMy has dramatic changes in the 1250–1050 cm^{-1} region, which is quantified by the ratio of ν(CO)/ν(CN) at 1150 cm^{-1}/1080 cm^{-1} (Fig. 3b–d).[36] Gd20 contains 4 threonine (T) and My contains a significant amount of amino acids with CO and CN in the side groups (ESI Fig. 1†) so the profound increase in ν(CO) and ν(CN) would indicate these amino acids release from My α-helices and aggregate with each other.

Modulus results for X large fibrils and XMy tapes, obtained from AFM nanoindentation in contact mode, support the conclusion that XMy continues self-assembly into a stable large tape with an increasing modulus, while X forms a metastable large fibril as evidenced by a decreasing modulus over time (Fig. 2d). These moduli are much lower than previously reported results for fibrils, fibers, and tapes.[13,15,37] The *in vivo* formed XMy tapes (Fig. 2b) show that the large fibrils are not fully aggregated together and thus do not produce as cohesive a tape as observed from *in vitro* systems.[13–15] This could be for several reasons: (1) some portion of the Gd20 template protein remains embedded in the cell membrane while the remainder allows for limited self-assembly with itself or My (Scheme 1) and (2) the molar concentration of fully excreted Gd20 may be sufficient to initiate My conformation change and addition into the self-assembling structure but that addition is limited due to a limited Gd20 concentration because the template : adder molar ratio has been shown to play a role in the self-assembly of large amyloid fibers.[13]

Conclusion

By utilizing *E. coli* to express an amyloid-forming template protein it is possible to grow micrometer sized amyloid tapes upon addition of a suitable adder protein. XMy forms tapes of the same size, morphology, and fibrillar hierarchy as observed *in vitro*.[14] These tapes can vary in modulus and can be coaxed to twist into cylinders to change morphology and properties.[15] By understanding self-assembly from the molecular to the macroscopic scale, it is possible to build fibers of predictable cross section, from rectangular to circular, and modulus, from soft to rigid, by controlling the type and amount of template and adder proteins. Since protein amino acid sequence can be controlled at the genetic level, it is then also possible to encode the properties of a macroscopic structure at the genetic level in a predictable and controllable manner. It is envisioned that large-scale structures for use in engineering applications could be encoded at the genetic level. The scheme also shows that it is possible to program cells to build their own fibrous scaffold, making the self-assembly process a unique tissue engineering motif. Furthermore, this method could be used to reconstruct the cell cytoskeleton or to recompartmentalize cells to make more robust organisms for industrial bioprocessing. It is hopeful that this study will provide the basis for future genetic engineering of spontaneously forming macroscopic biomaterials.

Acknowledgements

Generous funding through NSF-CMMI-0856262 and the USDA funded Virginia Tech Biodesign and Bioprocessing Research Center is gratefully acknowledged.

Notes and references

1 C. M. Dobson, *Trends Biochem. Sci.*, 1999, **24**, 329–332.
2 D. M. Fowler, A. V. Koulov, W. E. Balch and J. W. Kelly, *Trends Biochem. Sci.*, 2007, **32**, 217–224.
3 M. F. B. G. Gebbink, D. Claessen, B. Bouma, L. Dijkhuizen and H. A. B. Wosten, *Nat. Rev. Microbiol.*, 2005, **3**, 333–341.
4 D. E. Barlow, G. H. Dickinson, B. Orihuela, J. L. Kulp III, D. Rittschof and K. J. Wahl, *Langmuir*, 2010, **26**, 6549–6556.
5 S. Keten, Z. Xu, B. Ihle and M. J. Buehler, *Nat. Mater.*, 2010, **9**, 359–367.
6 T. P. J. Knowles and M. J. Buehler, *Nat. Nanotechnol.*, 2011, **6**, 469–479.
7 C. E. MacPhee and C. M. Dobson, *J. Am. Chem. Soc.*, 2000, **122**, 12707–12713.
8 M. Bouchard, J. Zurdo, E. J. Nettleton, C. M. Dobson and C. V. Robinson, *Protein Sci.*, 2000, **9**, 1960–1967.
9 T. P. Knowles, A. W. Fitzpatrick, S. Meehan, H. R. Mott, M. Vendruscolo, C. M. Dobson and M. E. Welland, *Science*, 2007, **318**, 1900–1903.
10 J. Adamcik, J.-M. Jung, J. Flakowski, P. De Los Rios, G. Dietler and R. Mezzenga, *Nat. Nanotechnol.*, 2010, **5**, 423–428.
11 M. Bouchard, J. Zurdo, E. J. Nettleton, C. M. Dobson and C. V. Robinson, *Protein Sci.*, 2000, **9**, 1960–1967.
12 L. Nielsen, S. Frokjaer, J. F. Carpenter and J. Brange, *J. Pharm. Sci.*, 2001, **90**, 29–37.
13 D. M. Ridgley, K. C. Ebanks and J. R. Barone, *Biomacromolecules*, 2011, **12**, 3770–3779.
14 D. M. Ridgley and J. R. Barone, *ACS Nano*, 2013, **7**, 1006–1015.
15 D. M. Ridgley, E. C. Claunch and J. R. Barone, *Soft Matter*, 2012, **8**, 10298–10306.
16 A. Vuorela, J. Myllyharju, R. Nissi, T. Pihlajaniemi and K. I. Kivirikko, *EMBO J.*, 1997, **16**, 6702–6712.

Published on 14 January 2014. Downloaded on 04/03/2014 16:54:39.

17 J. Cappello, J. Crissman, M. Dorman, M. Mikolajczak, G. Textor, M. Marquet and F. Ferrari, *Biotechnol. Prog.*, 1990, **6**, 198–202.
18 D. L. Kaplan, *Nat. Biotechnol.*, 2002, **20**, 239–240.
19 S. T. Krishnaji, G. Bratzel, M. E. Kinahan, J. A. Kluge, C. Staii, J. Y. Wong, M. J. Buehler and D. L. Kaplan, *Adv. Funct. Mater.*, 2013, **23**, 241–253.
20 T. Scheibel, R. Parthasarathy, G. Sawicki, X.-M. Lin, H. Jaeger and S. L. Lindquist, *Proc. Natl. Acad. Sci. U. S. A.*, 2003, **100**, 4527–4532.
21 J. Sambrook and D. W. Russell, *Molecular Cloning: A Laboratory Manual*, 2001.
22 A. Grote, K. Hiller, M. Scheer, R. Münch, B. Nörtemann, D. C. Hempel and D. Jahn, *Nucleic Acids Res.*, 2005, **33**, W526–W531.
23 *Innova AFM User Manual*, Bruker Instruments, 2013.
24 S. Guo and B. B. Akhremitchev, *Biomacromolecules*, 2006, **7**, 1630–1636.
25 L. L. del Mercato, G. Maruccio, P. P. Pompa, B. Bochicchio, A. M. Tamburro, R. Cingolani and R. Rinaldi, *Biomacromolecules*, 2008, **9**, 796–803.
26 A. W. P. Fitzpatrick, G. T. Debelouchina, M. J. Bayro, D. K. Clare, M. A. Caporini, V. S. Bajaj, C. P. Jaroniec, L. Wang, V. Ladizhansky, S. A. Müller, C. E. MacPhee, C. A. Waudby, H. R. Mott, A. De Simone, T. P. J. Knowles, H. R. Saibil, M. Vendruscolo, E. V. Orlova, R. G. Griffin and C. M. Dobson, *Proc. Natl. Acad. Sci. U. S. A.*, 2013, **110**, 5468–5473.
27 D. M. Ridgley, E. C. Claunch and J. R. Barone, *Appl. Spectrosc.*, 2013, **57**, 1417–1426.
28 C. C. Lara, J. Adamcik, S. Jordens and R. Mezzenga, *Biomacromolecules*, 2011, **12**, 1868–1875.
29 J. L. Jiménez, E. J. Nettleton, M. Bouchard, C. V. Robinson, C. M. Dobson and H. R. Saibil, *Proc. Natl. Acad. Sci. U. S. A.*, 2002, **99**, 9196–9201.
30 S. Krimm and J. Bandekar, in *Advances in Protein Chemistry*, ed. C. B. Anfinsen, J. T. Edsall and F. M. Richards, Academic Press, Inc., Orlando, 1986, vol. 38, pp. 181–364.
31 A. Dong, P. Huang and W. S. Caughey, *Biochemistry*, 1990, **29**, 3303–3308.
32 D. W. A. Buchan, S. M. Ward, A. E. Lobley, T. C. O. Nugent, K. Bryson and D. T. Jones, *Nucleic Acids Res.*, 2010, **38**, W563–W568.
33 G. Zandomeneghi, M. R. H. Krebs, M. G. McCammon and M. Fändrich, *Protein Sci.*, 2004, **13**, 3314–3321.
34 M. Fandrich, M. A. Fletcher and C. M. Dobson, *Nature*, 2001, **410**, 165–166.
35 A. Sethuraman, G. Vedantham, T. Imoto, T. Przybycien and G. Belfort, *Proteins: Struct., Funct., Bioinf.*, 2004, **56**, 669–678.
36 A. Barth, *Prog. Biophys. Mol. Biol.*, 2000, **74**, 141–173.
37 J. F. Smith, T. P. Knowles, C. M. Dobson, C. E. MacPhee and M. E. Welland, *Proc. Natl. Acad. Sci. U. S. A.*, 2006, **103**, 15806–15811.

This journal is © The Royal Society of Chemistry 2014

Chapter 8. Conclusion

Functional amyloids have demonstrated that self-assembling amyloid fibers have potential applications as industrial biomaterials. This study introduces a cooperative template and adder mechanism which utilizes a variety of proteins that interact to self-assemble into amyloid fibers with morphological and structural properties determined by the composition of the protein mixtures. A short hydrophobic "template" peptide initiates conformation change within a highly α-helical "adder" protein to self-assemble into β-sheets that continue to assemble from the molecular level to form micrometer sized amyloid fibers. As is the case with most materials, processing conditions play an integral role in the structural characteristics of the end product. The amyloid fibers formed here are no different. Altering solution pH, temperature, ionic strength and protein mixture yield fibers of varying morphology. Interestingly, near physiological processing conditions (pH 8 and 37°C) formed the greatest fiber quantities and the highest Young's Modulus for their respective protein mixtures which suggests that the template and adder mechanism may be the method that nature employs for amyloid self-assembly.

The results show that aliphatic amino acids initiate amyloid self-assembly and polyglutamine repeats (Q-blocks) form Q hydrogen bonds to reinforce the structure, creating a cylindrical amyloid fiber of higher modulus. The influence of these amino acids has been shown with spectroscopy and microscopy over long times to reveal the hierarchical self-assembly process of amyloid fibers within the differing protein mixtures. The work performed here demonstrates that it is possible to produce large amyloid fibers of a tailored modulus and morphology by manipulating the processing conditions and the adder proteins within the protein mixture. Furthermore, the aliphatic amino acid content of the α-helices is a determining factor in the amount of high density β-sheet aggregation within the protein mixture. Thus, it is possible to

predict the propensity of a protein to undergo conformation change and spontaneously assemble into an amyloid structure based on the secondary structure and amino acid composition of the protein. Furthermore, the molecular weight and aliphatic index of the adder protein was shown to be a good predictor of amyloid fiber morphology. These results introduce the possibility of engineering amyloid fibers of tailored properties simply by altering the amino acid sequence of the adder proteins. Again, this could offer substantial insight into naturally occurring amyloid forming systems.

The *in vitro* methods used for most of this thesis are not cost effective techniques for large scale industrial production of amyloid fibers. Gd20 was expressed in *E. coli* and combined with extracellular myoglobin to form micrometer sized amyloid fibers. Consequently, it is possible to genetically engineer a robust biomaterial over four orders of magnitude of scale. This study opens up several potential applications for the genetically encoded 3D printing (GET Print) of amyloid structures as tissue scaffolds, method for cell compartmentalization, biosensors or the immobilization of *E. coli* on a surface for metabolic processes.

This thesis provides the basis for future production of amyloid fibers as an industrial biomaterial by identifying the template plus adder mechanism of self-assembly, effect of processing conditions, the hierarchical self-assembly and the amino acids that dictate the structural properties of the fibers. Finally, this study has introduced a cost effective method for the genetic engineering of large amyloid fibers. It is the hope of this author that this research will provide the foundation for future industrial biomaterial applications for large amyloid fibers.

Appendix A.

Supporting Information: The Role of Protein Hydrophobicity in Conformation Change and Self-Assembly into Large Amyloid Fibers

Ridgley, D. M., E. C. Claunch, P. W. Lee, and J. R. Barone. 2014. The Role of Protein Hydrophobicity in Conformation Change and Self-Assembly into Large Amyloid Fibers. *Biomacromolecules*, DOI: 10.1021/bm401815u. - Reproduced with the generous permission of the American Chemical Society.

Table S1. Hydrophobic moment parameters using Kyte-Doolittle scale: $m\mu_{H,rel,i}$, $m\mu_{H,i}$, mH_i, L_i.

Protein	α_1	α_2	α_3	α_4	α_5
Ac	0.05, 0.14, 3.00, 13	*0.56, 1.61, -0.11, 5*	0.42, 1.22, -0.86, 10	0.29, 0.84, -1.31, 17	0.78, 2.24, -3.50, 2
Al	0.16, 0.47, 2.17, 14	*0.86, 2.49, -1.01, 8*	0.46, 1.34, 0.53, 11	0.38, 1.09, 0.71, 8	0.40, 1.17, -0.65, 8
Am	0.22, 0.64, 0.96, 19	0.45, 1.29, -1.09, 13	0.47, 1.36, -0.53, 13	0.40, 1.16, -0.82, 17	0.56, 1.61, -0.75, 14
Hm	0.12, 0.35, -0.39, 14	0.36, 1.05, 0.01, 15	0.32, 0.93, 0.18, 19	*0.46, 1.33, 0.26, 12*	0.80, 2.29, -3.55, 2
In	0.15, 0.43, 1.86, 16	0.40, 1.15, 1.80, 2	*0.45, 1.31, 1.24, 12*	0.14, 0.40, -0.38, 10	0.68, 1.95, 2.80, 2
My	0.32, 0.92, -0.58, 16	0.43, 1.23, 0.58, 15	*0.78, 2.24, -1.36, 6*	0.19, 0.56, -1.44, 5	*0.48, 1.40, 0.07, 20*

Protein	α_6	α_7	α_8	α_9	α_{10}
Ac	0.41, 1.18, -0.75, 15	0.43, 1.24, -1.33, 8	*0.56, 1.63, -0.41, 15*		
Al					
Am	0.53, 1.52, 0.56, 8	0.23, 0.67, -0.38, 8	0.75, 2.18, -0.45, 7	0.27, 0.78, 1.25, 11	0.50, 1.45, -0.83, 16
Hm	0.2, 0.59, 1.18, 15	*0.48, 1.37, 0.71, 19*			
In	*0.59, 1.70, -0.78, 7*				
My	0.17, 0.49, -0.82, 14	*0.58, 1.69, 1.21, 15*	0.66, 1.92, -2.35, 2	0.27, 0.80, -0.5, 24	

$m\mu_{H,rel,i}$ is the mean relative hydrophobic moment of the α-helix (hydrophobic moment normalized to a perfectly amphiphilic α-helix), $m\mu_{H,i}$ is the mean hydrophobic moment of the α-helix, mH_i is the mean hydrophobicity of the α-helix using the Kyte-Doolittle scale, L_i is the length of the α-helix in # of amino acids. α-helices go from N- to C-terminus in the prediction. Italicized data are for the highest mean relative hydrophobic moment α-helices discounting the 2 amino acid α-helices predicted by PSIPRED.

Table S2: The fiber morphology, molecular weight (MW), aliphatic index (AI), grand average hydropathicity (GRAVY) score, and isoelectric point (pI) for the six adder proteins used in this study.

Protein	Morphology	MW (kDa)	AI	GRAVY	pI
Ac	Flat	24.53	85.19	-0.481	4.98
Al	Ellipse	16.25	91.27	-0.169	4.92
Am	Flat	58.55	69.55	-0.607	6.33
Hm	Ellipse	15.25	93.45	0.013	8.72

In	Twist	11.98	102.91	0.193	5.22
My	Ellipse	17.18	88.77	-0.381	7.20

Appendix B.

Supporting Information: Genetically Encoded Self-Assembly of Large Amyloid Fibers

Ridgley, D. M., B. G. Freedman, P. W. Lee, and J. R. Barone. 2014. Genetically Encoded Self-Assembly of Large Amyloid Fibers. *Biomater. Sci.* 2(4):560-566. - Reproduced with generous permission of the Royal Society of Chemistry.

Table I: Comparison of template (Gd20) and adder (myoglobin) protein properties.

Protein	# amino acids	mol. wt. (g/mol)	pI	GRAVY	AI	α (%)	TANGO
Gd20	20	2060	9.4	1.820	171.0	85	1477
Myoglobin	154	17083	7.2	-0.381	88.77	79	207

mol. wt. is the molecular weight in g/mol; pI is the isoelectric point; GRAVY is the grand average of hydropathicity; AI is the aliphatic index; α is the percent α-helix predicted from PSIPRED; TANGO is an algorithm that predicts the potential for the protein to form an amyloid structure. Gd20 has a high propensity for amyloid formation and myoglobin a low propensity.

```
Gd20        TFLILALLAI VATTATTAVR

Myoglobin   MGLSDGEWQQ VLNVWGKVEA DIAGHGQEVL IRLFTGHPET LEKFDKFKHL KTEAEMKASE
            DLKKHGTVVL TALGGILKKK GHHEAELKPL AQSHATKHKI PIKYLEFISD AIIHVLHSKH
            PGDFGADAQG AMTKALELFR NDIAAKYKEL GFQG
```

Figure 1: Amino acid sequences of Gd20 and myoglobin.

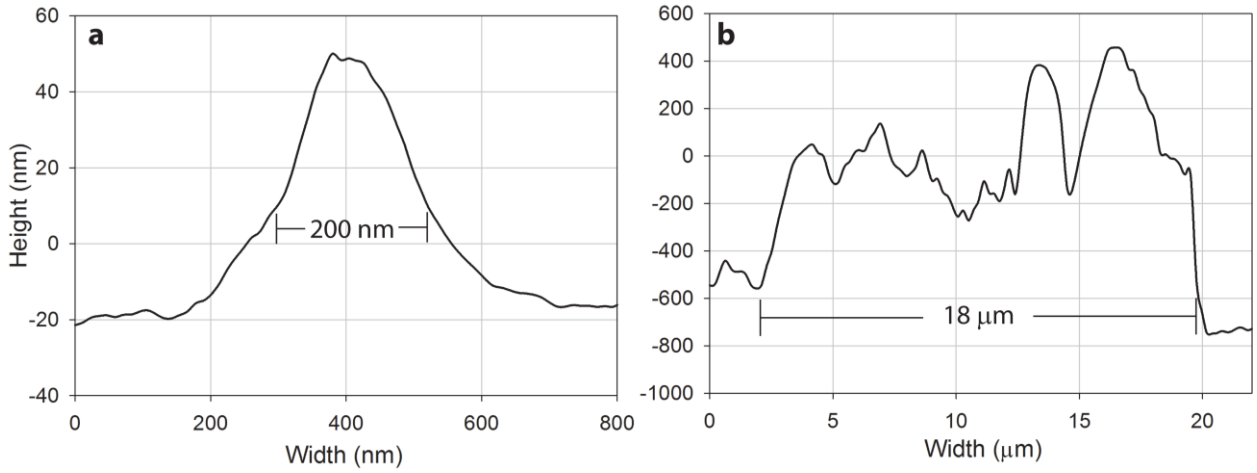

Figure 2: Cross sections of (a) X large fibrils and (b) XMy tapes at 72 hours. These graphs correspond to the AFM images of Figure 2a and 2b in the manuscript. The individual large fibrils comprising the XMy tape can be identified in the cross section.